

**Miniaturization of Features in Microfluidic Paper-based  
Analytical Devices for User-friendly Testing and Diagnosis  
Using Small Sample Volumes**

by

Md. Almostasim Mahmud

A thesis submitted to the  
School of Graduate and Postdoctoral Studies in partial  
fulfillment of the requirements for the degree of

Doctor of Philosophy in Mechanical Engineering

The Faculty of Engineering and Applied Science

University of Ontario Institute of Technology

Oshawa, Ontario, Canada

April 2019

© Md. Almostasim Mahmud, 2019

# Thesis Examination Information

Submitted by: **Md. Almostasim Mahmud**

Thesis title: Miniaturization of features in microfluidic paper-based analytical devices for user-friendly testing and diagnosis using small sample volumes

An oral defense of this thesis took place on April 10, 2019 in front of the following examining committee:

## Examining Committee:

Chair of Examining Committee	Dr. Amirkianoosh Kiani
Research Supervisor	Dr. Brendan D. MacDonald
Examining Committee Member	Dr. Atef Mohany
Examining Committee Member	Dr. Martin Agelin-Chaab
University Examiner	Dr. Liliana Trevani
External Examiner	Dr. Scott Tsai, Ryerson University

The above committee determined that the thesis is acceptable in form and content and that a satisfactory knowledge of the field covered by the thesis was demonstrated by the candidate during an oral examination. A signed copy of the Certificate of Approval is available from the School of Graduate and Postdoctoral Studies.

# Abstract

Microfluidic paper-based analytical devices ( $\mu$ PADs) are a promising platform for analytical testing, particularly for medical diagnosis. One of the main advantages of  $\mu$ PADs is the capacity for inexpensive, portable and user-friendly diagnostic devices for people who do not have access to traditional lab-based medical diagnosis. Miniaturization of  $\mu$ PADs can further reduce the material cost, reagent cost, and enhances the user-friendliness of the device. However, it is challenging to produce inexpensive and miniaturized  $\mu$ PADs using existing fabrication techniques because the techniques that offer high-end fabrication resolution are expensive, require multiple steps in fabrication, and are not suitable for mass production. Based on this research need, I have developed an inexpensive and high-resolution fabrication technique that enabled the fabrication of user-friendly miniaturized  $\mu$ PADs. The technique is rapid, capable of mass production, and offers the highest fabrication resolution compared to existing fabrication techniques. Small-scale paper channels are fabricated using a wide range of commercially available paper materials and it is found that the fibre width of the paper materials is the dominant parameter in creating the smallest features with the capability of fluid flow. The capillary flow speeds through small-scale paper channels are investigated to provide an understanding to predict fluid flow in miniaturized  $\mu$ PADs.

Two different types of miniaturized  $\mu$ PADs are developed using the newly developed fabrication technique: (a) compact  $\mu$ PAD for multiplexed testing and (b) lateral flow assay (LFA)-type  $\mu$ PAD for semi-quantitative test readout. The com-

pact multiplexed  $\mu$ PAD enables detection of eight analytes using 2  $\mu$ L of samples and the efficacy of this device is demonstrated by performing dye tests and glucose tests. The LFA-type  $\mu$ PAD enables analytical tests using sub-microlitre volume of samples and provides user-friendly semi-quantitative test readouts. The efficacy of the LFA-type  $\mu$ PAD is demonstrated by performing dye tests, glucose tests, and human immunoglobulin E (IgE) tests. Thus, the fabrication technique demonstrates its capability in the development of functional miniaturized  $\mu$ PADs and such devices are able to provide inexpensive and user-friendly diagnostic tests.

**Keywords:** Paper-based; Microfluidics; Miniaturization; Laser-cutting fabrication; Counting-based detection

## Author's Declaration

I hereby declare that this thesis consists of original work of which I have authored. This is a true copy of the thesis, including any required final revisions, as accepted by my examiners.

I authorize the University of Ontario Institute of Technology to lend this thesis to other institutions or individuals for the purpose of scholarly research. I further authorize University of Ontario Institute of Technology to reproduce this thesis by photocopying or by other means, in total or in part, at the request of other institutions or individuals for the purpose of scholarly research. I understand that my thesis will be made electronically available to the public.

Md. Almostasim Mahmud

---

## Statement of Contributions

Part of the work described in Chapter 3 and 4, and small portions from other chapters of this thesis have been published as:

**M. A. Mahmud**, E. J. M. Blondeel, M. Kaddoura, and B. D. MacDonald. Creating compact and microscale features in paper-based devices by laser cutting. *Analyst*, 141(23):6449-6454, 2016.

**M. A. Mahmud**, E. J. Blondeel, M. Kaddoura, and B. D. MacDonald. Features in microfluidic paper-based devices made by laser cutting: How small can they be? *Micromachines*, 9(5): 220, 2018.

The work described in Chapter 5, and small portions from other chapters of this thesis have been submitted for publication as:

**M. A. Mahmud**, E. J. Blondeel, and B. D. MacDonald (2019). Miniaturized counting-based microfluidic paper-based analytical devices for semi-quantitative test readouts.[Manuscript submitted for publication.]

I performed the literature review, all the experiments and associated data analysis, and presented the findings for the above mentioned publications and the submitted manuscript.

I have conceived, designed and performed all the experiments and associated data analysis for the works reported in Chapter 3, 4 and 5.

## Acknowledgements

I would like to express my sincere gratitude to my research supervisor Dr. Brendan D. MacDonald for his continuous support, encouragement, and guidance throughout my MAsc and PhD studies. He taught me essential research skills, technical writing skills, presentation skills and guided me to develop my own ability to solve the research problems.

I would like to thank Dr. Atef Mohany, Dr. Martin Agelin-Chaab, Dr. Liliana Trevani and Dr. Scott Tsai for dedicating their time to assess my work.

Special thanks to my family members for being extremely supportive throughout my study, without that it would be impossible for me to continue this study.

Thanks to all the members of the MacDonald Lab: Henry Fung, Michael Crawly, Salvatore Ranieri, William Oishi, Justin Rizzi and Anders Nielsen for all the valuable discussions and feedbacks. I would also like to thank the members of 'ExVivo Labs' for sharing the information on the potential application of  $\mu$ PADs in allergy testing.

# Contents

<b>Abstract</b>	<b>iii</b>
<b>Acknowledgements</b>	<b>vii</b>
<b>Table of Contents</b>	<b>xi</b>
<b>List of Tables</b>	<b>xii</b>
<b>List of Figures</b>	<b>xix</b>
<b>List of Abbreviations and Symbols</b>	<b>xx</b>
<b>1 Introduction</b>	<b>1</b>
1.1 Motivation . . . . .	2
1.2 Background . . . . .	4
1.2.1 Microfluidic devices . . . . .	4
1.2.2 Different types of $\mu$ PADs . . . . .	6
1.2.3 Fabrication of $\mu$ PADs . . . . .	9
1.2.4 Samples and analytes involved in medical diagnosis using $\mu$ PADs	11
1.2.5 Detection techniques used in the $\mu$ PADs . . . . .	14
1.2.6 Capillary flow . . . . .	17
1.2.7 User-friendly design of $\mu$ PADs . . . . .	19
1.2.8 User-friendly sample collection and small sample volume . . . . .	19
1.2.9 Miniaturization and compactness of $\mu$ PADs . . . . .	21
1.3 Scope of the thesis . . . . .	21
1.3.1 Objectives . . . . .	23



1.4	Thesis outline . . . . .	24
<b>2</b>	<b>Literature review</b>	<b>25</b>
2.1	Fabrication techniques developed for $\mu$ PADs . . . . .	26
2.2	Fabrication resolution and capability of small scale fabrication . . . . .	31
2.3	Characterization of capillary flow through paper channel . . . . .	32
2.4	Quantification of test results . . . . .	36
2.4.1	Intensity-based . . . . .	36
2.4.2	Distance-based . . . . .	38
2.4.3	Counting-based . . . . .	40
2.5	Summary of the chapter and perspective of this thesis . . . . .	43
2.5.1	Fabrication . . . . .	43
2.5.2	Flow characterization . . . . .	44
2.5.3	semi-quantitative test result . . . . .	44
<b>3</b>	<b>Development of fabrication technique for <math>\mu</math>PADs</b>	<b>46</b>
3.1	Materials and chemicals . . . . .	47
3.2	Development of fabrication technique . . . . .	48
3.2.1	Fabrication principle . . . . .	48
3.2.2	Fabrication procedure . . . . .	49
3.2.3	Laser power and speed adjustment for optimum barrier width . . . . .	55
3.3	Fabrication of compact and miniaturized $\mu$ PAD . . . . .	58
3.3.1	Dye test . . . . .	59
3.3.2	Glucose test . . . . .	61
3.3.3	Cost analysis . . . . .	63
3.3.4	Mass production of $\mu$ PAD . . . . .	64
3.4	Smallest features fabricated out of different paper materials . . . . .	65

3.4.1	Influence of fibre width on the miniaturization . . . . .	72
<b>4</b>	<b>Flow through small-scale features</b>	<b>77</b>
4.1	Experimental method . . . . .	78
4.2	Characteristics of flow through small scale features . . . . .	80
4.3	Difference in flow behaviour through cellulose and nitrocellulose paper materials . . . . .	86
<b>5</b>	<b>Development of LFA-type <math>\mu</math>PADs</b>	<b>89</b>
5.1	Materials and chemicals used in the Glucose test and human IgE test	90
5.2	Design and fabrication of the LFA-type $\mu$ PAD for counting-based test readout . . . . .	91
5.3	Operation of the LFA-type $\mu$ PAD . . . . .	93
5.4	Spotting reagents . . . . .	94
5.5	Device preparation for the glucose test and the test procedure . . . . .	95
5.6	Counting-based results obtained from the glucose test . . . . .	98
5.7	Device preparation for the IgE test and the test procedure . . . . .	101
5.8	Counting-based test results obtained from the IgE test . . . . .	104
<b>6</b>	<b>Conclusion</b>	<b>109</b>
6.1	Fabrication of $\mu$ PADs . . . . .	109
6.1.1	Fabrication technique . . . . .	109
6.1.2	Fabrication resolution . . . . .	110
6.1.3	Physical properties of paper that limit miniaturization . . . . .	110
6.1.4	Compact and miniaturized $\mu$ PAD developed for multiplexed testing . . . . .	111
6.2	Flow characterization of small scale channels . . . . .	111
6.3	Diagnostic tests using counting-based miniaturized LFA-type $\mu$ PAD .	112
6.4	Inexpensive and user-friendly $\mu$ PADs . . . . .	112

6.5	Research contributions . . . . .	113
6.6	Recommendation for the future works . . . . .	115
	<b>Bibliography</b>	<b>116</b>
	<b>Appendices</b>	<b>134</b>
	<b>A Permissions for reproducing author’s own work</b>	<b>135</b>
	<b>B Permission for reproducing figures from literature</b>	<b>137</b>

# List of Tables

3.1	Smallest channel widths for successful fluid flow for five different commercially available paper types using the foil-backed (all paper types) and non-foil-backed (1 Chr only) technique, reproduced from Ref. [113].	71
4.1	Design widths and corresponding actual widths fabricated from different paper types used for flow speed measurements, reproduced from Ref. [113]. . . . .	81

# List of Figures

Figure 1.1	A wide range of microfluidic devices developed for analysing different types of analytes (biomarkers, cells, viruses, bacteria), some of microfluidic devices are shown with common types of analytes as example: The lateral flow assay (LFA)-type $\mu$ PADs and microfluidically patterned $\mu$ PADs are primarily used for detection of biomarkers [top-left]; single cell detection system for the detection of cells [bottom-left]; digital microfluidic devices for the detection of viruses [bottom-right]; and sorting device for the bacteria detection [top-right]. Reproduced from Ref. [19] . . . . .	5
Figure 1.2	Basic operations of different kinds of the $\mu$ PADs: (a) simple microfluidically patterned $\mu$ PAD with a sample input zone and two detection zones, the test-ready device is shown at the left and the device with a colorimetric detection is shown at the right; (b) basic layout of LFA-type $\mu$ PAD where a test line and a control line are spotted with reagent, the analyte selectively binds at the test line ‘T’ and provides detection [bottom] and (c) basic layout of a dipstick with multiple detection zones, commonly used in urine analysis to detect multiple biomarkers. In this kind of device, the test readout can be performed based on intensity-variation of the same colour (R2, R3) or change in colour (R1, R4, R5) . . . . .	7
Figure 1.3	The conventional fabrication technique used for the LFA-type $\mu$ PADs where different hydrophilic pads and membranes are assembled together. Reproduced with permission from Ref. [29].	11

Figure 1.4	Basic operation of an LFA-type $\mu$ PAD based on the immunoassay. (a) The device is spotted with all necessary antibodies. (b) The sample flow to the conjugation pad and the analyte binds with anti-analyte antibody 1 (conjugated with a tracer). (c) The analyte selectively binds with the immobilized anti-analyte antibody 2 and the unbound anti-analyte antibody 1 with tracer binds with antibody 3 of the control line. (d) The tracer conjugated with anti-analyte antibody 1 provides detection at both test and control lines. Adapted with permission from Ref. [37]. . . . .	13
Figure 1.5	Different types of detection techniques used in the development of $\mu$ PADs: (a) colorimetric detection of glucose and protein, adapted with permission from Ref. [39]; (b) electrochemical detection of glucose, adapted with permission from Ref. [41]; (c) fluorescence detection of formaldehyde, adapted with permission from Ref. [47]; and (d) electrochemiluminescence (ECL) detection of 2-(dibutylamino)ethanol (DBAE), adapted with permission from Ref. [45]. . . . .	15
Figure 1.6	(a) The capillary flow of liquid through a paper channel confined by the hydrophobic barrier, adapted with permission from Ref. [54]; (b) an illustration of the porous hydrophilic matrix of the paper channel with capillary flow paths, adapted with permission from Ref. [55]. . . . .	18
Figure 1.7	(a) The assembly of the microneedle integrated $\mu$ PAD with device casing and PDMS touch switch to generate suction in needle, (b) different parts of the $\mu$ PAD and (c) steps of the device operation. Reproduced with permission from Ref. [30].	20
Figure 2.1	(a) Steps of wax printing technique for the fabrication of $\mu$ PAD, adapted with permission from Ref. [28]; (b) wax spreading behaviour to make the hydrophobic barrier, adapted with permission from Ref. [28]; (c) multiple steps required in the photolithography technique. Reproduced with permission from Ref. [39]. . . . .	28
Figure 2.2	(a) A laser cutting fabrication technique without any backing where some portions of the paper-sheet is left intact to support the $\mu$ PAD, reproduced with permission from Ref. [87]; and (b) a laser etching fabrication technique with the risk of through cutting because the backing is permeable to the laser beam, adapted with permission from Ref. [86]. . . . .	30

Figure 2.3	(a) Washburn flow characteristics where the flow speeds do not depend on the channel width, reproduced with permission from Ref. [68]; (b) Wider channel widths result faster flow, reproduced from Ref. [52]; and (c) Wider channel widths result slower flow after a certain the threshold, reproduced with permission from Ref. [93]. . . . .	35
Figure 2.4	Intensity-based glucose test readout, reproduced with permission from Ref. [36]: (a) colorimetric detection of glucose and (b) correlation between the colour intensity and glucose concentration. . . . .	37
Figure 2.5	Different distance-based test read out techniques reported in the literature: (a) distance-based detection of glucose level, adapted with permission from Ref. [101]; (b) the effect of sample volume on the sensitivity of the distance-based test readout, adapted with permission from Ref. [101]; (c) the distance-based test readout developed for fluorescence detection, adapted with permission from Ref. [103]; and (d) distance-based detection of H <sub>2</sub> O <sub>2</sub> level, adapted with permission from Ref. [104]. . . . .	39
Figure 2.6	(a) An illustration of the counting-based test readout where the gold nano-particles were used in the sandwich type immunoassay as the tracer for the analyte, adapted with permission from Ref. [105]; (b) the counting-based test readout produced by the gold nano-particles, adapted with permission from Ref. [105]; and (c) the counting-based test readout produced by the enzyme and corresponding substrate, adapted with permission from Ref. [107]. . . . .	42
Figure 3.1	Schematic of the fabrication process for a $\mu$ PAD with compact and microscale features, reproduced with permission from Ref. [112]. . . . .	49
Figure 3.2	The different steps involved in the preparation of foil-backed sheet of a paper material. . . . .	51
Figure 3.3	The laser unit is connected with a computer where the pattern is drawn [top] and the enclosed working table where the foil-backed sheet of paper material is placed for the fabrication [bottom]. . . . .	52
Figure 3.4	(a) Securing the sheet of paper with magnet and adjusting the working table height for focusing the laser; (b) the array of the $\mu$ PADs have been fabricated by the laser. . . . .	53

Figure 3.5	The inspection of the $\mu$ PAD and its hydrophobic barriers using a USB microscope . . . . .	54
Figure 3.6	Circular features cut in foil backed paper and tested with red dye at different values of laser power and cutting head speed to find the minimum width of the hydrophobic barrier without cross-barrier bleeding, reproduced with permission from Ref. [112]. . . . .	56
Figure 3.7	Plot of average hydrophobic barrier width for varying laser power at different laser head speeds, reproduced with permission from Ref. [112]. . . . .	58
Figure 3.8	(a) The pattern of the compact $\mu$ PAD with 8 detection zones, (b) The device with blue dye below a Canadian nickel (5 cent coin) to show the relative size, adapted with permission from Ref. [112]. . . . .	59
Figure 3.9	(a) Test device spotted with 8 different dye colours, and (b) after 2 $\mu$ L of yellow dye was added, adapted with permission from Ref. [112]. . . . .	60
Figure 3.10	(a) The test device for glucose test with reagents in 8 readout zones, and (b) image taken 5 minutes after sample placement, showing successful glucose test using 2 $\mu$ L of artificial urine sample where dark brown colour indicates the presence of glucose, adapted with permission from Ref. [112]. . . . .	62
Figure 3.11	Schematic of a possible manufacturing line for mass production of $\mu$ PADs, reproduced with permission from Ref. [112]. . . . .	65
Figure 3.12	(a) Schematic of the fabrication technique used to generate small-scale features in the different paper types. (b) Overhead view of a dye flow test with the fabricated small-scale channels, adapted from Ref. [113]. . . . .	67
Figure 3.13	Testing small-scale channels of different width with a dye solution to determine the smallest channel width that can be fabricated from a particular paper type. One of the three sets of channels fabricated from RC-55 are shown in the figure. The actual width is listed as N/A for cases where the channel failed to provide a continuous flow path and so no successful width could be listed, adapted from Ref. [113]. . . . .	68
Figure 3.14	Measurement of successful channel widths using the microscope. . . . .	70



Figure 3.15	Scanning electron microscope (SEM) images of the fibre structure for the different paper types, reproduced from Ref. [113].	73
Figure 3.16	The smallest channel widths in each of the paper types for successful fluid flow plotted against fibre widths, reproduced from Ref. [113]. . . . .	74
Figure 3.17	SEM images of the channels generated in the different paper types showing one intact channel with successful fluid flow (on the top) and one narrower channel where fluid flow was not successful (on the bottom), for (a) FP-50, (b) 3MM Chr, (c) 1 Chr, and (d) RC-55. Reproduced from Ref. [113]. . . . .	76
Figure 4.1	Schematic of the experimental procedure for measuring the flow speeds of dye solution through varying channel widths, adapted from Ref. [113]. . . . .	79
Figure 4.2	Flow behavior through varying channel widths fabricated in Whatman 1 Chr chromatography paper (1 Chr): (a) flow speed and (b) relation of $L$ with $\sqrt{t}$ . Adapted from Ref. [113].	83
Figure 4.3	Flow behavior through varying channel widths fabricated in Whatman 3MM Chr chromatography paper (3MM Chr): (a) flow speed and (b) relation of $L$ with $\sqrt{t}$ . Adapted from Ref. [113]. . . . .	84
Figure 4.4	Flow behavior through varying channel widths fabricated in Whatman regenerated cellulose membrane 55 (RC-55): (a) flow speed and (b) relation of $L$ with $\sqrt{t}$ . Adapted from Ref. [113]. . . . .	85
Figure 4.5	Photographs of the flow of red dye in NC and RC-55. (a) Cross-sectional views after red dye flowed through NC and RC-55. (b) Overhead view showing the concave flow profile of red dye in NC indicating faster flow along the sides of the channel, adapted from Ref. [113]. . . . .	87
Figure 5.1	(a) Schematic of the LFA-type $\mu$ PAD designed to analyse small sample volumes. (b) Relative size of the miniaturized $\mu$ PAD is shown against a Canadian nickel (five cent coin) and finger tips. (c) Schematic of the $\mu$ PAD showing placement of the simulated sample (blue dye) and simulated running liquid (yellow dye). (d) Photographs of the dye test showing the flow of the simulated sample (blue dye) over time for visual confirmation of successful sample flow across the detection zone, reproduced from Ref. [114]. . . . .	92

Figure 5.2	Spotting sub-microlitre reagent volumes on the test dots ‘T1-T3’ using a syringe pump, micro-bore tubing, and finger tips, reproduced from Ref. [114]. . . . .	95
Figure 5.3	Steps for the glucose test: (a) the reagents were spotted on the sample input zone and detection zone of the $\mu$ PAD, (b) the test was performed by pipetting the simulated blood plasma sample followed by DI water as the running liquid, and (c) colorimetric detection of glucose over the test dots ‘T1-T3’ (with ‘T1’ and ‘T2’ coloured as dark brown as an example of the reaction with glucose), reproduced from Ref. [114]. . . . .	96
Figure 5.4	The camera set-up to monitor and capture the image of test results obtained from counting-based testing using the LFA-type $\mu$ PAD . . . . .	97
Figure 5.5	Photographs of the detection zones after completion of the glucose tests for three sets of experiments conducted with 0.5 $\mu$ L of the simulated blood plasma samples containing various concentration of glucose (0-12 mmol/L). The test dots changed to a dark brown colour if they reacted with glucose; therefore the number of dark brown dots in each test corresponds with the level of glucose in the sample, reproduced from Ref. [114]. . . . .	99
Figure 5.6	The glucose concentrations were plotted against the number of test dots that changed to a dark brown colour. For each test dot, the plot distinguished between the progression of two colorimetric states that were observed: a portion of the test dot changed to a dark brown colour or the entire test dot changed to a dark brown colour, reproduced from Ref. [114]. . . . .	100
Figure 5.7	Steps for the IgE test: (a) the sample solution (a mixture of the simulated blood plasma (containing IgE) and ‘abHRP’) was placed on the sample input zone followed by the placement of the running buffer in the running liquid input zone, (b) IgE-bound ‘abHRP’ was captured at the test dots, and unbound ‘abHRP’ was captured at the control dot as the sample solution flowed over them, and (c) HRP of the ‘abHRP’ turned blue after adding TMB solution on the detection zone (with ‘T1’ and ‘T2’ shown as blue coloured as an example), reproduced from Ref. [114]. . . . .	102
Figure 5.8	The incubator and rocker used in the preparation of the LFA-type $\mu$ PADs for human IgE test . . . . .	103

Figure 5.9	Photographs of the detection zones after completion of the IgE tests for three sets of experiments conducted with 1 $\mu\text{L}$ of the simulated blood plasma samples containing various concentration of human IgE (0-400 ng/mL). The test dots changed to a blue colour if they bound with IgE; therefore the number of blue dots in each test corresponds with the level of IgE in the sample, reproduced from Ref. [114]. . . . .	105
Figure 5.10	The IgE concentrations were plotted against the number of test dots that changed to a blue colour. For each test dot, the plot distinguished between the progression of two colorimetric states that were observed: a portion of the test dot changed to a blue colour or the entire test dot changed to a blue colour, reproduced from Ref. [114]. . . . .	107

# LIST OF ABBREVIATIONS AND SYMBOLS

## Abbreviations

abC	Goat anti-mouse IgG unconjugated antibody
abHRP	Mouse monoclonal anti-human IgE (Fc) antibody conjugated with HRP
abT	Cross-absorbed goat anti-human IgE antibody unconjugated
DAB	3,3'-diaminobenzidine
FP-50	Whatman filter paper grade 50
GOx	Glucose oxidase
HRP	Peroxidase from horseradish
IgE	Human immunoglobulin E
LFA	Lateral Flow Assay
NC	Amershan Protran 0.45 nitrocellulose membrane
PBS	Phosphate buffered saline
RC-55	Whatman regenerated cellulose membrane 55
TMB	3,3',5,5'-Tetramethylbenzidine
1 Chr	Whatman 1 Chr chromatography paper
3MM Chr	Whatman 3MM Chr chromatography paper
$\mu$ PAD	Microfluidic Paper-based Analytical Device

## Symbols

$L$	Distance travelled by the liquid front
$t$	Time required by the liquid front to travel a certain distance
$r$	Average pore radius of the paper materials
$\gamma$	Surface tension of the flowing liquid
$\theta$	Contact angle between the capillary wall and the flowing liquid
$\mu$	Dynamic viscosity of the liquid

# Chapter 1

## Introduction

Limited access to analytical testing, particularly in diagnostic tests, has been an issue for people living in resource-poor regions. Different types of portable microfluidic devices have been developed for analytical testing to address this issue. However, the existing challenge is to produce devices that are inexpensive and user-friendly, so that the users can afford to buy the devices and can use them with confidence and convenience. Microfluidic paper-based analytical devices ( $\mu$ PADs) are a promising platform for analytical testing because they allow the use of inexpensive paper materials in the fabrication of  $\mu$ PADs, enable equipment free operation, and easy disposal of the  $\mu$ PADs after use.  $\mu$ PADs have been developed for a wide range of applications including medical diagnosis [1–8]; environmental testing [9–11] such as water quality monitoring [12] and soil testing [13]; and other analytical tests such as metal-ion detection [14], pesticide detection in food [15–17] and explosives detection [18]. Low manufacturing costs (fabrication, reagents, materials) and user-friendly design are crucial for  $\mu$ PADs to make them inexpensive and easy to use.

In the experimental study reported in this thesis, I have designed and developed miniaturized  $\mu$ PADs which will reduce the manufacturing cost and improve the user-friendliness of  $\mu$ PADs. An inexpensive fabrication technique was newly developed to facilitate fabrication of the miniaturized  $\mu$ PADs. In addition, a counting-based test readout was designed and employed with the miniaturized  $\mu$ PADs to make the test readout user-friendly.

This chapter describes the motivation of the work, relevant background and the scope of this thesis.

## 1.1 Motivation

Development of inexpensive and user-friendly  $\mu$ PADs with a goal to help the underprivileged people living in resource-poor regions motivates me the most. I have personally witnessed how the lack of medical diagnostic labs severely affected the health of the people living in rural areas of Bangladesh. People living in some rural areas travel long distances to get a medical diagnosis done, which may consume the working hours of that day for a return trip. Usually, such visits require a follow-up trip on another day to get the test results. The cost of diagnosis and trips become a substantial financial burden on people with low income. The perception developed from such an experience often leads to people being unwilling to seek medical diagnosis and ignoring the syndromes of bad health conditions, which eventually causes severe health damage or even death. Inexpensive and user-friendly  $\mu$ PADs can help these populations get many of their essential medical diagnoses in home-based set-

tings and make them aware of the health conditions that may require further medical treatments.

User-friendly  $\mu$ PADs can also be a good choice for urgent and emergency medical diagnosis because they are capable of providing instant test results. It is challenging and often impossible to get quick results from classical lab-based medical diagnostic systems because of the test procedures and sometimes because of the unavailability of lab experts. Under such situations, the quick diagnostic tests can be done by the healthcare provider (e.g. doctor) using the  $\mu$ PADs, which will enable them to provide rapid and life-saving treatments.

In this thesis, I have developed miniaturized and user-friendly  $\mu$ PADs using a newly developed inexpensive and high-resolution fabrication technique. I believe that this contribution will have a significant impact on the development of user-friendly and inexpensive  $\mu$ PADs to provide medical diagnosis access to underprivileged people and patients in urgent or emergency situations.



## 1.2 Background

### 1.2.1 Microfluidic devices

The potential of microfluidics is being harnessed in the development of different kinds of microfluidic devices: such as microfluidic chips, microfluidic paper-based analytical devices ( $\mu$ PADs), microwell array, and digital microfluidics; to use them in medical diagnosis and in other analytical tests [19], as shown in Figure 1.1. These devices are being developed to analyse a wide range of analytes for medical diagnosis including biomarkers (e.g. protein, glucose) [20], cells [21, 22], viruses [23] and bacteria [19, 24]. Microfluidic chips primarily consist of the microfluidic channels made out of glass, silicone, polydimethylsiloxane (PDMS) or other polymers and they are used as different types of analytical devices, such as analyte sorting or separating devices and cell detection devices [19], as shown in Figure 1.1. Microwell arrays are used as a platform for chemical analysis [25] which are commonly made out of glass or plastic materials but reportedly they can also be made out paper materials [20]. Digital microfluidics is used in the procedures of analytical testing where manipulation of droplets on a plane facilitates chemical analysis [26]. In  $\mu$ PADs, the interaction between the target analyte of a sample and the reagent happens on the paper surface to cause analyte-specific detection [20]. The  $\mu$ PADs enable performing the analytical tests without sophisticated lab apparatus and trained personnel. Each type of microfluidic device has some competitive advantages over the others and among them,  $\mu$ PADs are generally considered as an inexpensive option for analytical testing.

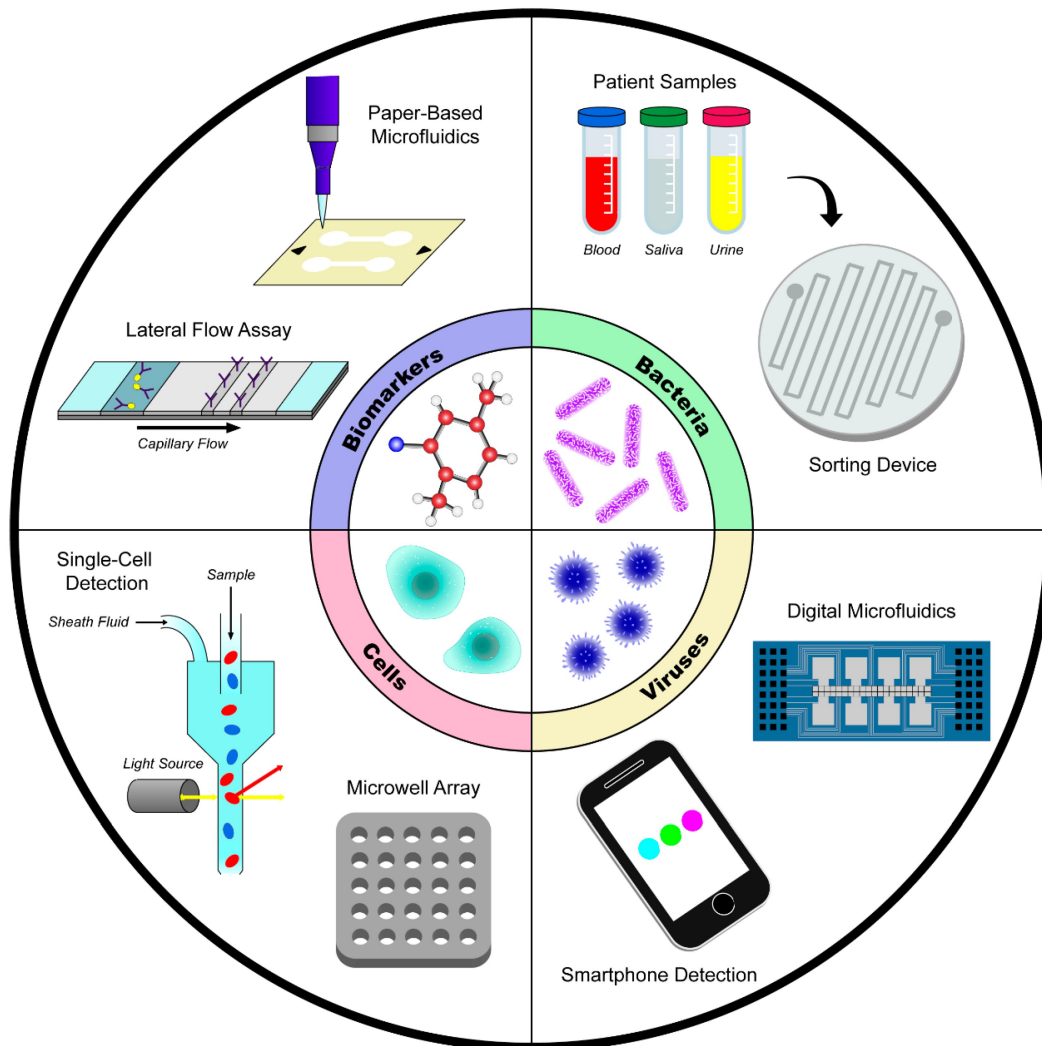
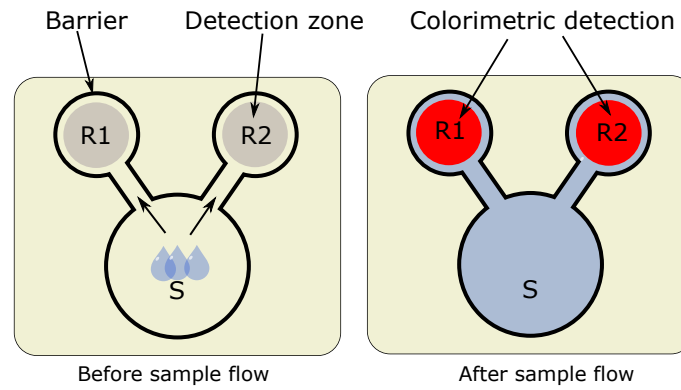
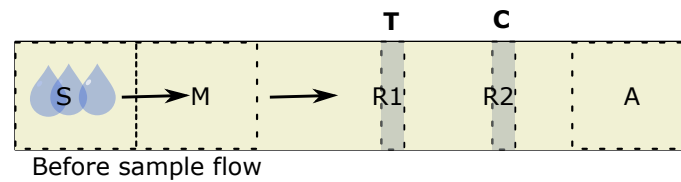
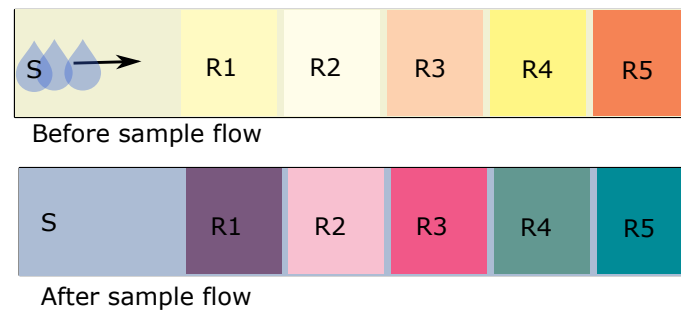


Figure 1.1: A wide range of microfluidic devices developed for analysing different types of analytes (biomarkers, cells, viruses, bacteria), some of microfluidic devices are shown with common types of analytes as example: The lateral flow assay (LFA)-type  $\mu$ PADs and microfluidically patterned  $\mu$ PADs are primarily used for detection of biomarkers [top-left]; single cell detection system for the detection of cells [bottom-left]; digital microfluidic devices for the detection of viruses [bottom-right]; and sorting device for the bacteria detection [top-right]. Reproduced from Ref. [19]

### 1.2.2 Different types of $\mu$ PADs

Microfluidic analytical devices made out of paper are considered as  $\mu$ PADs where the word ‘paper’ may simply mean a thin sheet of porous structure that consists of cellulose fibre. However, a broader definition of paper includes sheets or membranes of other paper-like porous materials [27] such as nitrocellulose membranes, polyvinylidene difluoride (PVDF) membranes and regenerated cellulose membranes (‘paper materials’ will be used herein to indicate all these materials including cellulose). A common type of paper-based device is the microfluidically patterned  $\mu$ PAD, as illustrated in Figure 1.2(a). Lateral flow assay (LFA) devices (such as pregnancy test strips) and dipsticks (used in urine analysis) are two other kinds of paper-based devices. Generally, these two types of  $\mu$ PADs are fabricated as a strip by assembling different hydrophilic pads made of different paper materials, as illustrated in Figure 1.2(b-c). In this thesis, ‘LFA-type  $\mu$ PADs’ will be used to refer LFA-type paper-based devices and ‘ $\mu$ PADs’ will be used to refer microfluidic paper-based analytical devices in general.

(a)  $\mu$ PAD(b) LFA-type  $\mu$ PAD

(c) Dipstick

Figure 1.2: Basic operations of different kinds of the  $\mu$ PADs: (a) simple microfluidically patterned  $\mu$ PAD with a sample input zone and two detection zones, the test-ready device is shown at the left and the device with a colorimetric detection is shown at the right; (b) basic layout of LFA-type  $\mu$ PAD where a test line and a control line are spotted with reagent, the analyte selectively binds at the test line ‘T’ and provides detection [bottom] and (c) basic layout of a dipstick with multiple detection zones, commonly used in urine analysis to detect multiple biomarkers. In this kind of device, the test readout can be performed based on intensity-variation of the same colour (R2, R3) or change in colour (R1, R4, R5)

The conceptual design of a simple microfluidically patterned  $\mu$ PAD is illustrated in Figure 1.2(a)[left] where it consists of three basic types of features: a sample input zone ‘S’, the detection zones spotted with the analyte-specific reagents ‘R1,R2’, and the connecting channels to facilitate sample flow from zone ‘S’ to detection zones ‘R1,R2’. The sample flow in a  $\mu$ PAD is facilitated by the capillary flow through the porous structure of paper which eliminates the need for an external pump. During the test, the analytes of interest flow to the detection zones ‘R1,R2’ with the sample and interact with the analyte-specific reagents which produce detection signals for the test results, as illustrated by red coloured zones in Figure 1.2(a)[right].

As shown in Figure 1.2(b)[top], the classical design of LFA-type  $\mu$ PADs consist of four basic features made out of hydrophilic paper materials: the sample input pad ‘S’, the conjugation pad or mixing zone ‘M’, the detection membrane (which contains test line ‘T’ and control line ‘C’ spotted with the specific reagents ‘R1,R2’) and the absorption pad ‘A’. During the test, the sample is placed in the zone ‘S’ which flows to the zone ‘M’ where the analyte is tagged with a label or tracer. After that, the sample with labelled analyte flows over the test line ‘T’ and the analyte interact or binds with the reagent ‘R1’ which produces a detection signal, as illustrated by the red colour in Figure 1.2(b)[bottom]. The control line ‘C’ always produces a signal when the reagent ‘R2’ comes in contact with the sample and thus it confirms successful sample flow to the end of the assay. Unlike the patterned  $\mu$ PAD, the LFA-type  $\mu$ PADs selectively binds the analyte at the test line and allows the rest of the sample to flow to the absorption zone ‘A’. Such selective binding is crucial to detect a specific analyte, when other substances of similar properties are present in the sample, such as

detecting a target antibody from a sample containing other antibodies and proteins.

A dipstick consists of a number of detection zones on a test strip spotted with analyte-specific reagents ‘R1-R5’, as illustrated in Figure 1.2(c)[top]. This kind of  $\mu$ PADs is usually designed for urine analysis where the available sample volume is large. During the test, the sample input zone ‘S’ of the device is exposed to a large volume of sample or the entire device is dipped in a sample. Thus the entire test strip becomes saturated with the sample and the reagents cause analyte specific detections (colorimetric signal), as shown in Figure 1.2(c)[bottom]. Dipsticks are primarily used in urine analysis whereas microfluidically patterned  $\mu$ PADs and LFA-type  $\mu$ PADs are suitable for both urine and blood-based diagnostic tests.

### 1.2.3 Fabrication of $\mu$ PADs

The fabrication of patterned  $\mu$ PAD refers to the process of creating the hydrophobic barriers according to a pattern which confines the liquid flow within the designated zones, as shown in Figure 1.2(a). The fabrication techniques can be divided into two groups based on the types of barriers: (i) forming methods and (ii) removing methods. In the forming methods, the hydrophobic substances (e.g. wax, hydrophobic ink, polymer etc.) are infused into the porous structure of paper following the pattern of the  $\mu$ PAD to create the barrier. However, the compatibility of the hydrophobic substance with the sample and other chemicals is important. For example, wax-based hydrophobic barriers are not compatible with organic liquids which can bleed through the wax barriers [28]. In addition, if the hydrophobic substances interfere with the

chemistry then they may cause false positive test results. The cutting or removing methods are the alternative to forming methods, where the paper material is removed following a pattern by cutting or burning and the capillary discontinuity created by the absence of paper material acts as the hydrophobic barrier. The describable traits for a fabrication technique are high fabrication resolution, low number of steps involved in the fabrication, and cost-effectiveness. The fabrication resolution refers to the precision and consistency of the width of the hydrophobic barrier where a high-resolution fabrication technique is essential to create miniaturized  $\mu$ PADs.

Unlike the patterned the  $\mu$ PADs, the LFA-type  $\mu$ PADs and dipsticks are commonly fabricated as a strip. The classical LFA-type  $\mu$ PAD consists of rectangular pieces of the sample pad, conjugation pad, reagent spotting membrane (e.g. nitrocellulose membrane) and the absorption pad which are assembled together to make a strip, as shown in Figure 1.3. Based on the application, a wide range of porous paper materials (e.g. cellulose paper, nitrocellulose membranes, PVDF membranes, glass fibre membrane, polyester membranes etc.) are used in the fabrication of LFA-type  $\mu$ PADs. Different types of paper materials offer a wide range of physical (pore size, fibre size, porous structure etc.) and surface properties (protein affinity, hydrophilicity, charge etc.). Therefore, it is important to select suitable paper materials in the fabrication of  $\mu$ PADs which are compatible with the chemistry and the sample used in the analytical tests.

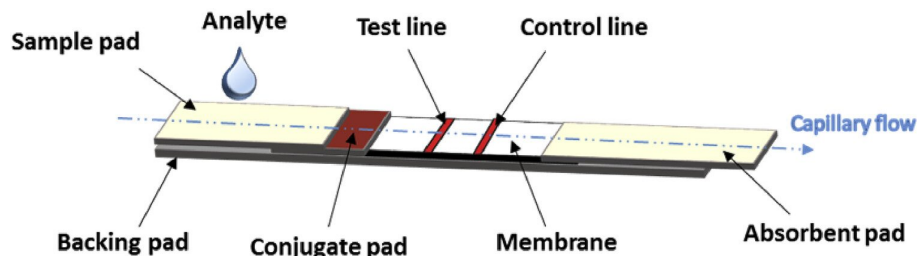


Figure 1.3: The conventional fabrication technique used for the LFA-type  $\mu$ PADs where different hydrophilic pads and membranes are assembled together. Reproduced with permission from Ref. [29].

### 1.2.4 Samples and analytes involved in medical diagnosis using $\mu$ PADs

In medical diagnosis, whole blood [30] or blood plasma and urine [31] are the most commonly used sample types. However, depending on the type of target analyte, interstitial fluid [32], sweat [33, 34], stool [35], tear [36], and saliva [31, 33] are also used as a sample. A wide range of biomarkers (analyte) is targeted for testing to identify the diseases and to monitor health conditions. For environmental and other analytical tests, a natural liquid sample (e.g. water quality monitoring) or a liquid sample prepared from the solid sample (e.g. testing solid food sample) can be used for tests [12, 15–17].

The selection of a suitable type of  $\mu$ PAD depends on the type of analyte and associated chemistry. If multiple analytes with the same chemical properties are present in a sample, then it may require selective binding of the target analyte from the rest of the chemically similar substances present in the sample. The LFA-type  $\mu$ PADs are good for detecting an analyte by selectively binding it at the detection zone from the rest of the sample. If the chemical properties of the analyte are unique,



then for detection it may not require selective binding of the analyte from the rest of the sample. For such tests, patterned  $\mu$ PAD shown in Figure 1.2(a) can be a good option as it simply detects the presence of the analyte at the detection zones. Chapter 3 of this thesis demonstrates the use of a compact and miniaturized  $\mu$ PAD for diagnostic test without the selective binding of the target analyte (glucose test) and chapter 5 of this thesis demonstrates the use of a miniaturized LFA-type  $\mu$ PAD for counting-based analyte detection by selectively binding the target analytes at the detection zone (human IgE test, and glucose test).

A large number of medical diagnosis involves the detection of the disease-specific antibodies (also known as immunoglobulins, which are protein) where the antibodies have similarity in chemical properties with other types of protein present in a human sample, such as blood plasma. Therefore, the selective binding of the target antibody from the rest of the proteins is required to avoid false positive test result. The procedures associated with the detection of antibodies is known as immunoassay and the LFA-type  $\mu$ PADs are commonly used in such detection, as shown in Figure 1.4. During the test, the sample is placed at the sample pad (as shown in Figure 1.4(a)) and when the sample reaches the conjugation pad the analyte binds with the first anti-analyte antibody-1 which is previously spotted in the conjugation pad 1.4(b). The antibody-1 is usually tagged with a tracer which later produces the detection signal. The analyte bound with antibody 1 reaches to the test line and binds with the anti-analyte antibody 2. Thus, in the test line the analyte is captured between two anti-analyte antibodies which is known as a sandwich assay, as shown in Figure 1.4(c). The rest of the sample flows forward to the control line and the unbound

anti-analyte antibody-1 tagged with tracer binds with the antibody 3 (which is anti-analyte antibody 1). Thus, if the analyte is present in the sample, the tracer of anti-analyte antibody 1 cause positive signal in the test line and the tracer signal at the control line confirms sample flow to the end of the detection zone, as shown in Figure 1.4(d). The absence of the tracer-signal at control line indicates that the test is invalid, as shown in Figure 1.4(d).

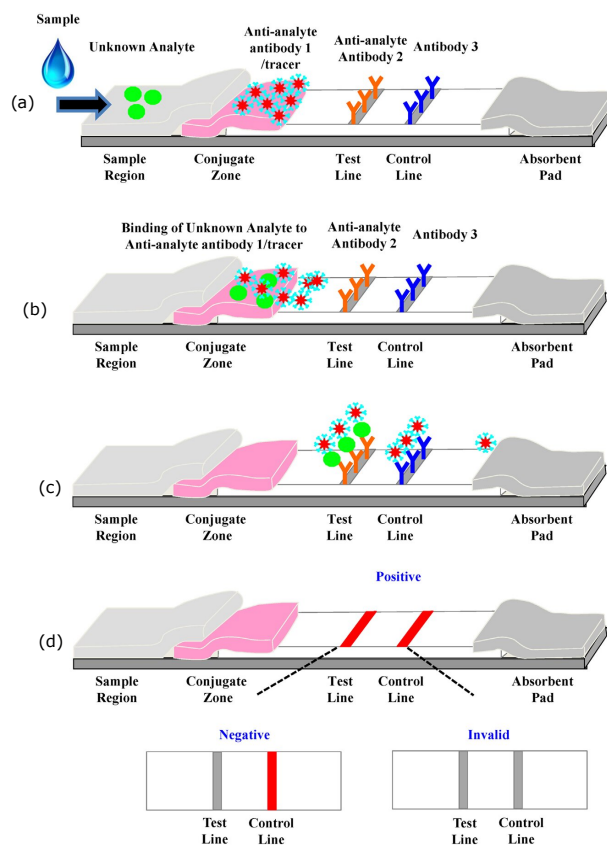


Figure 1.4: Basic operation of an LFA-type  $\mu$ PAD based on the immunoassay. (a) The device is spotted with all necessary antibodies. (b) The sample flow to the conjugation pad and the analyte binds with anti-analyte antibody 1 (conjugated with a tracer). (c) The analyte selectively binds with the immobilized anti-analyte antibody 2 and the unbound anti-analyte antibody 1 with tracer binds with antibody 3 of the control line. (d) The tracer conjugated with anti-analyte antibody 1 provides detection at both test and control lines. Adapted with permission from Ref. [37].

### 1.2.5 Detection techniques used in the $\mu$ PADs

The detection technique refers to the methods of acquiring a signal caused by the interaction between the target analyte and the detection reagents. A number of detection techniques have been introduced in the development of  $\mu$ PADs including colorimetric detection [18, 38, 39], electrochemical detection [40–42], chemiluminescence or electrochemiluminescence(ECL) detection [43–45] and fluorescence detection [46–48], as shown in Figure 1.5.

In the colorimetric detection, the detection zone changes its colour in contact with the target analyte present in the sample. Figure 1.5(a) shows how different concentration of glucose and bovine serum albumin (BSA) protein changes the detection zone's colour from clear to dark brown and yellow to green respectively [39].

In electrochemical detection, the electrodes are created in the detection zones of a  $\mu$ PAD (shown in 1.5(b)[top] ) and the detection chemistry is designed in such a way that the electrical signal (commonly current) obtained through the electrode corresponds to the concentration of the analyte. Figure 1.5(b)[bottom] shows how the current changes corresponding the concentration of the glucose present in the sample [41].

In fluorescence detection, the detection chemistry produces a fluorophore after reacting with the analyte or a standard fluorophore-tagged analyte is selectively bound on a detection zone. The fluorophore emits light of known frequency after being excited by the light of lower frequency, such a UV light. The emitted light is often within the visible light spectrum which passes through a filter and provide visible

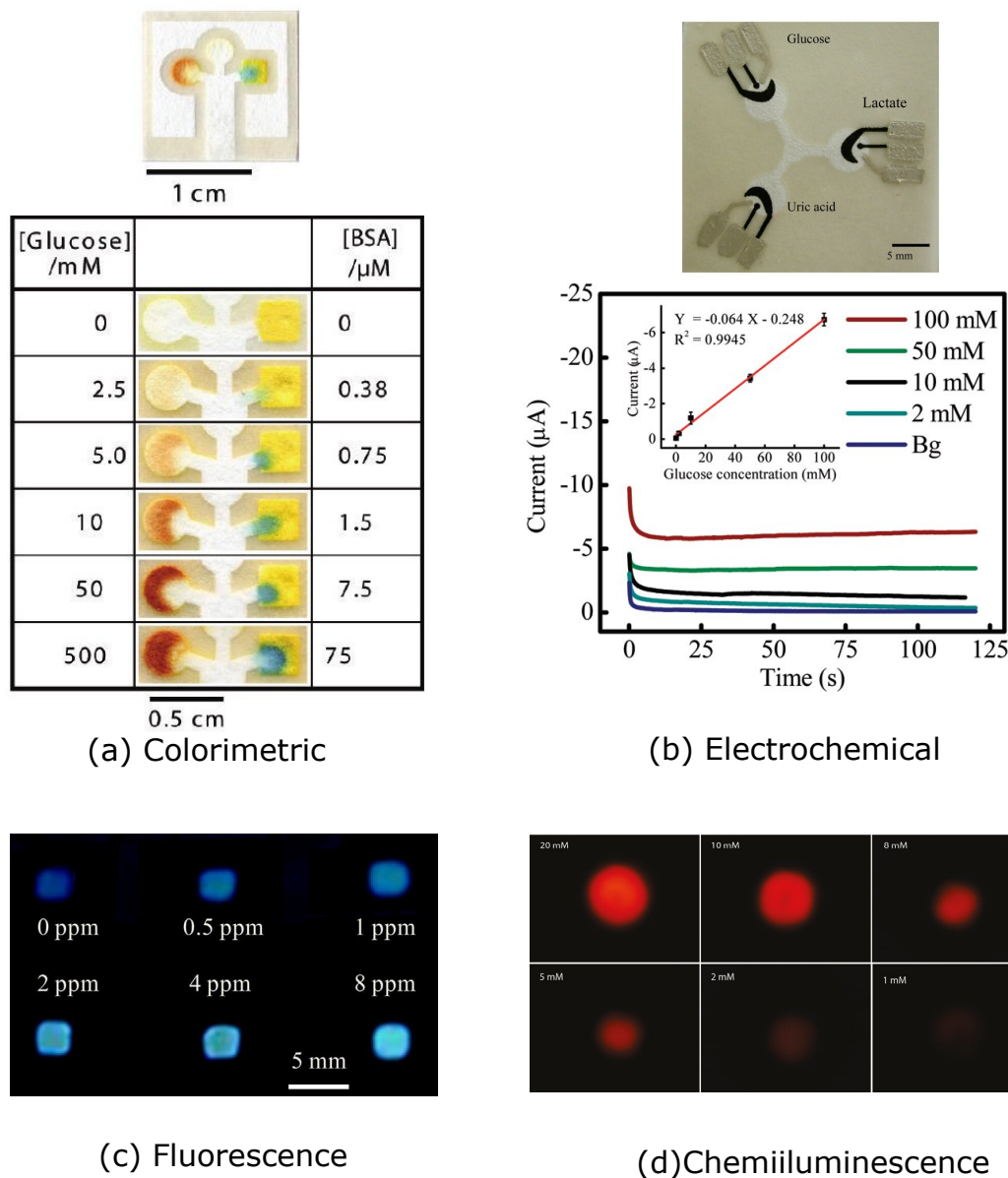


Figure 1.5: Different types of detection techniques used in the development of  $\mu$ PADs: (a) colorimetric detection of glucose and protein, adapted with permission from Ref. [39]; (b) electrochemical detection of glucose, adapted with permission from Ref. [41]; (c) fluorescence detection of formaldehyde, adapted with permission from Ref. [47]; and (d) electrochemiluminescence (ECL) detection of 2-(dibutylamino)ethanol (DBAE), adapted with permission from Ref. [45].

detection. Figure 1.5(c) shows the fluorescence detection of formaldehyde where the different concentration of the analyte corresponds to the different intensity of the fluorescence [47]. This detection technique requires some external equipment, such as a

fluorescence reader (e.g. microscope), UV lamp, camera with the appropriate filters etc.

Chemiluminescence (CL) and electrochemiluminescence (ECL) both utilize light emitting chemical substance (e.g. luminol which emits blue light ) in the detection. A common approach is to tag the analyte with the light emitting chemical and the light emission is triggered by certain type of chemicals (in CL) or by the applied electric field (in ECL). Figure 1.5(d) shows an ECL detection where the intensity of the emitted light corresponds to the different concentration of 2-(dibutylamino)ethanol (DBAE) and in this work a smart-phone camera was used to capture the photograph of the emitted light [45].

Among all the above mentioned detection techniques, the colorimetric detection is the most popular technique used in the development of  $\mu$ PADs. This technique is equipment free and intuitive, which can be considered as a user-friendly test readout technique. Primarily the colorimetric detection provides a qualitative result which simply indicates the presence or absence of the analyte, such as a pregnancy test strip. However, in many tests, the concentration of the target analyte needs to be determined, which is quantitative data. Different kind of test readout techniques have been reported in the literature to get quantitative test results using  $\mu$ PADs. However, obtaining exact concentration of analyte requires highly accurate test readout techniques and to avoid that  $\mu$ PADs are often designed for semi-quantitative test readouts where an approximate concentration of the analyte or a range of analyte concentration can be obtained as the test result. Techniques for semi-quantitative test readout are briefly reviewed in section 2.4 of this thesis. An easy interpretation

of the colorimetric detection signal into a quantitative or semi-quantitative test result is essential to develop user-friendly  $\mu$ PADs.

### 1.2.6 Capillary flow

The capillary flow through porous paper materials enables the operation of analytical testing on the  $\mu$ PAD without the help of an external pump. The flow influences the analyte flow behaviour towards the detection zone, detection signal, and the time required for the test. Therefore, the understanding of capillary flow behaviour through the porous fibrous structure of the paper materials is essential to design microfluidic flow paths in a  $\mu$ PAD.

In general, the paper is a hydrophilic porous material and the pores make a continuous capillary flow path through the fibrous matrix of paper, as shown in Figure 1.6(b). The pores are formed by the inter-fibre gaps and even by the gaps present inside the fibres [49, 50]. The capillary flow in a  $\mu$ PAD refers to the sample flow through that porous structure, as illustrated in Figure 1.6(b). A common approach to determine capillary flow behaviour is to make paper channels with different widths and measure the speed of the liquid front through the channels, as shown in Figure 1.6(a). In such experimentations, the one end of the paper channel is provided with an abundant volume of liquid (water with some dye is often used [51, 52]) and the speed of the liquid front is monitored and calculated using the visualization techniques such as video recording using a camera. The understanding of flow behaviour through the paper channels with varying widths helps to determine the feature sizes suitable

for the  $\mu$ PAD to be used for a specific test. The physical properties of the porous flow path (pore size, material type, hydrophilicity, fibre structure) and environmental conditions (temperature, humidity) [52, 53] also influence the capillary flow in a paper channel (the details are described in section 2.3 of this thesis). Theoretical prediction of such flow behaviour is challenging due to the random fibrous structure of the paper material and therefore the experimental study of such capillary flow behaviour is essential to get better understanding as compared to the theoretical approach. The understanding of the capillary flow through small-scale paper channels made out of different paper materials will be helpful for the development of miniaturized  $\mu$ PADs.

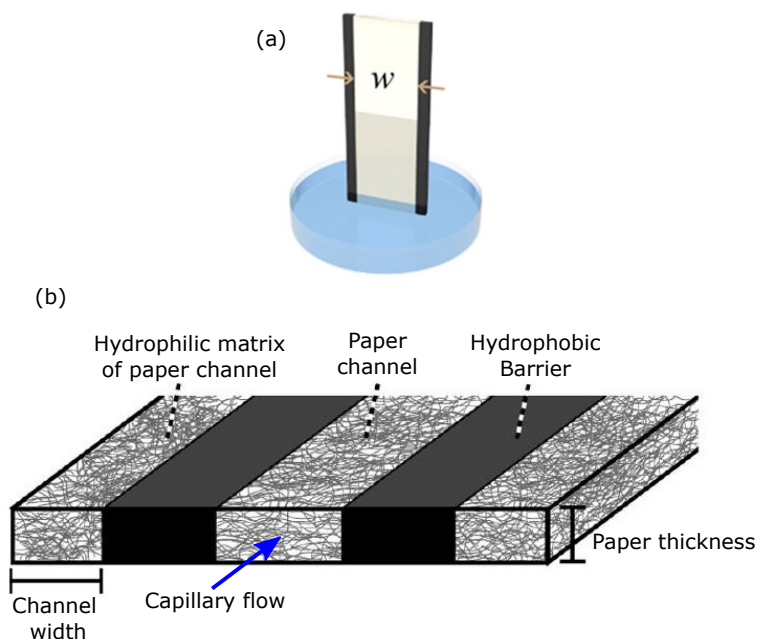


Figure 1.6: (a) The capillary flow of liquid through a paper channel confined by the hydrophobic barrier, adapted with permission from Ref. [54]; (b) an illustration of the porous hydrophilic matrix of the paper channel with capillary flow paths, adapted with permission from Ref. [55].

### 1.2.7 User-friendly design of $\mu$ PADs

The word ‘user-friendliness’ is a broad term that typically refers to the capability for  $\mu$ PAD tests to be easily used and the test results interpreted by untrained personnel [56], which enables the tests to be used in low-resource and home-based settings. The user involvement in the operation of  $\mu$ PADs determines the nature of user-friendliness where lesser involvement leads to a more user-friendly device and vice versa [27]. If the sample collection system is integrated with the  $\mu$ PADs, then it will eliminate the need for user-input in sample collection and its introduction onto the  $\mu$ PADs. For the user-friendly test result interpretation, the user should be able to get rapid qualitative or quantitative test results without operating sophisticated equipments, preferably by simple visual observation. Therefore, the integration of sample collection systems and incorporation of simple test readout techniques will make the  $\mu$ PADs user-friendly.

### 1.2.8 User-friendly sample collection and small sample volume

The collection of the blood sample using finger pricking [57] or micro-needles [58–60] can be considered as user-friendly compared to the use of hypo-dermal needle which is invasive in nature and damages skin cells. The use of hypo-dermal needle during the venous draw requires expertise where its use by an untrained individual may cause shrinkage in the blood vessel and other medical conditions [61].

Microneedles are suitable for a user-friendly sample collection system. Research has been conducted to develop different types of the microneedle and on its integration with  $\mu$ PAD for direct sample input. Figure 1.7 shows the design of a microneedle



integrated  $\mu$ PAD reported in the literature where the  $\mu$ PAD uses a single microneedle for the sample collection. A polydimethylsiloxane (PDMS) suction system was used with the microneedle to collect the sample by applying negative pressure. This device successfully performed glucose and cholesterol tests, as shown in Figure 1.7(c).

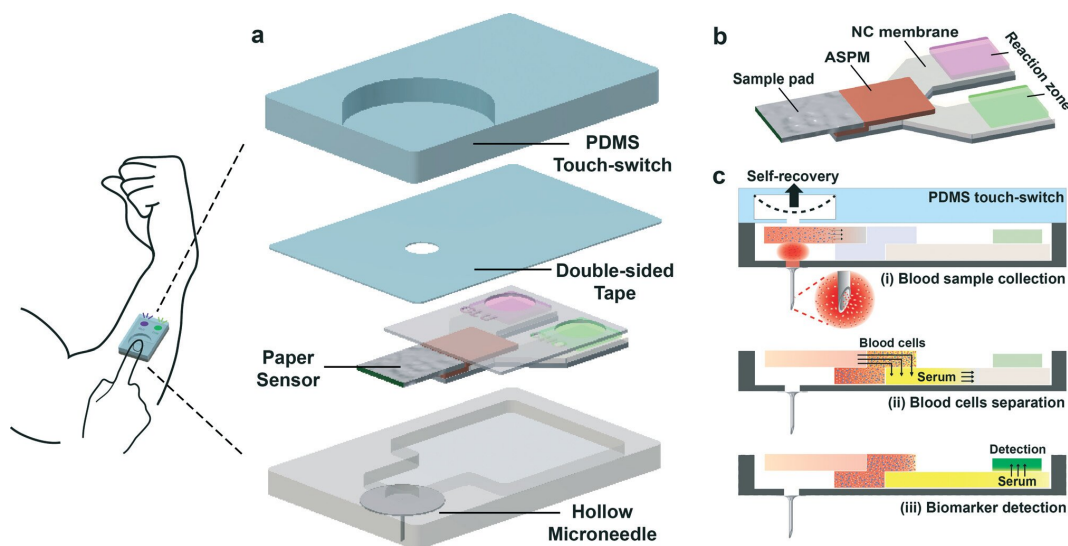


Figure 1.7: (a) The assembly of the microneedle integrated  $\mu$ PAD with device casing and PDMS touch switch to generate suction in needle, (b) different parts of the  $\mu$ PAD and (c) steps of the device operation. Reproduced with permission from Ref. [30].

Simple sample collection techniques will eliminate the challenges involved in conventional sample collection techniques. However, in absence of external suction device the sample volume collected by the microneedles [58–60] and finger prick [57] is relatively small (in the range of 1  $\mu$ L to 20  $\mu$ L) [57, 58, 60] and therefore the development of miniaturized  $\mu$ PADs capable analysing small sample volume is essential to allow the integration of user-friendly sample collection system.

### 1.2.9 Miniaturization and compactness of $\mu$ PADs

Miniaturized and compact  $\mu$ PADs enable testing with small sample volume and it can be integrated with a user-friendly sample collection system. The miniaturization of a  $\mu$ PAD simply means creating smaller scale devices and the compactness of the device refers to a design that keeps all the features of a device close together. A high-resolution fabrication technique that can create the narrow hydrophobic barriers accurately and precisely, is capable of fabricating the small scale features required for a compact and miniaturized  $\mu$ PAD. Such  $\mu$ PADs use less fabrication materials and reagents; therefore the reduced reagent costs and material costs will eventually make the final device inexpensive. In addition, the sample needs to travel a shorter distance in a small scale  $\mu$ PAD which may reduce the time required to complete the test. Thus, the user will be able to obtain rapid test result from a miniaturized  $\mu$ PAD. The compactness of the device will accommodate multiple detection zones closer to the sample input zone which allows the simultaneous detection of multiple analytes using a single sample input (commonly known as multiplexed testing). Therefore, a miniaturized and compact  $\mu$ PAD has the potential to be adopted as an inexpensive and user-friendly test device for analytical testing and medical diagnosis.

## 1.3 Scope of the thesis

The experimental study reported in this thesis was pursued in three phases. In the first phase, an inexpensive, rapid and high-resolution fabrication technique was developed for  $\mu$ PADs that incorporates a  $\text{CO}_2$  laser cutter. The technique enabled

the fabrication of miniaturized and compact  $\mu$ PADs required for inexpensive and user-friendly paper-based analytical devices. A wide range of commercially available paper materials was used to fabricate the smallest possible hydrophilic features that allowed successful liquid flow and it is essential to investigate the feasibility of using the materials in miniaturized  $\mu$ PADs. The dominant physical parameter of the paper materials that limits the miniaturization of paper-based devices was determined which will help material selection for future development of the miniaturized  $\mu$ PADs. To prove the concept, a miniaturized and compact  $\mu$ PAD was fabricated, which is capable of analysing multiple analytes using a small volume of sample (multiplexed detection of eight analytes using only 2  $\mu$ L of sample).

In the second phase, capillary flow through the small scale features (paper-based microfluidic channel) fabricated from three different paper materials were investigated to understand the potential sample flow behaviour in the miniaturized  $\mu$ PADs. The flow characterization provided an understanding that is essential to design miniaturized paper-based devices.

In the third phase, a miniaturized counting-based LFA-type  $\mu$ PAD was designed and developed that is capable of providing a semi-quantitative test result using a small volume of sample. To demonstrate the efficacy of the device, glucose test and human immunoglobulin E (IgE) tests were performed using the sub-microlitre volumes of simulated blood plasma samples (0.5  $\mu$ L for the glucose test and 1  $\mu$ L for the human IgE test). Glucose is a non-protein analyte present in the human blood sample which is an important biomarker to determine diabetes and hypoglycemia conditions [62]. IgE is a protein analyte (antibody) present in the human blood sample which is an

important biomarker for allergic symptoms [63–65]. Thus the miniaturized  $\mu$ PADs that successfully performed the tests for these two analytes are also capable of testing for a wide range of other analytes. The counting-based test readout is user-friendly which simply requires counting the number of coloured test dots to get the semi-quantitative test result.

### 1.3.1 Objectives

Based on the above mentioned scope, the objectives of this thesis are as follows:

1. Develop a high resolution fabrication technique that enables fabrication of miniaturized features in the  $\mu$ PADs.
2. Discover the smallest possible feature size with the capability of fluid flow that can be fabricated from different commercially available paper materials.
3. Experimentally determine the liquid flow speed through small-scale channels fabricated from different paper materials.
4. Develop a compact and miniaturized  $\mu$ PAD which enables multiplexed testing using small volumes of biologically relevant samples.
5. Develop a miniaturized counting-based LFA-type  $\mu$ PAD for semi-quantitative test readout and demonstrate its efficacy to use small volumes of biologically relevant samples.

## 1.4 Thesis outline

This thesis contains six chapters. Chapter 1 provides the introduction, motivation, relevant backgrounds, and the scope of the thesis. Chapter 2 presents the literature review on the different aspects of the development of  $\mu$ PADs related to the work reported in the thesis. Chapter 3 contains all the work done in the first phase including the development of a fabrication technique, demonstration of the multiplexed testing using a compact and miniaturized  $\mu$ PAD, and the miniaturization of  $\mu$ PADs and its relation to the physical properties of the paper materials. Chapter 4 presents the characterization of capillary flow through small scale features fabricated from different paper materials which was performed in the second phase of this study. Chapter 5 describes the design and development of miniaturized LFA-type  $\mu$ PADs with a counting-based test readout technique, which was done in the third phase of this experimental study. Chapter 6 contains concluding remarks on the different findings of this study along with the recommendations for future study.

# Chapter 2

## Literature review

The development of microfluidically patterned  $\mu$ PADs for analytical tests can be traced back to the 1940s [66]. However, throughout the twentieth century, the development of paper-based devices was somewhat limited to urine test strips (LFA-type  $\mu$ PADs and dipstick). In 2007, use of microfluidically patterned  $\mu$ PADs for analytical testing was reported again and since then the development of  $\mu$ PADs has grown rapidly [39]. In this chapter, the different aspects of  $\mu$ PAD development will be reviewed to put this thesis into perspective including the fabrication techniques developed for the  $\mu$ PADs, the resolution of the fabrication techniques, flow characterization of the paper channels with varying widths, and research work on semi-quantitative test readout techniques.

## 2.1 Fabrication techniques developed for $\mu$ PADs

The fabrication technique is a crucial part of the  $\mu$ PAD development as it facilitates versatile designs and also contributes to the cost of the final device. The fabrication accuracy, capability of creating small features, number of steps required in the fabrication, the total time required for fabrication, cost of materials used in fabrication, and the mass production capability are normally the key considerations to adopt a technique for  $\mu$ PAD fabrication. As described in section 1.2.3, the forming and removing method of fabrications will be reviewed separately in this section.

The forming methods (e.g. wax patterning, inject printing) of  $\mu$ PAD fabrication are mainly about the different techniques to infuse hydrophobic substance (e.g. wax, hydrophobic ink, polymer etc.) into the porous paper materials according to the pattern of the  $\mu$ PAD. Historically, the use of wax to create the confined test zone on filter paper was first reported in 1937 [66]. After that, in 1949 a wax patterning technique was used to create a paper-based microfluidic device for analytical testing [67]. Nowadays, the wax patterning technique is one of the most popular techniques for  $\mu$ PAD fabrication [28, 55, 68–70] where a solid wax printer is often used to pattern the solid wax-ink on the paper layer followed by a heating process to infuse the molten wax into the paper [28], as shown in Figure 2.1(a). The resolution of the wax printer and also the wax infusion behaviour during the heating process affects the fabrication resolution [28]. Figure 2.1(b) shows how wax barrier laterally spreads inside the porous structure of the paper after heating and results in low resolution of the hy-

drophobic barrier. For example, a 500  $\mu\text{m}$  wide printed line of wax reportedly became approximately 1100  $\mu\text{m}$  [28], as shown in Figure 2.1(b). Such spreading behaviour of molten wax makes it challenging to fabricate a narrow and high-resolution hydrophilic barrier [28]. Another commonly used forming method is the photolithography technique where multiple steps are followed in a sequence to create patterned  $\mu\text{PADs}$  [39], as shown in Figure 2.1(c). The key concept of this technique is to soak the entire sheet of paper material in the photoresist and only the patterned path is exposed to UV light which cross-links the photoresist and forms the hydrophobic barrier, as shown in Figure 2.1(c). To date, many other forming methods of  $\mu\text{PAD}$  fabrication have been reported in the literature including screen printing [71, 72], patterning with permanent marker [73] or ink pen [74], plasma treatment [75], ink stamping [76, 77], inkjet printing [78, 79], inkjet etching [80], flexographic printing [81] and laser-based polymerization [82, 83]. A wide range of hydrophobic materials was used to create the hydrophobic barriers using different techniques. Each of the forming fabrication techniques has some advantages for specific fabrication requirements. However, the chemical methods of fabrication such as photolithography, require multiple steps in fabrication and may lead to a higher fabrication cost and slow production rate. Another concern is that the traces of chemicals used in the fabrication process and the hydrophobic substance used in the barrier may affect the analyte detection chemistry used in  $\mu\text{PADs}$ . In addition to that, some methods are complex in nature such as inkjet etching and some methods generally offer low fabrication resolution such as wax patterning, as described in the following section. Therefore, it is still challenging to adopt a forming method that will be rapid, inexpensive, capable of offering high



fabrication resolution and capable of mass production at the same time.

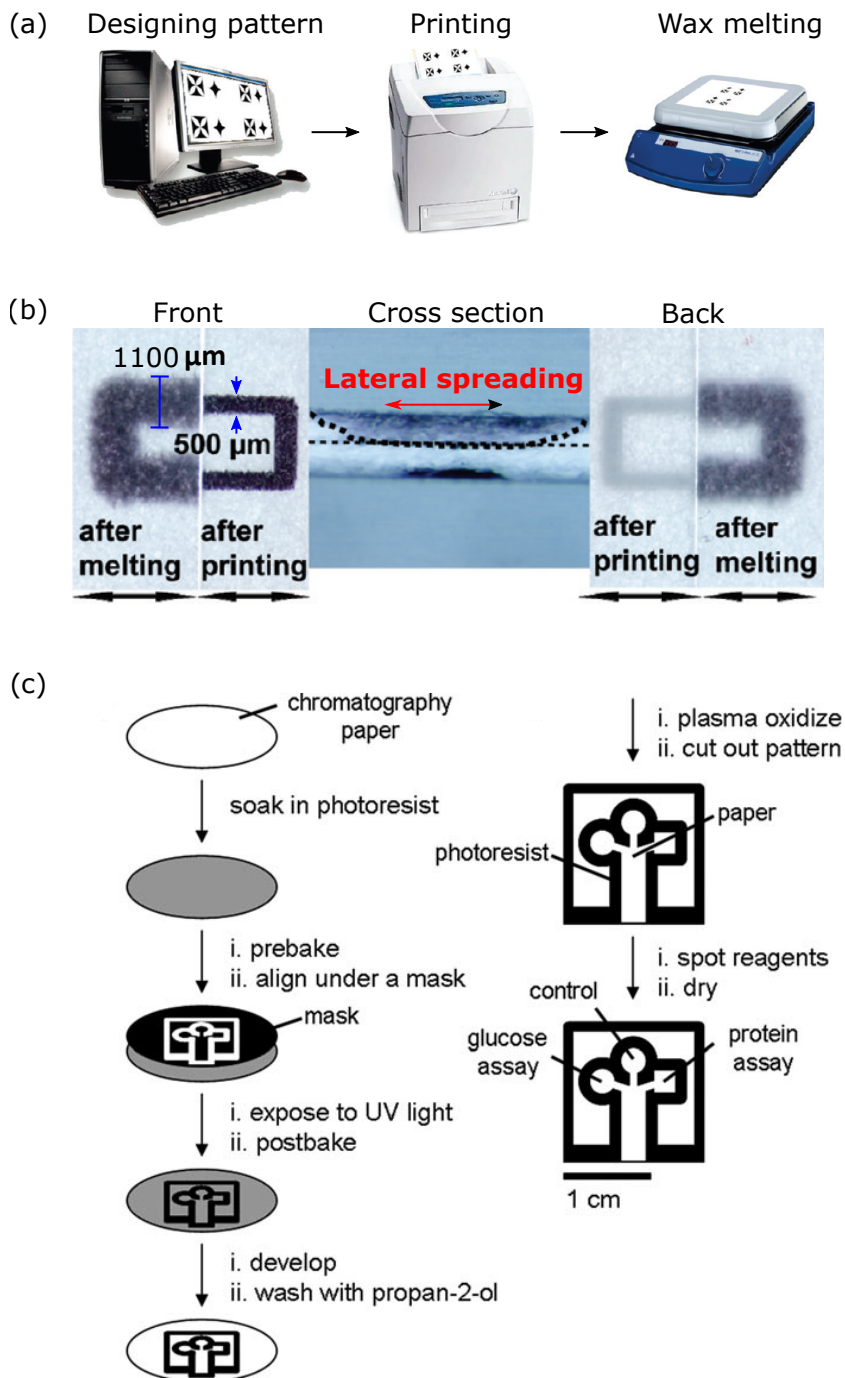


Figure 2.1: (a) Steps of wax printing technique for the fabrication of  $\mu$ PAD, adapted with permission from Ref. [28]; (b) wax spreading behaviour to make the hydrophobic barrier, adapted with permission from Ref. [28]; (c) multiple steps required in the photolithography technique. Reproduced with permission from Ref. [39].

In the removing methods (e.g. laser cutting), the paper material is removed according to the pattern of the  $\mu$ PAD and the resulting air gap or the discontinuity of porous structure acts as a hydrophobic barrier, as shown in Figure 2.2(a). Removing methods have been reported in the literature including the paper cutting and shaping technique [84, 85], laser etching technique [86] and laser cutting technique [87]. The laser cutting technique is very promising which exploits the precision of a laser beam to burn out the paper material from its cut-line that follows the pattern to create a precise and accurate hydrophobic barrier. In 2012, Nie et al. first reported the laser cutting technique for the microfluidically patterned  $\mu$ PAD where the laser beam burned the paper material along the cut-line following the pattern of the  $\mu$ PAD [87]. However, to hold the different features of the fabricated  $\mu$ PAD in place, some portions of the  $\mu$ PAD were left intact, as shown in Figure 2.2(a). Thus, the air gap or the hydrophobic barrier was not continuous which might led to the liquid leakage through the hydrophilic path of intact connections, as shown in Figure 2.2(a). In addition to that, since the paper layer did not have any support or backing, a thick paper sheet was used in the fabrication to provide enough strength to the  $\mu$ PAD. In 2013, Spicer-Mihalic et al. reported the laser etching technique to fabricate  $\mu$ PADs using polyester-backed nitrocellulose membrane, as shown in Figure 2.2(b). In this method, the careful laser power settings were used to remove nitrocellulose membrane following the pattern of the  $\mu$ PAD without cutting through the membrane backing, as shown in Figure 2.2(b). However, in this technique, an improper power setting can cut through the backing or engrave the backing which may create a secondary capillary flow path and make the  $\mu$ PAD weak. They also mentioned that the fabrication

technique was not suitable for high throughput mass production [86]. Therefore, the existing removing methods are promising as a rapid and inexpensive technique, but in terms of providing proper strength to the device and mass production capability, the methods are not suitable for the fabrication of inexpensive miniaturized  $\mu$ PADs.

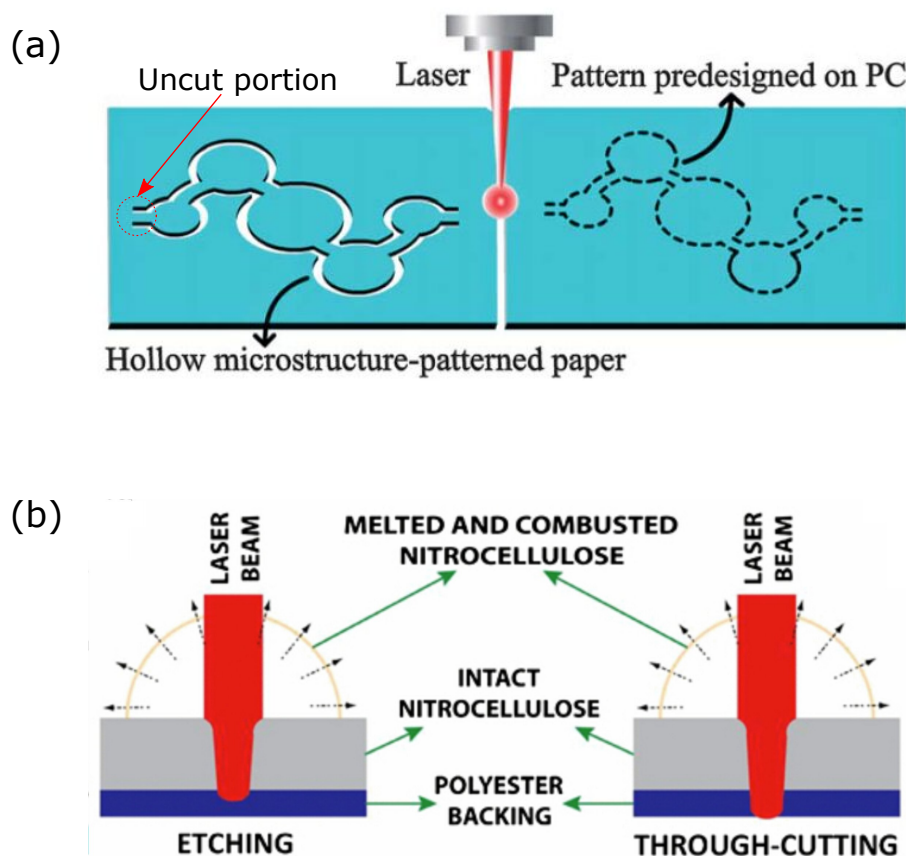


Figure 2.2: (a) A laser cutting fabrication technique without any backing where some portions of the paper-sheet is left intact to support the  $\mu$ PAD, reproduced with permission from Ref. [87]; and (b) a laser etching fabrication technique with the risk of through cutting because the backing is permeable to the laser beam, adapted with permission from Ref. [86].

## 2.2 Fabrication resolution and capability of small scale fabrication

The fabrication techniques reported in the literature offered a wide range of fabrication resolutions where the capability of creating small features was limited by the techniques and the paper materials used for fabrication. For example, in the cases where Whatman 1 Chr chromatography paper was used in the fabrication, the screen printing enabled fabrication of the channel widths of  $670 \pm 50 \mu\text{m}$  with the barrier widths of  $380 \pm 40 \mu\text{m}$  [72], the wax printing enabled fabrication of the channel widths of  $561 \pm 45 \mu\text{m}$  with the barrier widths of  $850 \pm 50 \mu\text{m}$  [28], the flexographic printing enabled fabrication of the channel widths of  $500 \pm 30 \mu\text{m}$  [81] and the fast lithographic activation of sheets (FLASH) method enabled fabrication of the channel widths of  $184 \pm 12 \mu\text{m}$  with the barrier widths of  $186 \pm 13 \mu\text{m}$  [88]. In the cases where nitrocellulose membrane was used in the fabrication, the laser etching enabled fabrication of the drawn line-to-line channel widths of  $150 \mu\text{m}$  with the barrier widths of  $85 \pm 5 \mu\text{m}$  [86], the wax printing enabled fabrication of the channel widths of  $100 \mu\text{m}$  with the barrier widths of  $86\text{--}118 \mu\text{m}$  [69], and the laser-based direct-write technique enabled the fabrication of an approximate channel widths of  $100 \mu\text{m}$  with a barrier width of  $60 \mu\text{m}$  [89]. The fast lithographic activation of sheets (FLASH) showed better ability to create the smallest feature using Whatman 1 Chr chromatography paper and in general, the nitrocellulose membrane enabled fabrication of relatively smaller feature than 1 Chr paper. However, the FLASH is a chemical fabrication method which requires multiple steps including, printing the hydrophobic material,

UV treatment, baking and finally developing the  $\mu$ PAD. Such a method may increase the fabrication cost and cause slow fabrication rate which is not favourable for the development of inexpensive  $\mu$ PADs. Therefore, with regards to the fabrication resolution, most of the existing fabrication techniques offer low fabrication resolutions and the methods that offer relatively better resolution, are time-consuming and require multiple steps in the fabrication of  $\mu$ PADs. In this context, a rapid and inexpensive technique with high fabrication resolution can have a significant contribution in the development of inexpensive miniaturized  $\mu$ PADs.

### **2.3 Characterization of capillary flow through paper channel**

In  $\mu$ PADs, the capillary flow through the hydrophilic paper features facilitates the analyte flow to the designated zone for the proper detection. The proper understanding of the capillary flow is crucial to design an effective  $\mu$ PAD that is capable of providing a consistent and accurate test result. A good number of works have been reported in the literature, where they investigated the capillary flow through hydrophilic fibrous matrix [90,91] of paper channels both experimentally and theoretically. Reportedly, the physical properties of paper materials (e.g. average pore size [92]), the dimension of the flow path (e.g. width of the flow path [52,53]), properties of flowing liquid (e.g. viscosity [92]) and surrounding environment [52,53] (e.g. temperature, relative humidity) influence the flow behaviour. For a certain operating condition, the capillary flow is mainly affected by the average pore size of the paper material [92] and the

width of the flow path [52, 53, 93]. In general, a larger pore size, less viscous flowing liquid, warmer surrounding and higher relative humidity of the surrounding air cause faster capillary flow and vice versa. However, the effect of channel width on the flow speed was not conclusive based on the research works reported in the literature.

A frequently used equation to describe the liquid flow through a paper channel is the Washburn equation [92], where the porous medium is approximated as a bundle of parallel cylindrical capillaries. The Washburn equation indicates that the distance travelled by the liquid front in time  $t$  is expressed by:

$$L(t) = \sqrt{\frac{rt\gamma\cos\theta}{2\mu}} \quad (2.1)$$

where  $L$  is the distance travelled,  $r$  is the average pore radius,  $\gamma$  is the surface tension of the flowing liquid,  $\theta$  is the contact angle between the capillary wall and the liquid, and  $\mu$  is the dynamic viscosity of the liquid. According to this equation, the distance travelled by the liquid front does not depend on the width of the paper channel. However, most of the experimental studies revealed that the flow through the paper channel does depend on the channel width [52, 53, 93] and in few cases Washburn flow was observed with insignificant effect of the channel width [68]. Figure 2.3(a) shows the flow characteristics through the 1 Chr chromatography paper channel of varying widths and an insignificant variation in capillary flow speeds were observed for different channel widths [68]. However, in these experiments, all three channels were within 1-2 mm of widths and thus the flow through a wide range of channel widths was not investigated. In another experimental study, the capillary flow characteristics through

the paper channels with 5-40 mm of widths made out of 1 Chr chromatography paper were investigated and it was found that the wider channels cause faster flow which does not follow the width-independent flow characteristics [52], as shown in Figure 2.3(b). In contrast to that, another experimental study of flow characteristics with 1-5 mm wide channels found that for the 2-5 mm wide channels the wider channels resulted in slower flow, but for the channels with under 2 mm of widths, the trend was opposite where narrower channels caused slower flow [93], as shown in Figure 2.3(c). Therefore, the different experimental investigations suggest that the capillary flow behaviour depends on the scale of the paper channels where the channels at a relatively larger scale may behave differently than the channels at a smaller scale.

In the miniaturization of  $\mu$ PADs, the width of the flow path is scaled down and therefore it is essential to know the characteristics of capillary flow through small scale channels. The findings of the experimental studies done on the the capillary flow through millimetre [51,53,54,68,90,93–95] and centimetre [52] scale paper channels are not sufficient to understand the flow characteristics of small-scale channels (including microscale) because it seems like the experimental conditions and varying range of channel widths correspond to different flow behaviours.

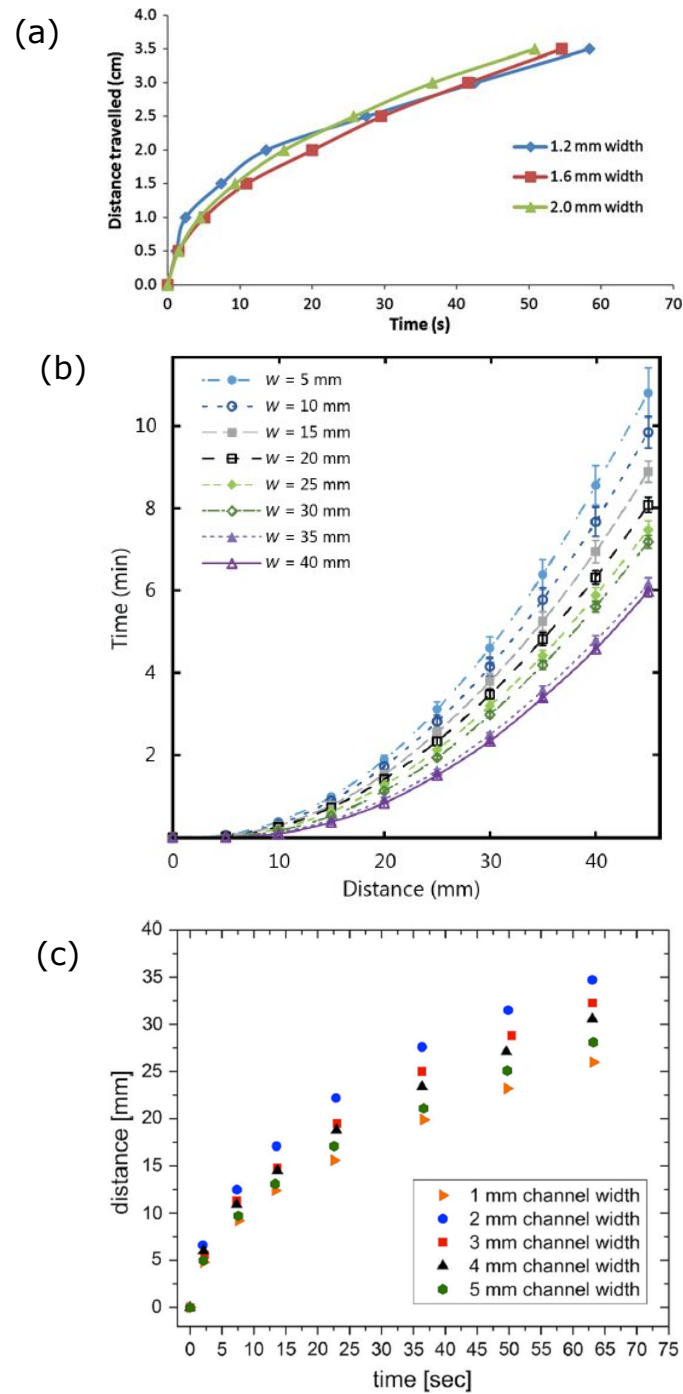


Figure 2.3: (a) Washburn flow characteristics where the flow speeds do not depend on the channel width, reproduced with permission from Ref. [68]; (b) Wider channel widths result faster flow, reproduced from Ref. [52]; and (c) Wider channel widths result slower flow after a certain the threshold, reproduced with permission from Ref. [93].



## 2.4 Quantification of test results

A simple, instrument free and user-friendly technique is required for the quantification of test results obtained from the  $\mu$ PADs. The detection signal alone is enough for the qualitative test result where the presence or absence of the target analyte is required, such as the commercially available pregnancy test strips. However, a semi-quantitative test readout technique is required for tests where the approximate concentration or concentration-range of the target analyte needs to be determined, such as a glucose level test. Different methods of obtaining semi-quantitative test results have been reported in the literature including intensity-based, distance-based and counting-based semi-quantitative techniques, but they all are not suitable for the inexpensive and user-friendly  $\mu$ PADs.

### 2.4.1 Intensity-based

The intensity-based quantification refers to a measurement technique where the intensity of the detection signal corresponds to the concentration of the analyte. The intensity of the colorimetric signal, fluorescence signal, chemiluminescence signal, and other similar detection signals can be used in the quantification test result. The intensity-based quantification of colorimetric detection is very common where the quantitative test result is obtained by correlating colour intensity to the concentration of the target analyte [12,96,97]. Figure 2.4(a) shows the  $\mu$ PAD developed for the glucose test where the intensity of the colorimetric detection successfully corresponded to the different concentration of glucose, as shown in Figure 2.4(b) [36].

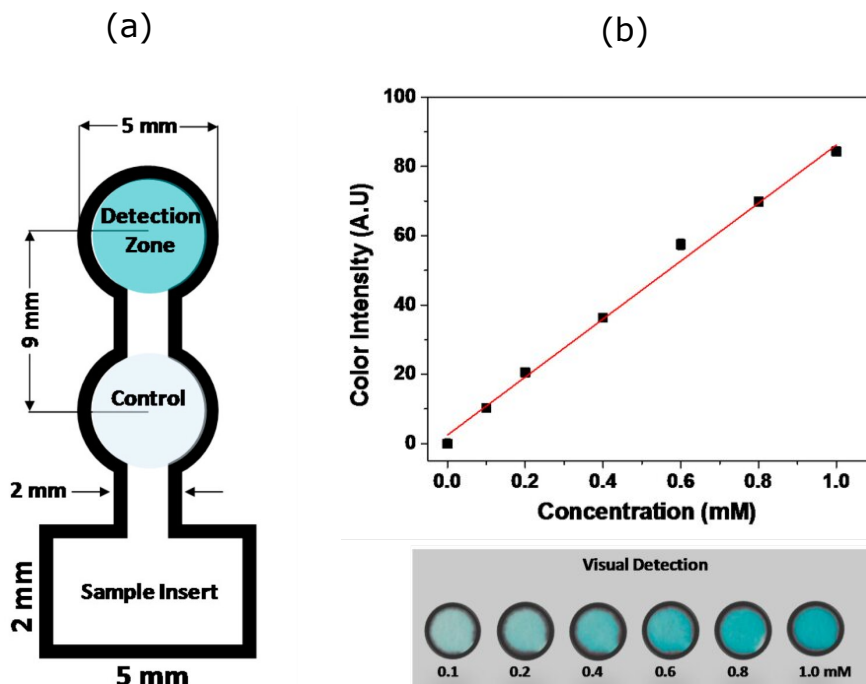


Figure 2.4: Intensity-based glucose test readout, reproduced with permission from Ref. [36]: (a) colorimetric detection of glucose and (b) correlation between the colour intensity and glucose concentration.

The intensity-based quantification of the colorimetric test result requires the use of external devices, such as a camera and image processing software. However, the visualization with naked eye can be an alternative to the intensity measurement where distinct intensities of colour or colour-change may provide semi-quantitative test results (a common test readout approach for the urine analysis using the dipsticks, as shown in figure 1.2(c)). However, based on the perception of the user, such interpretation of test result can be challenging [27] and may vary from person to person [56]. Thus, intensity-based quantification may hinder the simplicity of the test result interpretation needed for the user-friendliness and it may increase the likelihood of incorporating the user-error in the test result [56]. To eliminate the requirement of

intensity measurement, few other test readout techniques are reported in the literature that provide semi-quantitative test results, such as distance-based and counting-based test readouts.

### 2.4.2 Distance-based

The distance-based test readout technique refers a detection design of a  $\mu$ PAD where the length of the detection signal corresponds to the concentration of the analyte present in the sample, as shown in Figure 2.5(a). In this technique, a certain length of the sample flow path is designed as the detection zone and the detection reagents are immobilized along the detection zone. The detection reagent reacts with the target analyte present in the flowing sample and produces a coloured band of a certain length along the detection zone which correlates with the concentration of the analyte. Many distance-based test readout techniques were reported in the literature where different types of analytes were used in the tests [56,98–104]. Figure 2.5 (a) shows the distance-based test result for glucose level where the band of the dark brown coloured signal corresponds to the different concentration of glucose [101]. Reportedly, the distance-based detection was also accomplished with the fluorescence detection, as shown in Figure 2.5 (c) [103].

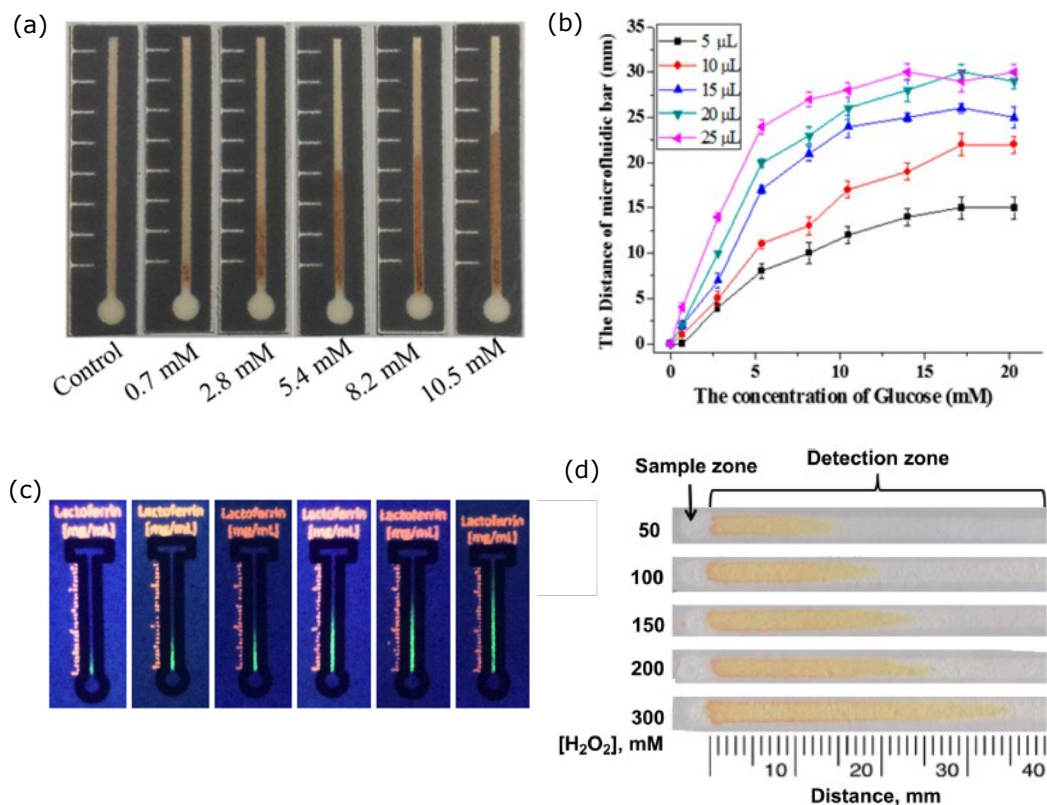


Figure 2.5: Different distance-based test read out techniques reported in the literature: (a) distance-based detection of glucose level, adapted with permission from Ref. [101]; (b) the effect of sample volume on the sensitivity of the distance-based test readout, adapted with permission from Ref. [101]; (c) the distance-based test readout developed for fluorescence detection, adapted with permission from Ref. [103]; and (d) distance-based detection of H<sub>2</sub>O<sub>2</sub> level, adapted with permission from Ref. [104].

The sample volume is crucial for the distance-based test readout. As shown in Figure 2.5 (b), the experiments on the distance-based glucose test revealed that a minimum volume of sample was required to get sensitive distance-based test device [101]. The plot shows that the relatively smaller sample volumes result in poor sensitivity in the device. Another aspect of the distance-based test readout is to properly identify the length of the coloured band. As shown in Figure 2.5 (d), the experimental study successfully developed distance-based test readout for H<sub>2</sub>O<sub>2</sub> detection on the  $\mu$ PAD

where different concentration of  $\text{H}_2\text{O}_2$  corresponded different lengths of the coloured detection band [104], but apparently it will be challenging to determine the end of the coloured band for such detection signal. Therefore, the distance-based test readout requires a relatively large volume of sample for better sensitivity and the chemistry should be selected in such a way that it is easy to identify the length of the coloured band. In addition to that, the requirement of larger sample volume may require a large amount of reagent to be immobilized on the entire length of the detection zone which will make the  $\mu\text{PAD}$  more expensive.

In a miniaturized  $\mu\text{PAD}$ , the sample volume used the test might be relatively small. Therefore, incorporating the distance-based test readout with the miniaturized  $\mu\text{PAD}$  can be challenging due to the required measurements of the small-scale coloured band obtained as the test result.

### 2.4.3 Counting-based

The counting-based test readout refers to a technique that enables obtaining a semi-quantitative test result by simply counting the number of coloured segments produced on the detection zone of a  $\mu\text{PAD}$ . The counting-based (also referred to as barcode-based) test readout method was successfully tested with LFA-type  $\mu\text{PAD}$ s [105–111] where multiple test lines or segments were spotted on the detection zone with the analyte-specific reagents along the sample flow path and the analyte concentrations

were determined by counting the number of coloured test lines or segments. In these works, the colorimetric detection by selective binding of the analyte was used as the test procedure (as shown in 2.6(a)) which is similar to the test procedure of common immunoassay as described in section 1.2.4. The coloured test lines were formed by different tracers such as gold nanoparticles (as shown in Figure 2.6(a-b)) or enzyme (as shown in Figure 2.6(c)) where the gold nano-particles naturally generated red coloured signal [105] and the enzyme needed a substrate to produce corresponding colour [107]. Figure 2.6(b-c) shows the counting-based test result reported by two separate experimental studies for different concentration of gliadin [105] and glucose [107] concentrations respectively. Relatively large volume of samples (25 to 120  $\mu\text{L}$ ) were used in these tests [105–111] because the devices were relatively large in size and a minimum sample volume is required to get successful counting-based test readout using a device [106]. Therefore, the reported works on the counting-based test readout suggest that the technique is promising for a user-friendly  $\mu\text{PADs}$  as it simply requires counting the number of coloured segments. However, the requirement of the larger sample volume needs to be addressed to adopt the counting-based test readout in the design of miniaturized counting-based  $\mu\text{PADs}$ .

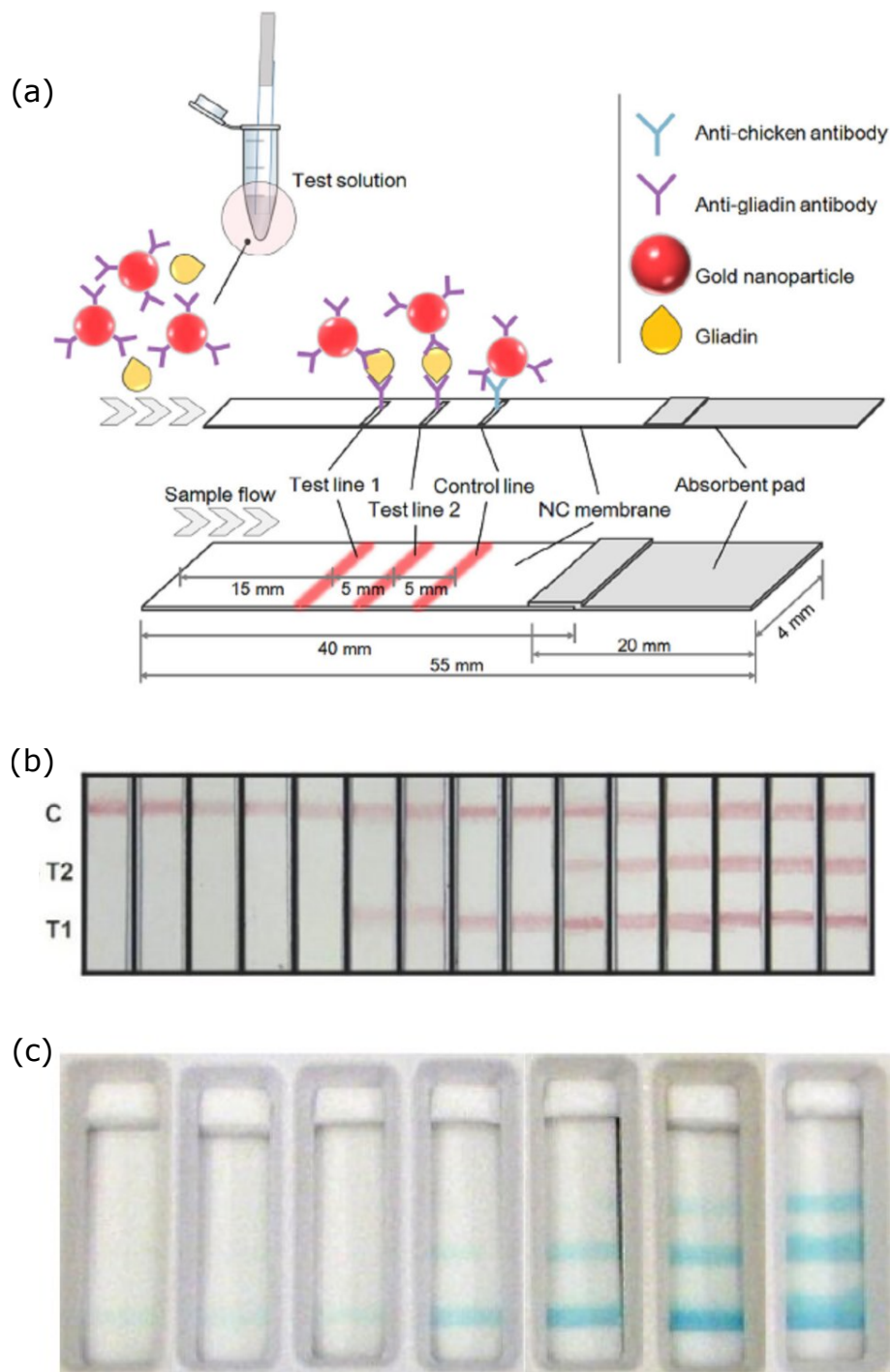


Figure 2.6: (a) An illustration of the counting-based test readout where the gold nano-particles were used in the sandwich type immunoassay as the tracer for the analyte, adapted with permission from Ref. [105]; (b) the counting-based test readout produced by the gold nano-particles, adapted with permission from Ref. [105]; and (c) the counting-based test readout produced by the enzyme and corresponding substrate, adapted with permission from Ref. [107].

## 2.5 Summary of the chapter and perspective of this thesis

In this chapter, the relevant literature was reviewed to find research needs for the development of user-friendly miniaturized  $\mu$ PADs and to provide a perspective for the research contributions reported in this thesis. Based on the research gaps present in the literature, the following goals have been set:

### 2.5.1 Fabrication

The literature review revealed that the different kinds of techniques were developed for the fabrication of  $\mu$ PADs but most of the forming methods offered a low fabrication resolution which will limit the miniaturization of  $\mu$ PAD. Some of the forming methods (such as FLASH or laser-based direct writing) offer relatively higher fabrication resolution but these techniques will increase the fabrication cost and they require multiple steps in fabrication which will result in slow production rate. The removing methods, particularly the laser cutting techniques, are promising because they enable rapid and single step fabrication. However, the existing laser cutting techniques experience challenges such as lack of support to the test device, low fabrication resolution, risk of cutting through the backing and inability of mass production.

To address the above mentioned issue, in the first phase of this study, a laser cutting fabrication technique was developed that offers high fabrication resolution, strong support to the final device, the capability the mass production of the  $\mu$ PAD and the fabrication of small scale features for miniaturized  $\mu$ PAD without the risk of



cutting through. The detailed fabrication technique is described in chapter 3 of this thesis. By harnessing the high fabrication resolution, a wide range of commercially available paper materials was used to create the smallest possible feature using the laser cutting technique to determine the physical limitation of paper materials in the miniaturization process.

### **2.5.2 Flow characterization**

In the literature, the characterization of capillary flow through millimetre scale and centimetre scale features were studied experimentally and the theoretical models were developed that could predict the experimental results. The experimental results obtained from different studies have some element of disagreement on the relation between the capillary flow and the channel width. In addition to that, the high-resolution fabrication technique enabled fabrication of microscale features for the miniaturization of  $\mu$ PAD and the flow through such small scale features were not studied in the literature. Therefore as part of this thesis, the flow speeds through the small scale features were investigated and compared with the previously reported works on the relatively larger scale features, the details of the study is described in chapter 4.

### **2.5.3 semi-quantitative test result**

Different types of test readout techniques were reported in the literature that are capable of providing semi-quantitative test results such as intensity-based, distance-based,

and counting-based test readout. The intensity-based test readout needs an external device to analyse the intensity of the signal which hinders the user-friendliness. The distance-based test readout is a good option but analysis of low sample volume and reading the distance measurement in the small length scale of a miniaturized  $\mu$ PAD can be challenging. The counting-based test readout is promising as a user-friendly technique for test result interpretation of a miniaturized  $\mu$ PAD because it does not involve any measurement in the process. Simple counting of the number of coloured segments is required for this kind of test readout which is intuitive in nature. However, the counting-based LFA-type  $\mu$ PADs as reported in the literature needed a relatively larger volume of the sample because of the larger device size. The conventional fabrication method used in LFA-type  $\mu$ PADs (as described in section 1.2.3) may have limited the miniaturization of the devices.

The counting-based colorimetric technique was expanded and adapted in the development of user-friendly miniaturized LFA-type  $\mu$ PADs as reported in chapter 5 of this thesis. Instead of the conventional fabrication technique, the LFA-type  $\mu$ PADs were patterned on foil-backed paper materials to produce the miniaturized devices. The challenges of developing counting-based test readout for the miniaturized device were addressed and the devices were successfully tested with medical diagnostic tests using sub-microliter volume samples. .

# Chapter 3

## Development of fabrication technique for $\mu$ PADs

A technique with high fabrication resolution is required for fabrication of compact and miniaturized  $\mu$ PAD. However, the existing fabrication techniques face challenges to meet the requirement of a simple, inexpensive and high-resolution fabrication for miniaturized  $\mu$ PAD, as described in section 2.1 and section 2.2. Based on this research need, a laser cutting technique was developed for the fabrication of small scale features with high resolution which are essential for creating user-friendly miniaturized  $\mu$ PADs. This fabrication technique is inexpensive, rapid, capable of mass production and offers the highest fabrication resolution as compared to the existing fabrication techniques.

The details of the fabrication technique and adjustment of the laser parameter for highest fabrication resolution is described in the first section of this chapter. The second section of this chapter describes the fabrication of compact and miniaturized  $\mu$ PADS using the newly developed fabrication technique. The capacity and efficacy of the miniaturized  $\mu$ PADS was demonstrated by a series of experiments. The third section of this chapter describes how the physical properties of different paper materials limit the miniaturization of  $\mu$ PADS. The narrowest hydrophilic paper channels that can be fabricated from different paper materials using the laser cutting fabrication technique were determined and these findings will help in the selection of paper materials for the future development of miniaturized  $\mu$ PADS.

### 3.1 Materials and chemicals

Five different types of paper that are commonly used for  $\mu$ PADS, were selected for the experiments: Whatman 1 Chr chromatography paper (1 Chr), Whatman 3MM Chr chromatography paper (3MM Chr), Whatman regenerated cellulose membrane 55 of 0.45  $\mu\text{m}$  pore size (RC-55) and Whatman filter paper grade 50 (FP-50) were purchased from VWR International (Mississauga, ON, Canada) and Amershan Protran 0.45 nitrocellulose membrane (NC) was purchased from Thermo Fisher Scientific (Mississauga, ON, Canada); all these types of paper are manufactured by GE health-care. A roll of positionable mounting adhesive film 568 by 3M<sup>TM</sup> (Maplewood, MN, USA) was purchased from Amazon.ca. Aluminum foil (Diamond-Reynolds Consumer Products Inc., thickness: 15  $\mu\text{m}$ ) and double-sided adhesive tape (Studio) were pur-

chased from a local retail store. Artificial urine sample with glucose (Water 98.89%, glucose 1%, Methaylparaben 0.1%, Alizarin Yellow 0.0035%, Thymol 0.0017%) were purchased from VWR International (Mississauga, Ontario, Canada). The red dye (Allura Red AC dye content 80%), deionized water, glucose oxidase (*aspergillus niger*), horseradish peroxidase (HRP) and potassium iodide were purchased from Sigma-Aldrich (Oakville, Ontario, Canada). Solutions were made using the deionized water. Allura Red dye solutions were prepared using distilled water and Allura Red dye. The coloured dyes used in the multiplexed testing were extracted from colour markers (felt-tip pens) manufactured by Studio.

## 3.2 Development of fabrication technique

### 3.2.1 Fabrication principle

In order to fabricate the compact and miniaturized  $\mu$ PADs, a laser cutting technique was developed that follows the principle of removing methods, as described in section 1.2.3. A 30 W laser cutter (Speedy 100, Trotec) and aluminium foil-backed sheets of paper material were used in the fabrication. The foundation for this fabrication technique is that a 30 W laser beam can cut through the paper layer (and adhesive layer) following the pattern of the  $\mu$ PAD, generating hydrophobic barriers where the material is removed, but leaves the foil layer intact because such laser cannot penetrate any metal layer as shown in the Figure 3.1. Thus, the fabrication technique eliminates the chance of cutting through the backing layer of the  $\mu$ PAD and provides

continuous support for the device. This technique offers high fabrication resolution and enables fabrication of small scale features for the user-friendly miniaturized  $\mu$ PAD with sufficient strength.

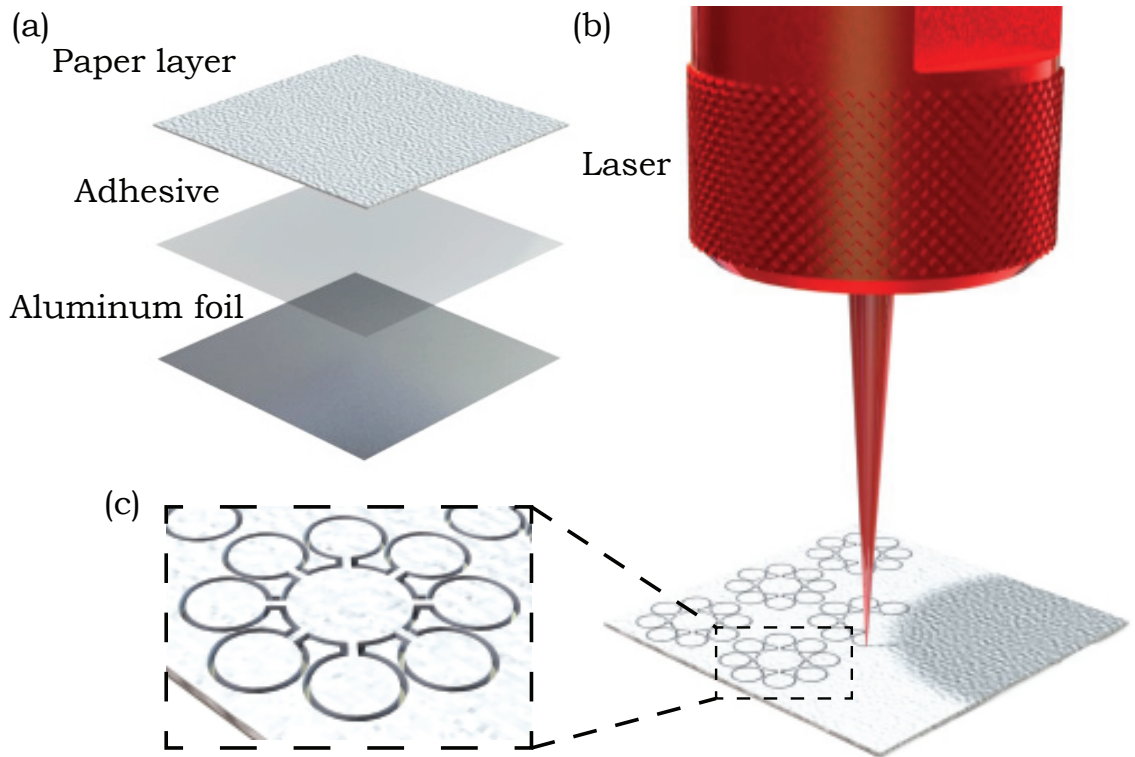


Figure 3.1: Schematic of the fabrication process for a  $\mu$ PAD with compact and microscale features, reproduced with permission from Ref. [112].

### 3.2.2 Fabrication procedure

The first part of the fabrication is to create the foil-backed sheet of the paper material by affixing a thin sheet of aluminium foil underneath the paper sheet. The layering procedure is shown in Figure 3.2 where the consecutive steps are shown by the arrows.

The first step is to layer the aluminium foil on an acrylic sheet to keep the foil

layer flat, as shown in 3.2(a). After that, an adhesive layer was created on the foil layer. Different types of adhesives including double-sided tape, glue and a positionable mounting adhesive film (3M<sup>TM</sup>) were found to be suitable for creating the adhesive layer but the use of positionable mounting adhesive film (3M<sup>TM</sup>) is a better option because it easily creates a uniform layer of adhesive. To use the adhesive film, it was placed on the foil layer and affixed on the foil layer using a squeegee (Figure 3.2(b-c)). The protective cover of the adhesive was peeled off and a uniform adhesive layer was formed on the foil layer (Figure 3.2(d-e)). After that, the sheet of paper material was placed on the adhesive layer and a squeegee was used to apply pressure on the paper layer so that it properly binds with the foil layer (Figure 3.2(f)). Finally, the unnecessary portion of foil was trimmed by a paper cutter (as shown in Figure 3.2(g)) and the foil-backed sheet of paper was ready for the fabrication of the  $\mu$ PADS.

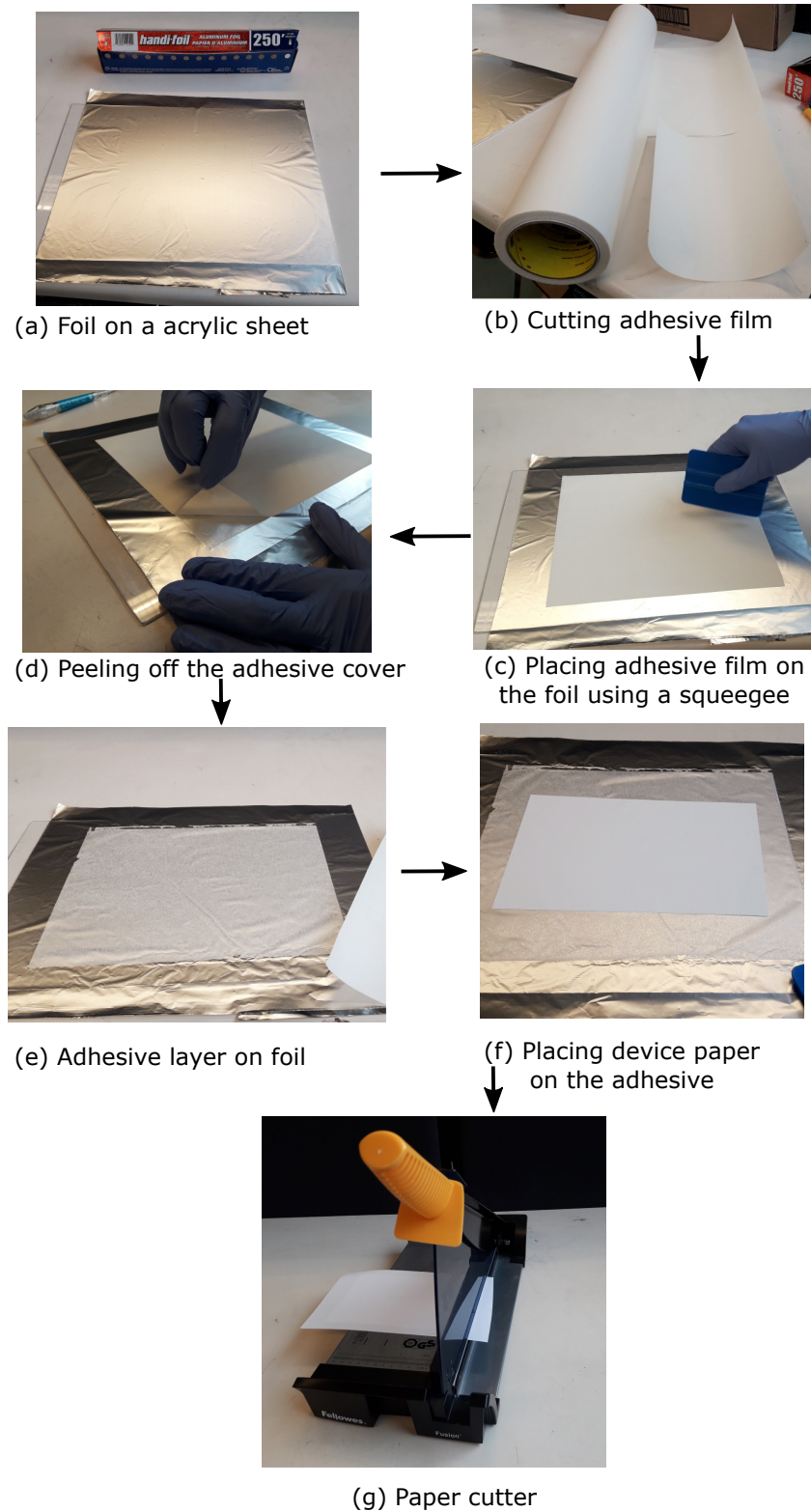
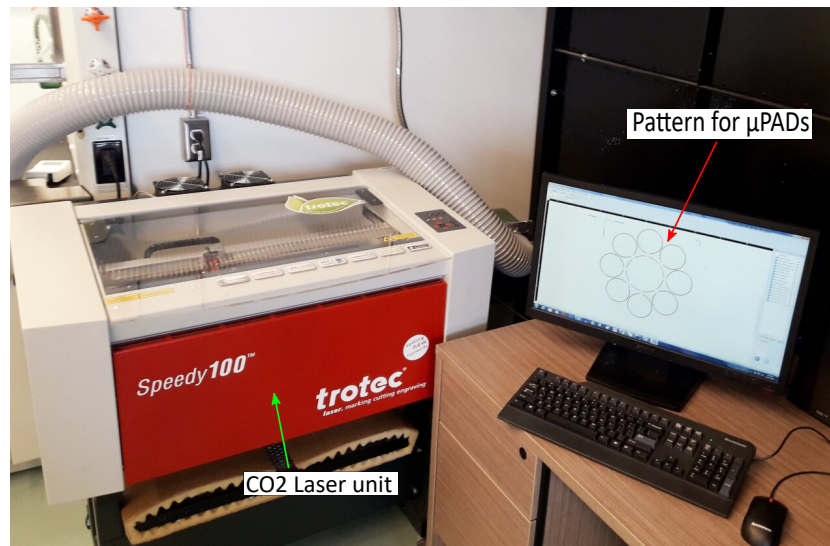


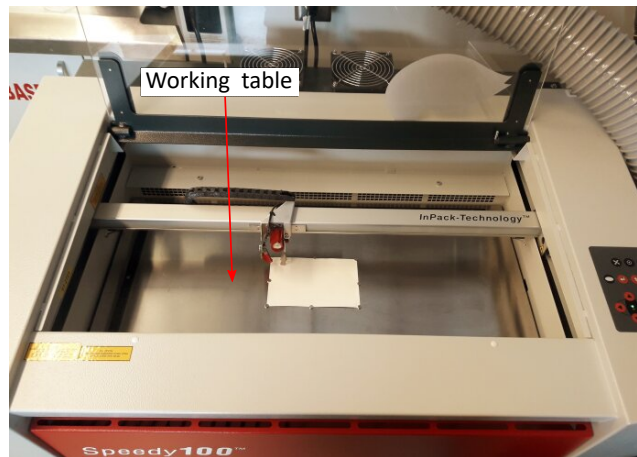
Figure 3.2: The different steps involved in the preparation of foil-backed sheet of a paper material.



The second part of the fabrication is to draw the pattern of the  $\mu$ PAD and fabricate the device accordingly. The pattern was drawn on a computer using 'InkScape software', as shown in Figure 3.3(a). The laser unit which is connected with the computer can take the instruction from the drawn pattern and the beam of the laser cutter follows a cut-line identical to the pattern by the help of the 'JobControl-Trotec software' that comes with the laser unit.



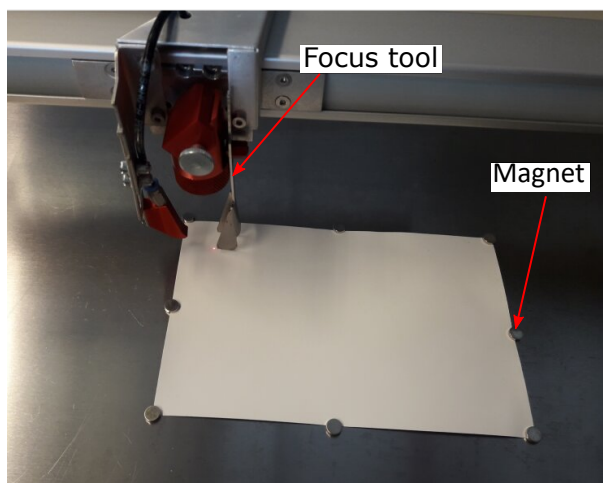
(a)



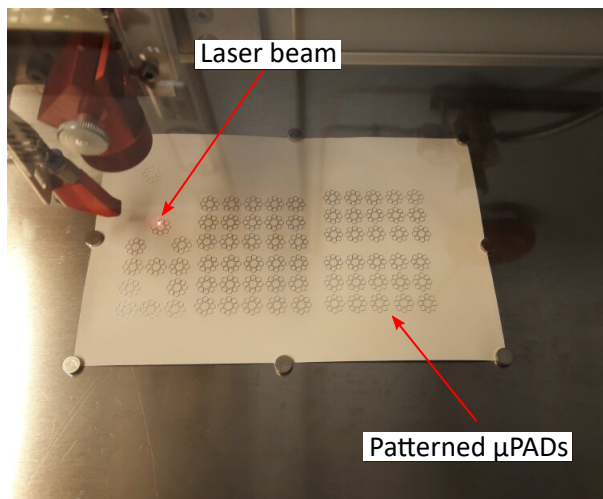
(b)

Figure 3.3: The laser unit is connected with a computer where the pattern is drawn [top] and the enclosed working table where the foil-backed sheet of paper material is placed for the fabrication [bottom].

During the fabrication, the foil-backed sheet of paper was placed on the working table of the laser unit (as shown in Figure 3.3(b) ) and the magnet pieces were used to secure the sheet on the table surface, as shown in Figure 3.4(a). After that, the height of the working table was adjusted to place the paper surface at the focal point of the laser beam using the focus tool provided with the laser unit, as shown in Figure 3.4(a).



(a) Focusing the laser



(b) Laser cutting

Figure 3.4: (a) Securing the sheet of paper with magnet and adjusting the working table height for focusing the laser; (b) the array of the  $\mu$ PADs have been fabricated by the laser.

Finally, the laser parameters (power, frequency and laser head speed) were selected for the cut-line and laser cutting was performed to fabricate the  $\mu$ PAD, as shown in Figure 3.4(b). Thus, the pattern becomes a  $\mu$ PAD on the sheet of foil backed paper material where different features of the devices are confined by hydrophobic barriers. A USB microscope (xcsOURCE, 20x-800x, 8 LED, 3D Digital Zoom Microscope) was used to inspect the hydrophobic barriers and the different features of the  $\mu$ PAD, as shown in Figure 3.5.

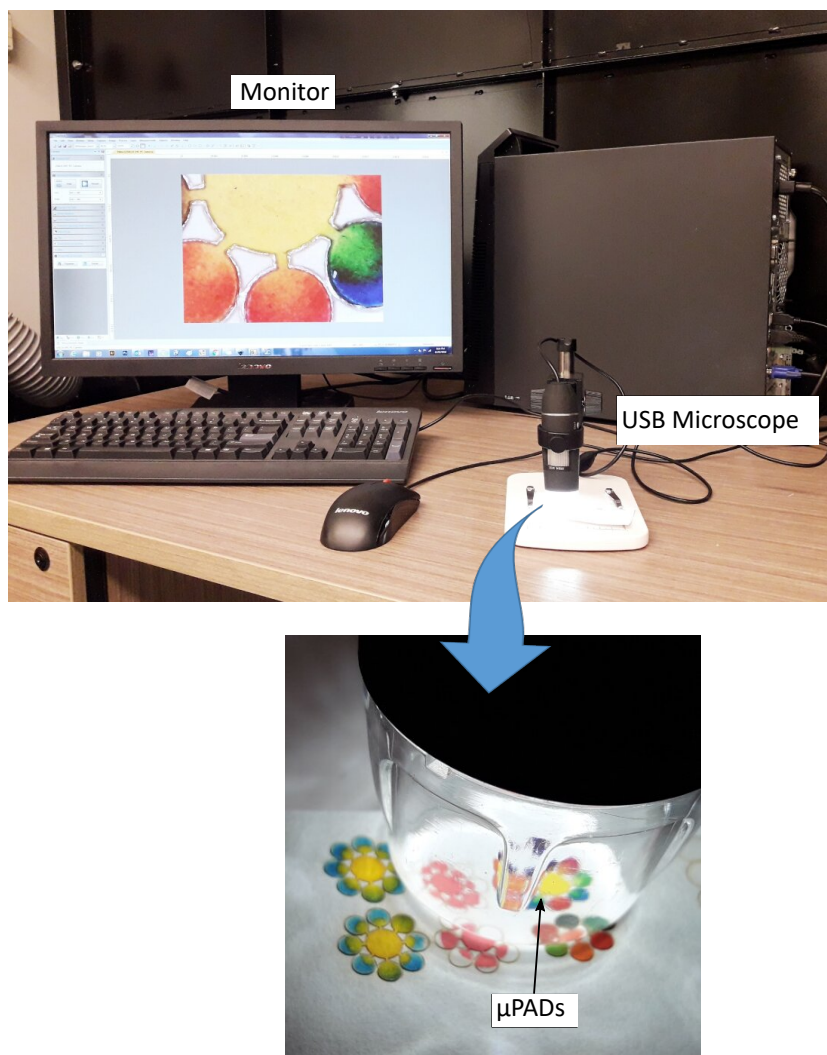


Figure 3.5: The inspection of the  $\mu$ PAD and its hydrophobic barriers using a USB microscope

### 3.2.3 Laser power and speed adjustment for optimum barrier width

The key concept of the laser cutting fabrication technique is to create the hydrophobic barrier which is identical to the pattern of the  $\mu$ PAD. An optimum hydrophobic barrier refers to the minimum value of its width that can successfully prevent the cross bleeding of the liquid confined by the barriers. A combination of the laser parameters (power, speed and frequency) controls the burning or removal rate of paper materials from the cut-line of the laser beam and hence it controls the resulting width of the barriers. The laser allows adjustment of its power at any percentage of the maximum power 30W, adjustment of its speed at any percentage of the maximum speed 80 cm/sec and adjustment of its frequency up to 10000Hz. A pattern consisting 9x8 array of the 3 mm diameter circles was used to determine the required combination of the laser parameters for the optimum hydrophilic barrier. A unique combination of speed and power was used to fabricate each circle of the pattern by keeping the frequency constant at 1000 Hz. The laser head speeds of 0.5% to 3% with increments of 0.25% and laser powers of 1 % to 8 % with increments of 1% were used in the unique power-speed combinations.

A sheet of Whatman 1 Chr chromatography paper (1 Chr) was affixed with a thin sheet of aluminium foil using double-sided tape and the layered sheet was used in the fabrication of the circular zones with unique power-speed combinations, as shown Figure 3.6. A 0.6  $\mu$ L of Allura red dye was pipetted in the centre of each circular zone to determine either the resulting hydrophobic barrier is capable of preventing cross barrier bleeding of the dye. The blue dash line shown in Figure 3.6 separates

the circular zones that successfully confined the dye and prevented from the cross bleeding (successful circular zones are the one under the dash blue line). The USB microscope was used to capture the images of successful circular zones which were analysed using ‘Toupview software’ to measure barrier widths of the circular zones, as shown in Figure 3.6.

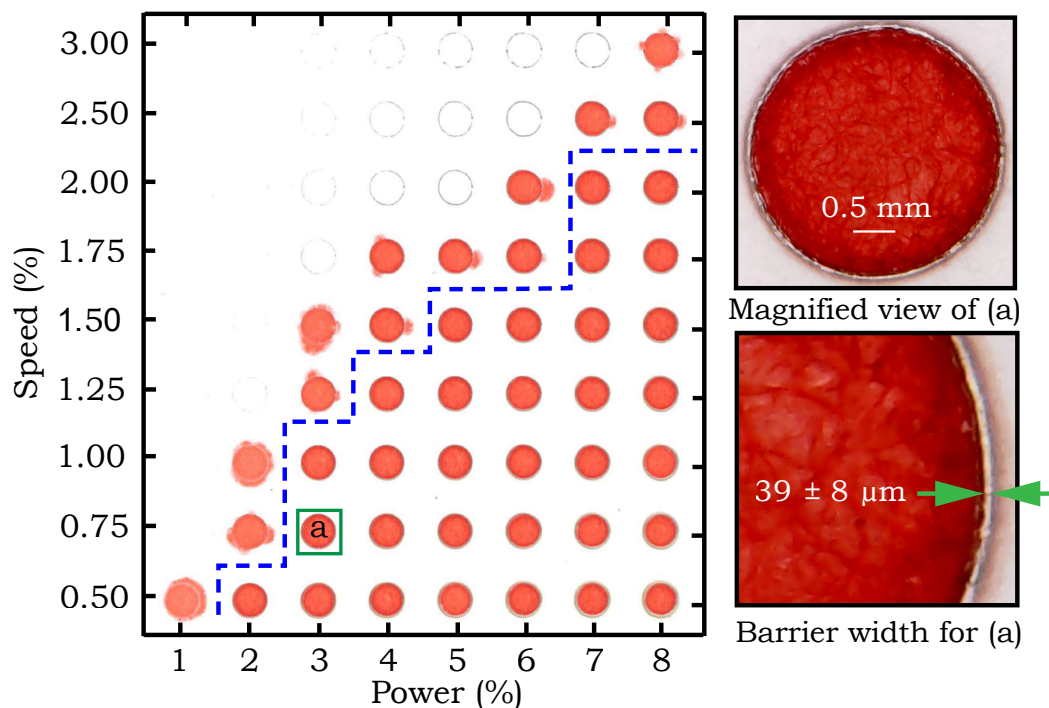


Figure 3.6: Circular features cut in foil backed paper and tested with red dye at different values of laser power and cutting head speed to find the minimum width of the hydrophobic barrier without cross-barrier bleeding, reproduced with permission from Ref. [112].

The barrier widths of the successful circular zones resulting from the different power-speed combinations are plotted in Figure 3.7. Width measurements were taken at five different locations along the barrier of a successful circular zone and the average of the measurements was used as the barrier width and one standard deviation

( $\pm\sigma$ ) of the measurements was used as the range. The error associated with the measurement procedure using the microscope was insignificant compared to the variation of barrier width around the circular shape, therefore one standard deviation ( $\pm\sigma$ ) of the width measurements was used as the range. Figure 3.7 shows that the combination of 3% laser power and 0.75% laser head speed creates the narrowest successful hydrophobic barrier width of  $39 \pm 8 \mu\text{m}$  on 1 Chr paper and this the narrowest hydrophobic barrier compared to those reported in the literature, as described in section 2.2. Figure 3.7 also confirms that slower speed values and high power values result in thicker barriers and vice versa. A wide range of laser power and speed combinations can be used depending on what size of the hydrophobic barrier is required for each application. A narrow and precise hydrophobic barrier will help in designing a compact and miniaturized  $\mu$ PAD because narrow barriers waste less area of the paper surface and allow the placement of multiple features of the device close to each other.

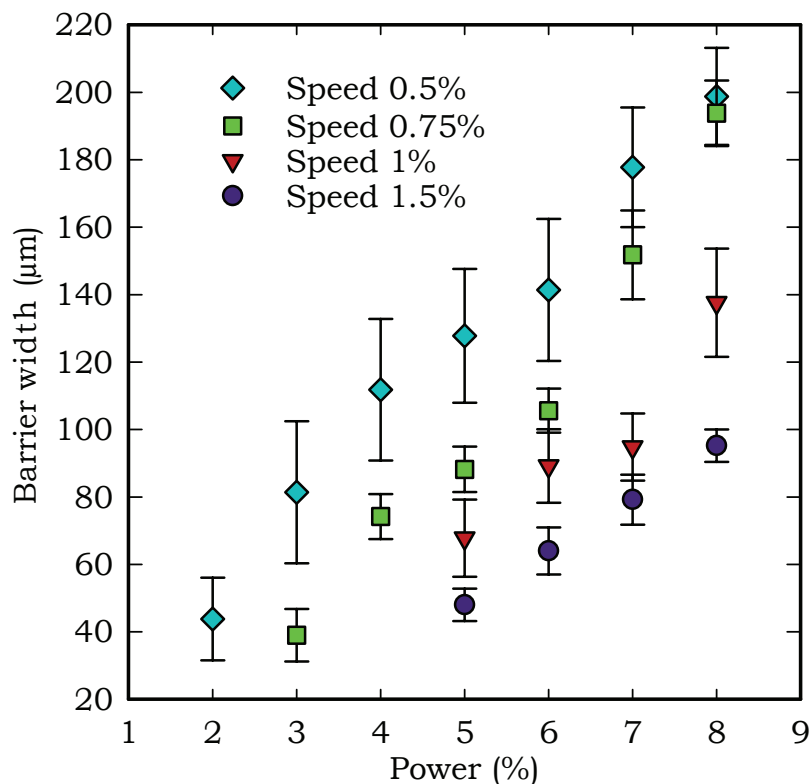


Figure 3.7: Plot of average hydrophobic barrier width for varying laser power at different laser head speeds, reproduced with permission from Ref. [112].

### 3.3 Fabrication of compact and miniaturized $\mu$ PAD

A compact and miniaturized  $\mu$ PAD was designed and fabricated on 1 Chr paper using the foil backed laser cutting technique and the device was used in a dye test and a glucose test to demonstrate the efficacy of the technique. The conceptual design was such that the device will be able to detect eight different analytes simultaneously using a small volume of sample (multiplexed testing). In the pattern, eight circular detection zones of 2 mm diameter were connected the central sample input zone of 3 mm diameter through the narrow channels of 280  $\mu$ m length and 300  $\mu$ m width, as

shown in Figure 3.8(a). The dimensions of the features in the final fabricated device were slightly smaller than the dimensions used in the pattern because the hydrophobic barrier reduces the feature size. The actual size of the miniaturized device is shown against the Canadian nickel coin in Figure 3.8(b). The glucose test and the dye test demonstrate how the miniaturization and compactness of the device enable the use of small sample and reagent volume in multiplexed diagnostic testing. This type of compact and miniaturized device can be used in the tests where selective binding of the analyte is not required, as described in section 1.2.4.

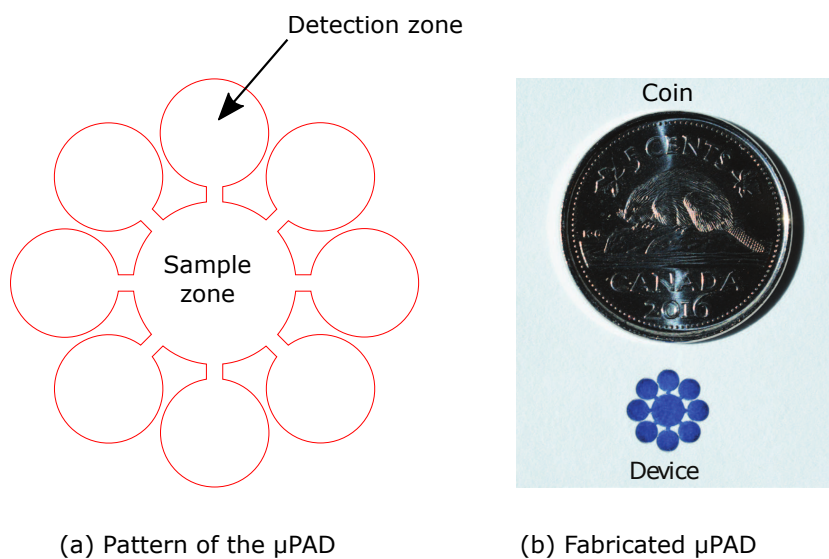


Figure 3.8: (a) The pattern of the compact  $\mu$ PAD with 8 detection zones, (b) The device with blue dye below a Canadian nickel (5 cent coin) to show the relative size, adapted with permission from Ref. [112].

### 3.3.1 Dye test

The dye test was performed using the compact and miniaturized  $\mu$ PAD to confirm proper sample flow to the surrounding detection zones and to get an understanding of sample volume and reagent volume required for the test. A sample volume of 2



$\mu$ L was found to be enough to reach the furthest end of the detection zones and a reagent volume of 0.2  $\mu$ L was found to be sufficient to spot each of the detection zones. For the dye test, a 0.2  $\mu$ L of aqueous dye solution of each of eight different colours (clockwise: green, orange, light blue, pink, blue, red, light green, and brown) were spotted in the detection zones where each colour represents the reagent for a certain analyte, as shown in Figure 3.9(a)[the images were captured using a DSLR Camera (Nikon D5200 with Nikon Af-s Dx Micro 40mm F2.8G lens)]. As a sample, a 2  $\mu$ L of yellow dye solution was placed in the centre zone which flowed to the detection zones to facilitate the interaction between the analytes and the detection reagents. The changes of colour to the dyes spotted at the detection zones in contact with the yellow sample visually confirms the sample-reagent interaction, as shown in Figure 3.9(b).

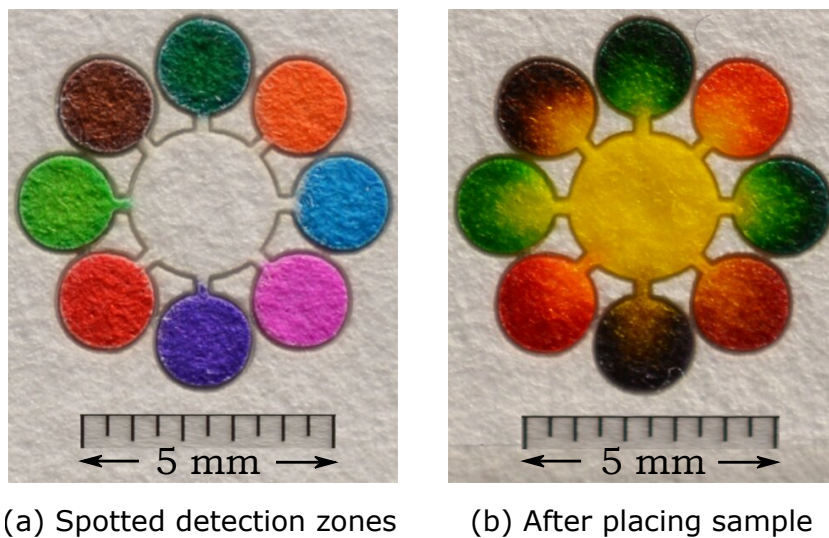


Figure 3.9: (a) Test device spotted with 8 different dye colours, and (b) after 2  $\mu$ L of yellow dye was added, adapted with permission from Ref. [112].

### 3.3.2 Glucose test

In order to demonstrate the efficacy of the compact and miniaturized  $\mu$ PAD in the diagnostic test, the glucose test was performed at all the eight detection zones using only 2 L of artificial urine sample. Each of the eight detection zones was spotted with 0.2  $\mu$ L of glucose detection reagents and allowed to dry at room temperature, as shown in Figure 3.10(a). The detection reagent included 0.1  $\mu$ L of 0.6M potassium iodide and 0.1  $\mu$ L of glucose oxidase-horseradish peroxidase solution (120 units/mL of glucose oxidase and 30 units/mL of horseradish peroxidase) prepared with distilled water (commonly used reagent for glucose test [96]). A 2  $\mu$ L of artificial urine sample was placed in the sample input zone which reached to the eight detection zones and changed their colour from clear to dark brown and thus indicated the presence of glucose in the sample, as shown in Figure 3.10(b) (the image was captured after approximately five minutes). At the detection zones, glucose is converted to gluconic acid and hydrogen peroxide by glucose oxidase. Subsequently the hydrogen peroxide reacts with potassium iodide in the presence of horseradish peroxidase and produces brown coloured potassium iodate. The eight detection zones could contain different reagents in practice for a variety of tests, but all of them were spotted with glucose assay just to prove the concept. This test demonstrates the successful use of the compact and miniaturized  $\mu$ PAD for multiplexed diagnostic testing using only 2 L of sample.

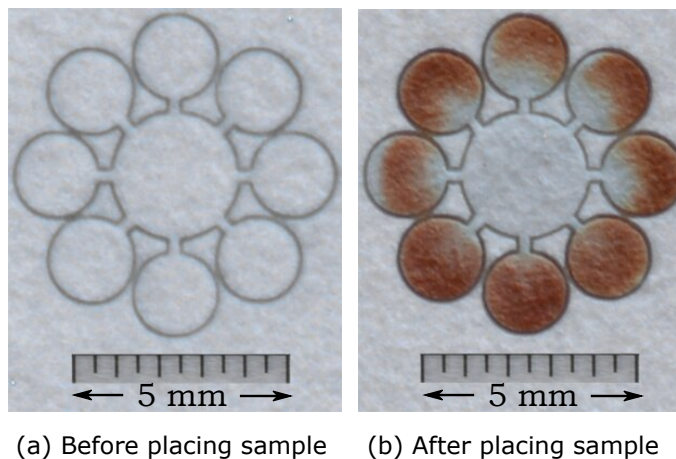


Figure 3.10: (a) The test device for glucose test with reagents in 8 readout zones, and (b) image taken 5 minutes after sample placement, showing successful glucose test using 2  $\mu$ L of artificial urine sample where dark brown colour indicates the presence of glucose, adapted with permission from Ref. [112].

This kind of colorimetric detection provides a rapid qualitative test result which only indicates the presence of the analyte (glucose) in the sample. However, the intensity of the dark brown colour can be measured and the intensity value could provide the semi-quantitative value of the glucose concentration, as described in section 2.4. However, in this study, the goal is to develop a semi-quantitative test readout technique without intensity measurement to make the test readout more user-friendly, which has been described in Chapter 5.

The sizes of the detection zones and the sample input zone used in the above described miniaturized  $\mu$ PAD (as shown in Figure 3.8(a)) could be further miniaturized as the foil-backing technique allows the fabrication of much smaller features. However, the feature sizes of the  $\mu$ PAD were chosen considering the manual pipetting of the detection reagent, visual test result interpretation with a naked eye and easy sample input. Therefore, depending on the application, target user, and test readout

technique, the  $\mu$ PADs can be miniaturized to varies degree to perform multiplexed testing.

### 3.3.3 Cost analysis

The cost of a miniaturized  $\mu$ PAD used in glucose test was estimated to provide an idea about the manufacturing cost. Based on the retail purchase, per unit square feet of 1 Chr chromatography paper was 1.2 USD, adhesive layer was 0.1 USD (for glue) and the aluminium foil was 0.01 USD which leads to a total cost of 1.31 USD per square feet of the layered paper. The miniaturized  $\mu$ PAD used in the glucose test will easily fit within a  $1 \text{ cm}^2$  area, therefore a total of about 930 devices can be manufactured from each square feet of layered paper which leads to a material cost of 0.0014 USD per unit  $\mu$ PAD. With regard to the reagent cost, cost of 0.6M potassium iodide was 0.00004 USD/ $\mu$ L, horseradish peroxidase was 0.00045 USD/ $\mu$ L and glucose oxidase costs 0.0004 USD/ $\mu$ L which leads to a total chemical cost of 0.0003 USD (approximately) per unit  $\mu$ PAD. Therefore, for the glucose test a total of 0.0016 USD (material cost and chemical cost) costs per unit  $\mu$ PAD. This cost estimation indicates that the manufacturing cost of a miniaturized  $\mu$ PAD can be very low for a test like glucose level detection. The raw materials and the chemicals required for the  $\mu$ PAD are available everywhere and bulk purchasing of the materials and chemicals, and large scale mass production will yield even lower costs for the miniaturized  $\mu$ PADs.

### 3.3.4 Mass production of $\mu$ PAD

The foil backed laser cutting technique is a rapid, inexpensive and one step fabrication technique which will also be suitable for the mass production of the miniaturized  $\mu$ PADs. In addition to the miniaturization of  $\mu$ PADs, if they are also fabricated through a mass production process then the  $\mu$ PADs will ultimately become inexpensive. Illustration of a potential mass fabrication system is shown in Figure 3.11 where the entire production system can be divided in three main processes: (i) creating the foil backed paper sheet, (ii) patterning or cutting the  $\mu$ PAD with laser and (iii) cutting each unit of final  $\mu$ PAD. However, if the deposition of the detection reagents are also done using an automated system then that process can be placed right after the laser cutting process. The foil backing process will involve the feeding of foil and paper materials from the respective rolls and the introduction of the adhesive layer on the foil sheet can be done by spraying the adhesive or using a previously made roll of adhesive film. When the foil backed sheet of paper material passes over the working table of the laser, the laser beam will rapidly pattern an array of the devices on the entire bed and send it to the next process. The patterned  $\mu$ PADs on the sheet of foil backed paper will proceed to the next step for the reagent deposition and the final device cutting processes. Complicated process design is not required for such production and hence the mass production of inexpensive, user-friendly and miniaturized  $\mu$ PADs will require minimum infrastructures.

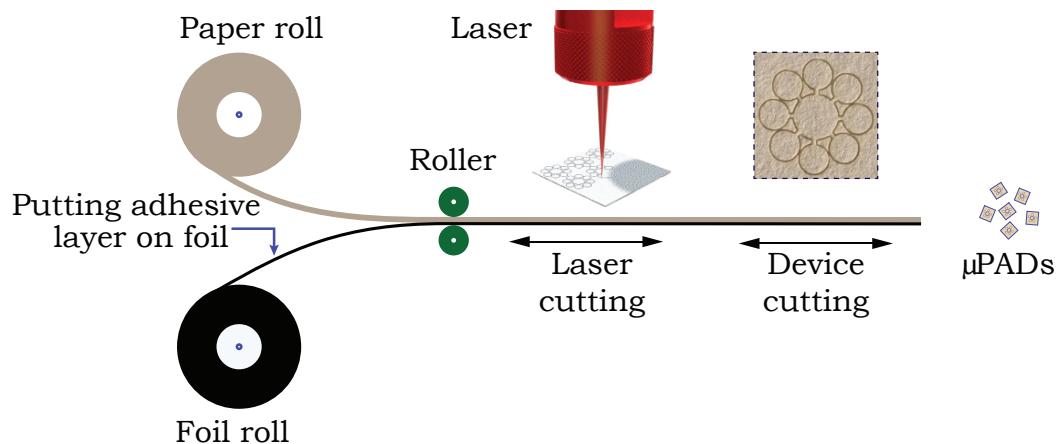


Figure 3.11: Schematic of a possible manufacturing line for mass production of  $\mu$ PADs, reproduced with permission from Ref. [112].

### 3.4 Smallest features fabricated out of different paper materials

To design and fabricate the miniaturized  $\mu$ PAD, it is essential to know the smallest feature size that can be fabricated using a certain paper material. However, the smallest feature of  $\mu$ PAD still has to be capable of fluid flow by maintaining a hydrophilic capillary flow path made of a minimum number of fibre. To address this aspect, five different commercially available paper materials of different physical properties were used to determine the smallest hydrophilic features with the capability of fluid flow that can be fabricated using these paper materials: (i) Whatman 3MM Chr chromatography paper (3MM Chr) , (ii) Whatman 1 Chr chromatography paper (1 Chr) , (iii) Whatman filter paper grade 50 (FP-50) , (iv) Whatman regenerated cellulose membrane 55 (RC-55) , and (v) Amershan Protran 0.45 nitrocellulose membrane (NC).

Since some of the paper materials were very delicate, therefore the preparation method of foil backed paper sheet was improved for this part of the experiments, as shown in Figure 3.12(a). A positionable mounting adhesive film (3M<sup>TM</sup>) was sandwiched between the sheets of paper material and foil, instead of the double sided tape and a cold roller machine was used to provide a uniform pressure in the bonding process. The rolling process eliminates the chance of trapping air between the layers and ensure strong foil backing to the paper materials, as shown in Figure 3.12(a). To determine the smallest feature, dumbbell-shaped  $\mu$ PADs were fabricated using each of the paper materials where the 1 mm long paper channels of varying widths connect two reservoirs at two sides, as shown in Figure 3.12(b). The experimental procedure was structured in a way that, the connecting channel will be fabricated with gradually smaller widths to determine the narrowest channel that allows fluid to flow from one reservoir to another, as shown in Figure 3.12(b). Thus, the width of the narrowest channel that allow fluid flow was considered as the smallest feature size with the capability of fluid flow that can be fabricated from that particular paper material. For each paper type, the three sets of dumbbell-shaped  $\mu$ PADs were fabricated where each set contained seven devices with different channel widths: the line-to-line design widths of 120  $\mu\text{m}$  to 240  $\mu\text{m}$  with an interval of 20  $\mu\text{m}$ , as shown in Figure 3.13. The actual widths of the channels that result on the paper material after cutting by the laser are smaller than the line-to-line design widths due to the width of the laser beam cut, and these actual resulting widths were reported and investigated in the analysis.

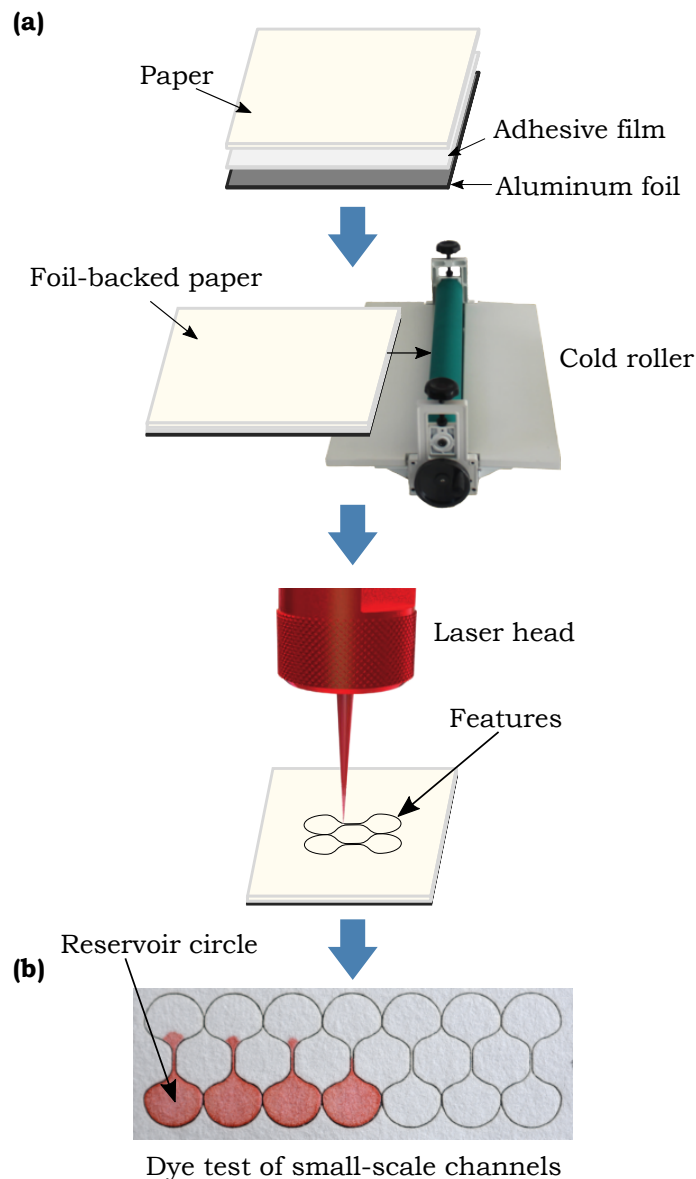


Figure 3.12: (a) Schematic of the fabrication technique used to generate small-scale features in the different paper types. (b) Overhead view of a dye flow test with the fabricated small-scale channels, adapted from Ref. [113].

During the experiments, to determine the successful channels that allow fluid flow, a cotton rod saturated with dye solution (0.5 g/L Allura Red) was brought in contact with the reservoirs at one side to see if the liquid flows to the reservoirs at another side, as shown in Figure 3.12(b). The narrowest channel that allowed the red dye to



flow from one reservoir to another, was measured and recorded as the smallest feature that can be fabricated from the respective paper material using the foil backed laser cutting technique, as shown in Figure 3.13.

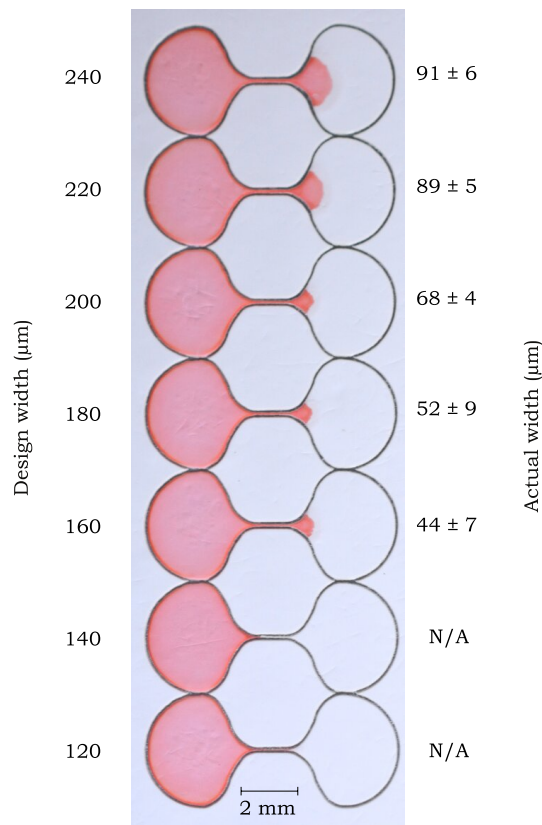
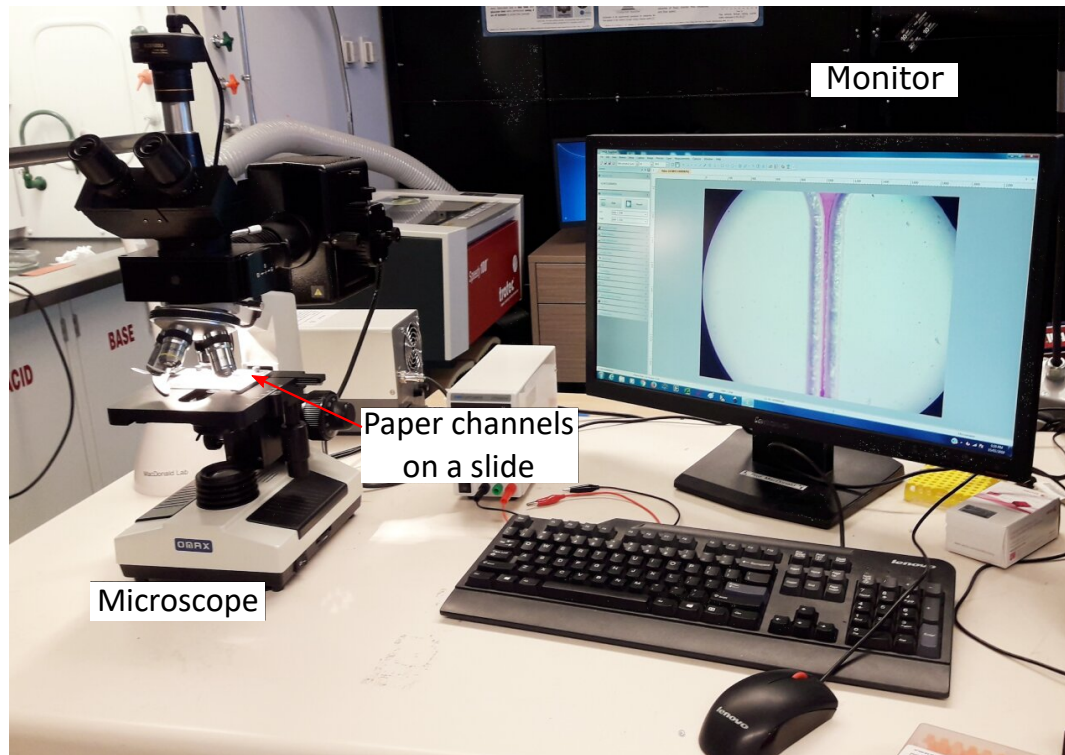


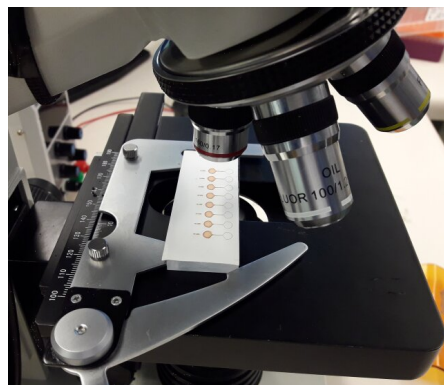
Figure 3.13: Testing small-scale channels of different width with a dye solution to determine the smallest channel width that can be fabricated from a particular paper type. One of the three sets of channels fabricated from RC-55 are shown in the figure. The actual width is listed as N/A for cases where the channel failed to provide a continuous flow path and so no successful width could be listed, adapted from Ref. [113].

The actual widths of the narrowest successful channels fabricated from five paper materials, were measured using a microscope (OMAX 40X-1600X professional EPI-fluorescence trinocular biological microscope with 10MP USB digital Camera, sold by MicroscopeNet Canada, Kitchener, ON, Canada, Amazon.ca) (as shown in Figure

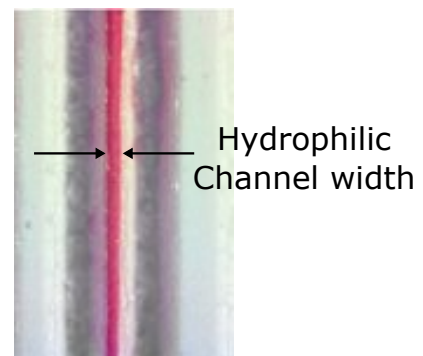
3.14) and the results are shown in Table 3.1. For each paper material, three smallest channels were determined by three sets of experiments and the actual widths of the three narrowest successful channels were measured. The width measurements were taken at 20 points over each of the three 1 mm long narrowest channel and hence a total of 60 measurements were recorded where the average of the measurements was recorded as the width of the narrowest successful channel and one standard deviation ( $\pm\sigma$ ) of that measurements was used as the range. The error associated with the measurement procedure using the microscope was insignificant compared to the variation of channel width along the length, therefore one standard deviation ( $\pm\sigma$ ) of the width measurements was used as the range. To investigate either the fabrication of the smallest feature is limited to the foil backed laser cutting technique or it is independent of foil backing, the smallest feature was also determined using 1 Chr paper without foil backing or adhesive layer.



(a) Microscope for channel width measurement



(b) Paper channels on the slide



(c) Dye flow

Figure 3.14: Measurement of successful channel widths using the microscope.

Table 3.1: Smallest channel widths for successful fluid flow for five different commercially available paper types using the foil-backed (all paper types) and non-foil-backed (1 Chr only) technique, reproduced from Ref. [113].

Paper Type	Smallest Channel Width ( $\mu\text{m}$ )
FP-50	$139 \pm 8$
3MM Chr	$130 \pm 11$
1 Chr (w/o foil)	$106 \pm 11$
1 Chr	$103 \pm 12$
RC-55	$45 \pm 6$
NC	$24 \pm 3$

Table 3.1 shows that, the cellulose papers: 1 Chr, 3MM Chr, and FP-50 offer relatively larger narrowest features (over  $100 \mu\text{m}$ ) where FP-50 enable creating the smallest feature of  $139 \pm 8 \mu\text{m}$  which is the widest among all the smallest features that can be fabricated from five different paper materials. The regenerated cellulose paper RC-55 and the nitrocellulose paper NC, offer relatively smaller narrowest features where the NC enables the fabrication of  $24 \pm 3 \mu\text{m}$  feature which is the smallest feature of a  $\mu$ PAD ever reported in the literature [69, 86, 89]. Table 3.1 shows the miniaturization limit for different paper materials and it is important to investigate the dominant physical parameter of the paper materials that allow different paper materials to create the smallest hydrophilic features to a different degree.

### 3.4.1 Influence of fibre width on the miniaturization

The previous section explained how the paper materials with varying physical properties set a different limit on the miniaturization where the smallest hydrophilic feature sizes that can be fabricated are different for different paper materials. Different physical parameters of the paper materials were compared with the data of Table 3.1 to determine the dominant physical parameter of a paper material that influences the smallest feature size. A correlation was found between the fibre widths and respective smallest feature sizes of the paper materials. The average fibre width of a paper material was measured using its scanning electron microscope (SEM) images, as shown in Figure 3.15. For each paper material, three SEM images taken at three different locations of paper surface were used for the fibre width measurements. The fibre width was measured at 50 spots of each of three images and the average of the 150 measurements were used as the fibre width and one standard deviation ( $\pm\sigma$ ) of measurements was used as the range. The error associated with the measurement procedure using the microscope was insignificant compared to the variation of fibre width along its length, therefore one standard deviation ( $\pm\sigma$ ) of the width measurements was used as the range.

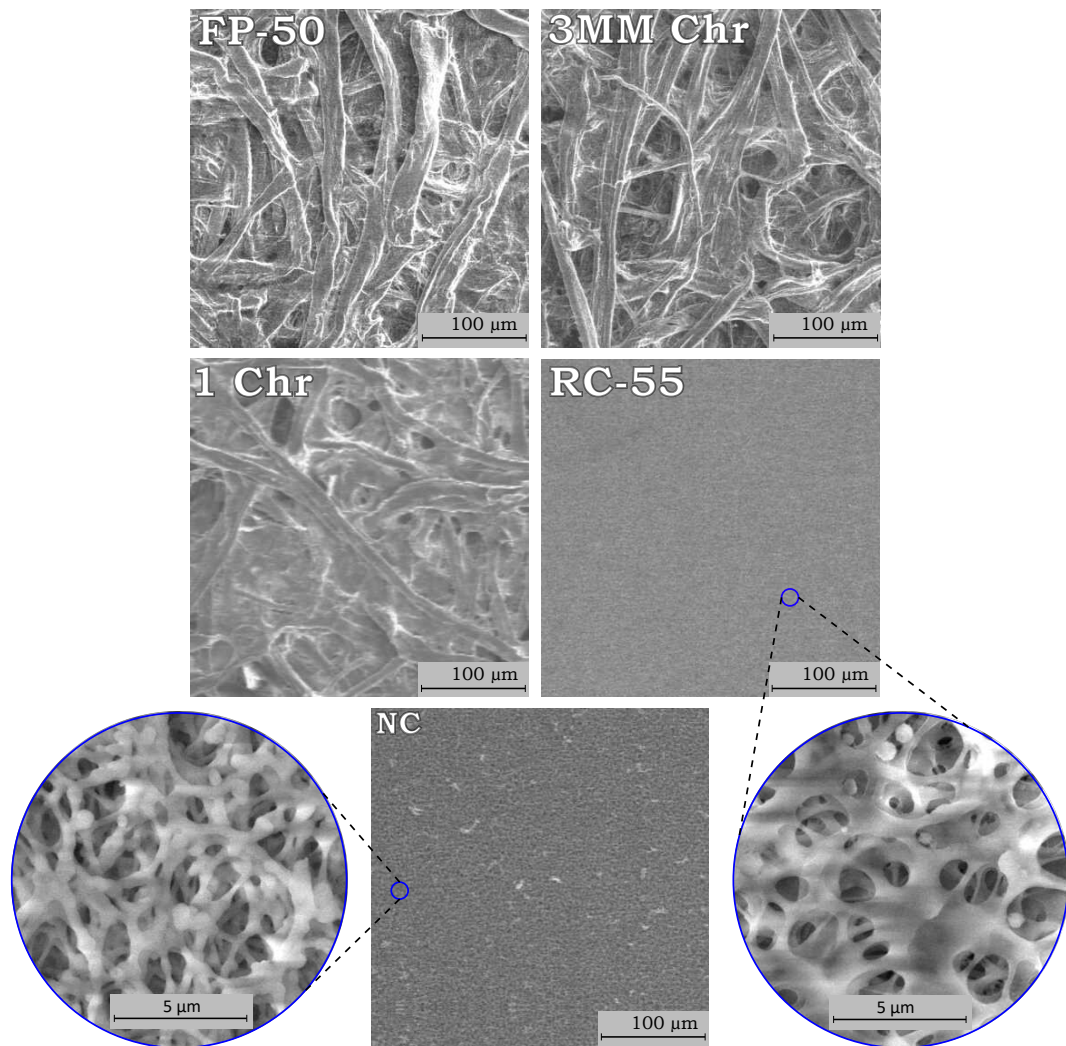


Figure 3.15: Scanning electron microscope (SEM) images of the fibre structure for the different paper types, reproduced from Ref. [113].

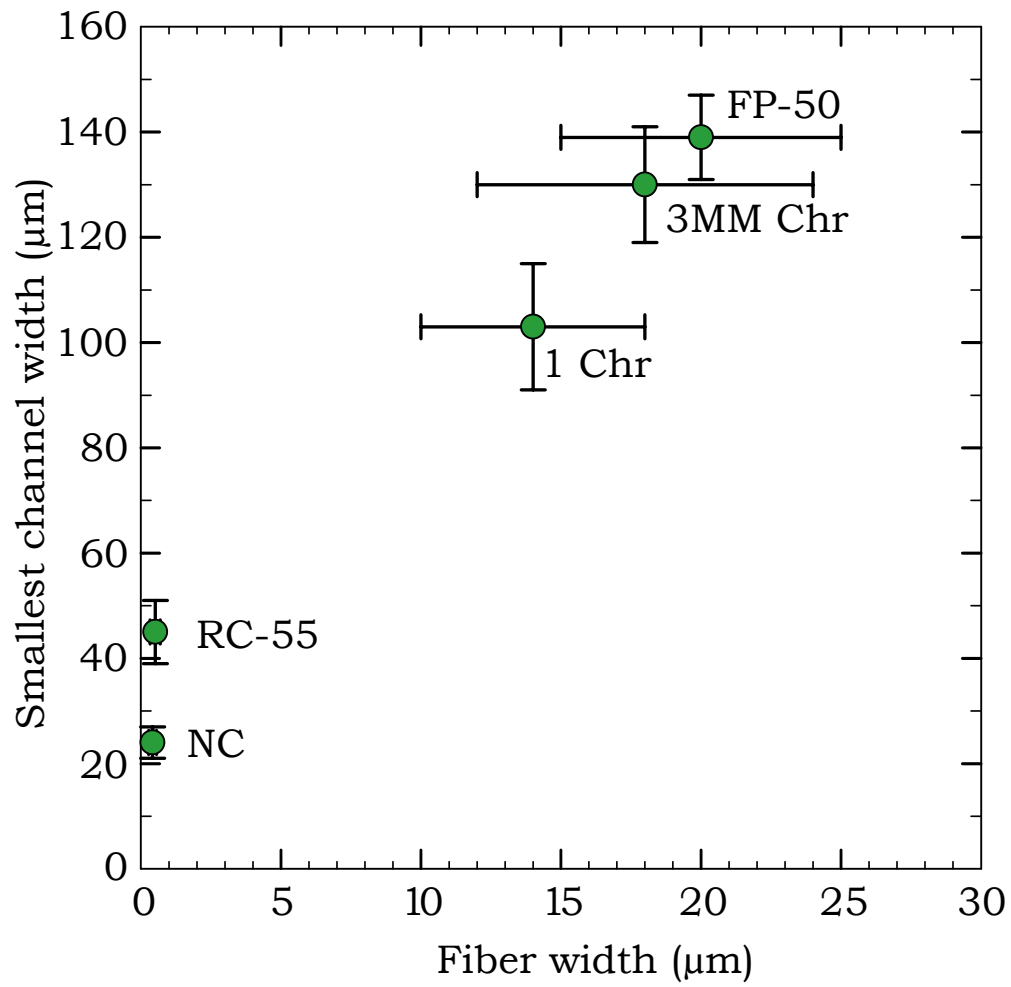


Figure 3.16: The smallest channel widths in each of the paper types for successful fluid flow plotted against fibre widths, reproduced from Ref. [113].

The fibre widths of the five different paper materials were plotted against the smallest channel widths in Figure 3.16. The plot shows that a smaller fibre width correlates with a lower value of the smallest channel width. For successful fluid flow through a paper channel, the fibre structure should be continuously linked along the channel pathway to ensure that the fluid is wicked along by capillary forces. A channel generally fails to carry liquid when the fibre network along the channel becomes disconnected due to fibres that are loose or broken. The SEM images in Figure 3.17 shows both successful and unsuccessful channels to illustrate how the fibre network becomes discontinuous as the channel widths are made too small. Therefore, the paper types with smaller fibre widths are capable of having continuous fibre networks along smaller channels and not disturbing the fluid pathway at smaller dimensions as compared to the larger fibre widths. Similar sized successful flow channels can be fabricated from both RC-55 and NC, with RC-55 shown in Figure 3.17(d), because both of their fibre widths are less than 1  $\mu\text{m}$ .

The relation between the physical properties of a paper material and its smallest hydrophilic feature with the capability of fluid flow suggests that the different paper materials allow different degree of miniaturization. The paper materials with smaller fibre width are suitable for the miniaturized  $\mu$ PADs because some features of the device can be small and not all the paper materials are capable of forming such a feature without disturbing the fluid pathway.



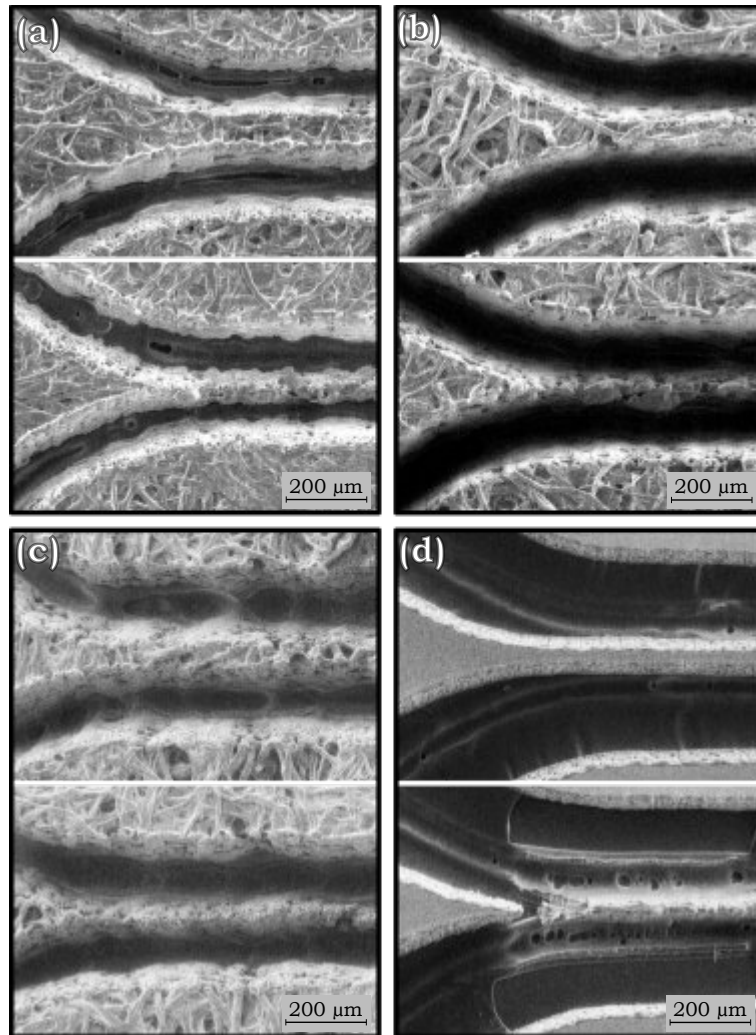


Figure 3.17: SEM images of the channels generated in the different paper types showing one intact channel with successful fluid flow (on the top) and one narrower channel where fluid flow was not successful (on the bottom), for (a) FP-50, (b) 3MM Chr, (c) 1 Chr, and (d) RC-55. Reproduced from Ref. [113].

# Chapter 4

## Flow through small-scale features

The understanding of the flow behaviour through the features of a  $\mu$ PAD helps in the designing of proper detection technique, test completion time and effective interaction between the analyte and the detection reagents. It is essential to know the characteristics of capillary flow through the features before using them in a  $\mu$ PAD. In the literature, flow characterization of millimetre [51, 53, 54, 68, 90, 93–95] and centimetre scale [52] channels were reported but their findings provided an inclusive understanding of the flow behaviour, as described in section 2.3. In addition, the high-resolution fabrication technique enabled the fabrication of small-scale features including the micro-scale features which can be used as the features of the miniaturized  $\mu$ PADs. Therefore, the characterization of capillary flow through small-scale features fabricated from different paper material is essential and it will provide an useful understanding of flow behaviour for future the development of the miniaturized  $\mu$ PADs.

This chapter describes the characterization of the capillary flow through 5 mm

long small-scale channels with varying widths that were fabricated using three paper materials (3MM Chr, 1 Chr, and RC-55). Different materials were used to investigate how the physical parameters of the paper material influence the capillary flow speeds through small-scale channels.

## 4.1 Experimental method

The capillary flow speeds of the dye solution were measured for the flow characterization of the 5 mm long small-scale channels with varying widths. The channels were fabricated from three different paper materials: Whatman 3MM Chr chromatography paper (3MM Chr), Whatman 1 Chr chromatography paper (1 Chr) and Whatman regenerated cellulose membrane 55 (RC-55). A schematic of the experimental procedure is shown in Figure 4.1. The paper channels were located on a petri dish and fed from a rectangular dye reservoir made from 1 Chr that contained an excess volume of red dye solution (10 g/L, Allura Red) on it. The surface of the petri dish was hydrophobic which enabled the dye to move directly to the channel without spreading along the petri dish. The edge of the dye reservoir was brought in contact with the inlet regions of the channels and provided an abundant fluid supply for continuous flow through each channel. The petri dish was covered with its lid at the moment when the edge of the dye reservoir was brought in contact with the inlet regions of the channels to reduce the effect of the evaporation loss on the system.

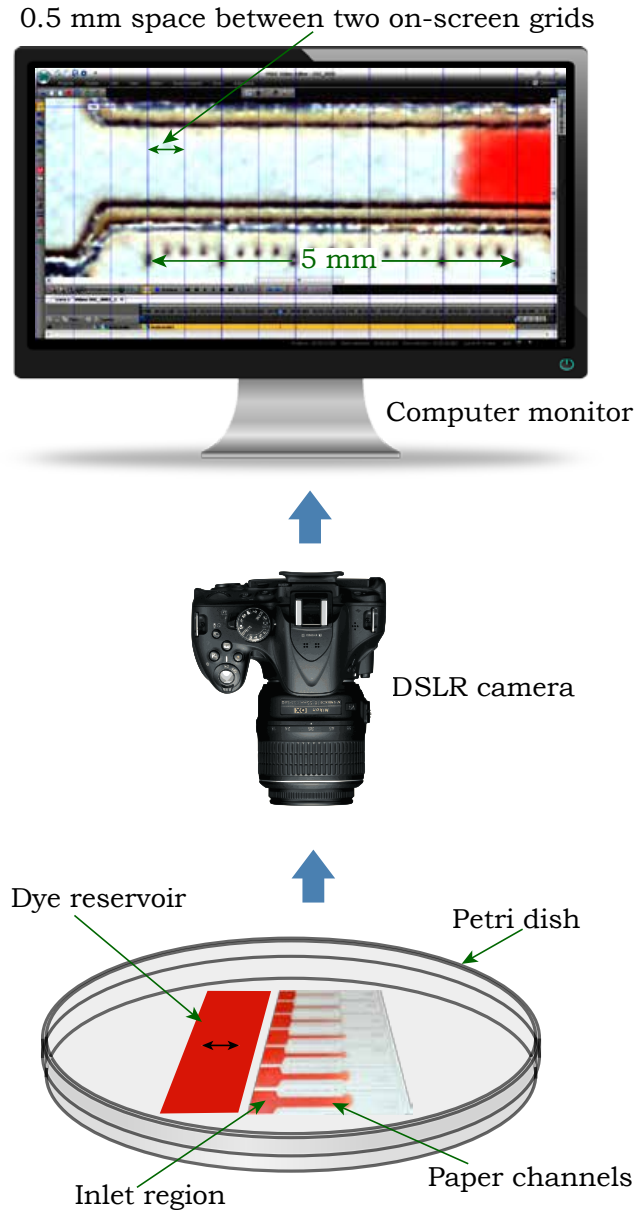


Figure 4.1: Schematic of the experimental procedure for measuring the flow speeds of dye solution through varying channel widths, adapted from Ref. [113].

The flow was recorded with a DSLR camera (Nikon D5200 with Nikon Af-s Dx Micro 40 mm F2.8G lens, Nikon Corporation, Tokyo, Japan) which was connected with a PC to observe the flow on the monitor. A 5 mm scale with  $250\ \mu\text{m}$  tick marks was cut with the laser along each channel to measure the time required by the liquid

front to travel a specific distance. To align the liquid front with the centre of the cut tick marks, an on-screen grid software (MB-Ruler, version 5.3, Markus Bader - MB-Softwaresolutions, Iffezheim, Germany) was used that generates grids with a precise tick mark spacing, as shown on the computer screen in Figure 4.1. The VSDC video editing software (Flash-Integro LLC., Vector Limited, Auckland, New Zealand) was used to measure the time required by the liquid front to travel between tick marks with millisecond increments.

## 4.2 Characteristics of flow through small scale features

To examine the flow behaviour through small-scale features in paper-based devices, the 5 mm long small-scale channels were fabricated from the tree paper materials: 1 Chr, 3MM Chr, and RC-55. The line-to-line design widths and corresponding actual widths of the paper channels that were used in these experiments are summarized in Table 4.1. To measure the width of each channel, 20 measurements were taken along the length of the channel and the average value is reported as the channel width in Table 4.1 one standard deviation ( $\pm\sigma$ ) of the measurements was used as the range. The error associated with the measurement procedure using the microscope was insignificant compared to the variation of channel width along the length, therefore one standard deviation ( $\pm\sigma$ ) of the width measurements was used as the range.

Table 4.1: Design widths and corresponding actual widths fabricated from different paper types used for flow speed measurements, reproduced from Ref. [113].

1 Chr		3MM Chr		RC-55	
Design Width ( $\mu\text{m}$ )	Actual Width ( $\mu\text{m}$ )	Design Width ( $\mu\text{m}$ )	Actual Width ( $\mu\text{m}$ )	Design Width ( $\mu\text{m}$ )	Actual Width ( $\mu\text{m}$ )
-	-	-	-	200	$54 \pm 3$
300	$210 \pm 12$	300	$212 \pm 10$	300	$148 \pm 4$
400	$314 \pm 8$	400	$298 \pm 8$	400	$248 \pm 3$
500	$396 \pm 11$	500	$405 \pm 7$	500	$341 \pm 6$
600	$492 \pm 9$	600	$521 \pm 9$	600	$459 \pm 5$
800	$699 \pm 9$	800	$750 \pm 8$	800	$642 \pm 3$
1100	$973 \pm 9$	1100	$1009 \pm 9$	1100	$931 \pm 4$

The smallest features that can be fabricated from each of the paper materials, were not used for the flow characterization because the relatively long length of the channels (5 mm) was  $\sim 50$  times larger than the smallest feature sizes, which led to some inconsistent flow behaviour for the smallest features. The benefit of the smallest feature sizes is to create miniaturized devices, so it is unlikely that the channels would flow a length of 50 times their width, and they were found to exhibit consistent flow speeds over shorter lengths ( $\sim 1$  mm), as was observed during the smallest feature experiments described in section 3.4. However, the 5 mm length was necessary to

provide flow observations that could be compared to previous studies at substantially larger length scales [52, 53, 93], which used lengths of multiple centimetres with the lowest data points at 5 mm.

To get the flow speed, the time required for the liquid front to travel 5 mm with intervals of 0.5 mm, was measured following the method as shown in Figure 4.1. For each channel width, the experiment was repeated three times and the average value of the time measurements was taken as the time value and one standard deviation ( $\pm\sigma$ ) of the measurements was used as the range. The travel distance and corresponding time required for the liquid front through the various channel widths made out of 1 Chr, 3MM Chr and RC-55 are plotted in Figures 4.2(a), 4.3(a) and 4.4(a). The results in Figures 4.2(a), 4.3(a) and 4.4(a) show a gradual increase in flow speed for increasing widths, except at the smallest widths, where the flow was substantially slower. These smallest width values are approximately the same size as the paper thickness in each of the three cases (thickness of 1 Chr: 180  $\mu\text{m}$ , 3MM Chr: 340  $\mu\text{m}$ , and RC-55: 75  $\mu\text{m}$ ). This indicates that the flow speeds do not vary as much when the channel width is substantially larger than paper thickness, but when the channel width and paper thickness are similar, the smaller width causes an appreciable reduction in the flow speed. Therefore, a greater dependence of the flow speed on the channel width was observed when the channel width is comparable to the paper thickness. Comparison with previous studies for significantly larger channels [52, 53] also shows the same trend of quicker flows for wider channels in the paper but with significantly quicker flow speeds compared to the microscale channels. Figure 4.4(a) shows that RC-55 also follows the same trend as the 1 Chr and 3MM Chr with the

smallest channel experiencing slower flow speed. However, for the the RC-55 paper, the overall flow speeds are slower than in the chromatography papers.

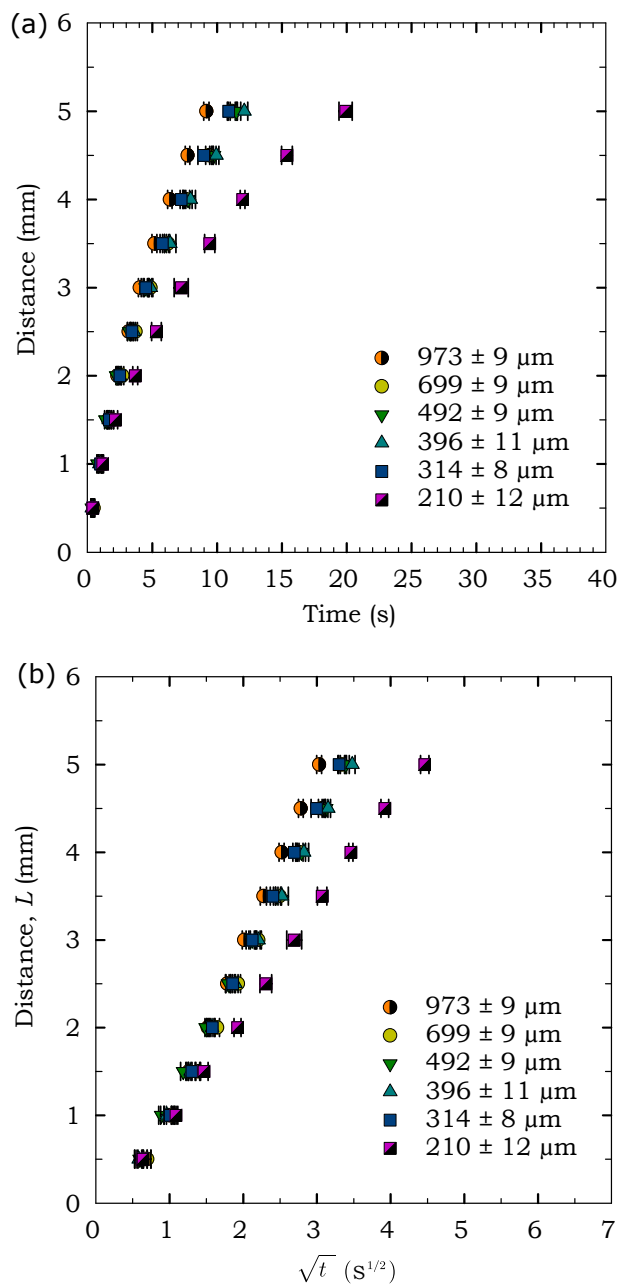


Figure 4.2: Flow behavior through varying channel widths fabricated in Whatman 1 Chr chromatography paper (1 Chr): (a) flow speed and (b) relation of  $L$  with  $\sqrt{t}$ . Adapted from Ref. [113].



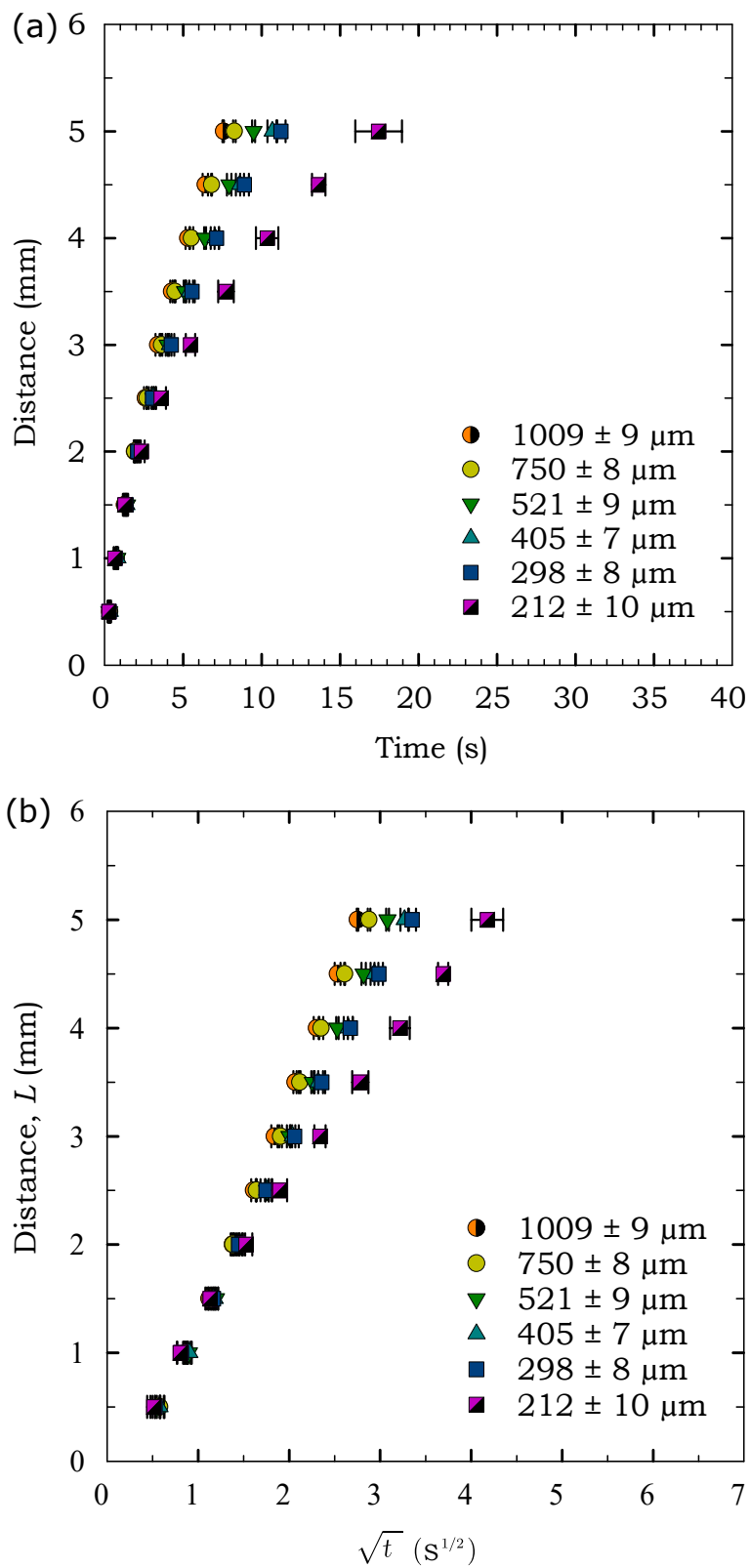


Figure 4.3: Flow behavior through varying channel widths fabricated in Whatman 3MM Chr chromatography paper (3MM Chr): (a) flow speed and (b) relation of  $L$  with  $\sqrt{t}$ . Adapted from Ref. [113].

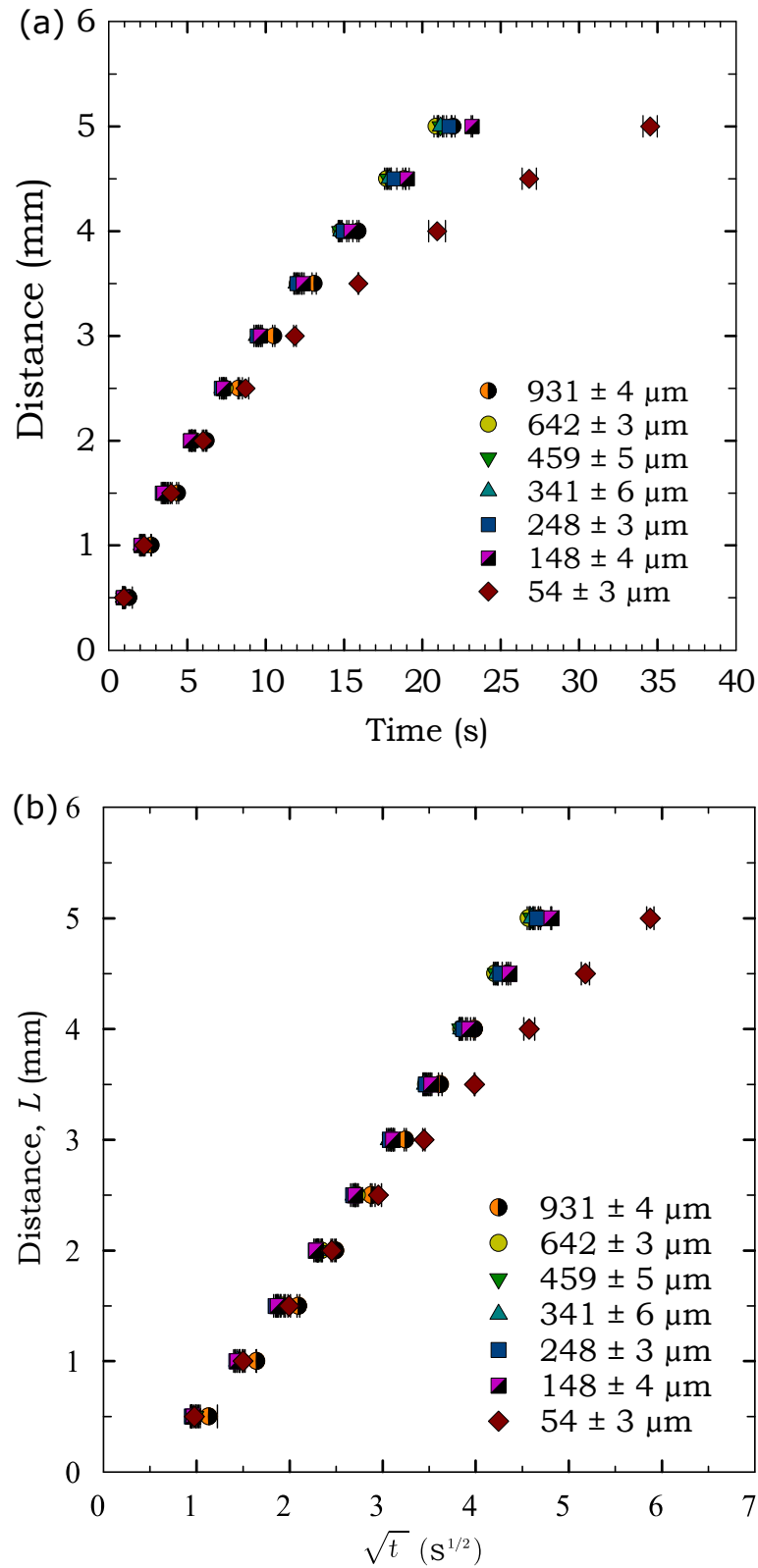


Figure 4.4: Flow behavior through varying channel widths fabricated in Whatman regenerated cellulose membrane 55 (RC-55): (a) flow speed and (b) relation of  $L$  with  $\sqrt{t}$ . Adapted from Ref. [113].

For all three paper types, the distance travelled by the liquid front was also plotted against  $\sqrt{t}$  to assess diffusive flow behaviour, as shown in Figures 4.2(b), 4.3(b) and 4.4(b). On these plots, the straight lines confirm diffusive flow behaviour for most widths, and only for the narrowest channel in each paper type were slightly curved lines observed. This confirms diffusive flow behaviour as predicted by the Washburn equation [92], but since the Washburn equation does not have any width dependence, then all the lines of each plot should have coincided. However, the lines do not coincide in Figures 4.2(b), 4.3(b) and 4.4(b) which indicates that the flow does depend on the channel width and was also previously shown by experimental studies [52, 53, 93]. Therefore, this work provides further confirmation that the Washburn equation alone is not sufficient for prediction of flows in paper-based microfluidic devices with features at smaller length scales, and highlights the importance of research exploring the complex dependence of the flow on various parameters, for various scenarios, such as the recent work by Castro et al. [53]. This study provides experimental data at the smaller length scales to help inform the future development of models to accomplish stronger predictive capacity for the capillary flow in miniaturized  $\mu$ PADs.

### 4.3 Difference in flow behaviour through cellulose and nitrocellulose paper materials

An attempt was made to measure the flow speed through 5 mm long small scale channels made out of a nitrocellulose membrane (Amershan Protran 0.45 nitrocellulose membrane (NC)) but the flow along the edge of the NC channel is significantly

faster than the middle area which generates a concave flow profile, as shown in Figure 4.5(b). Such profile was not favourable for accurate measurements of the flow speed within a flow path of 5 mm. The concave flow profile may possibly be attributed to the fabrication method and chemical properties, since the laser may be burning or otherwise altering the hydrophilicity of the membrane along the sides of the channel. In contrast, the cellulose papers (1 Chr, FP 50, and RC-55) make straight or slightly convex flow profiles which allow accurate measurements of the distance travelled by the liquid front, as shown on the monitor of Figure 4.1. Another difference that was observed between the cellulose and nitrocellulose membrane is that the red dye flows along the edges of the NC, whereas it is distributed more evenly through the entire thickness of cellulose paper (RC-55), as shown in 4.5(a).

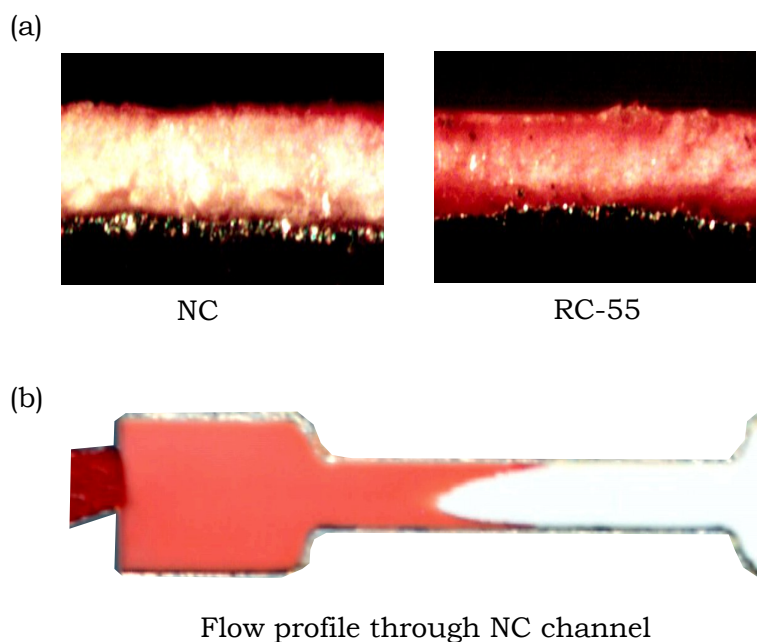


Figure 4.5: Photographs of the flow of red dye in NC and RC-55. (a) Cross-sectional views after red dye flowed through NC and RC-55. (b) Overhead view showing the concave flow profile of red dye in NC indicating faster flow along the sides of the channel, adapted from Ref. [113].

The understanding of the flow behaviour through the small scale channels will be helpful in the designing of the miniaturized  $\mu$ PADs to estimate the sample flow behaviour from the sample input zone to the multiple detection zones, to estimate the the volume of sample flowing through channels with varying widths, to design different test readout techniques and to design the microfluidic valve system for the miniaturized  $\mu$ PADs.

# Chapter 5

## Development of LFA-type $\mu$ PADs

This chapter describes the design and development of a counting-based miniaturized LFA-type  $\mu$ PAD with a semi-quantitative counting-based test readout that enables small sample volumes to be used for user-friendly testing. The efficacy of the LFA-type  $\mu$ PAD was demonstrated by performing glucose and human IgE tests using a small volume of simulated blood plasma sample (0.5  $\mu$ L for the glucose test and 1  $\mu$ L for the IgE test).

In the design of the counting-based test readout, three circular test dots were spotted along the sample flow path using small volumes of detection reagent (0.2  $\mu$ L for each dot) where the test dots changed their colour in the presence of the analyte and the number of coloured test dots successfully correlated to the concentration of the analytes and hence provided a semi-quantitative counting-based colorimetric test readout.

## 5.1 Materials and chemicals used in the Glucose test and human IgE test

Cross-absorbed goat anti-human IgE antibody unconjugated ('abT' will be used herein) was purchased from Fisher Scientific, (Hampton, New Hampshire, USA). Human IgE full length protein (IgE will be used herein), mouse monoclonal anti human IgE (Fc) antibody conjugated with HRP ('abHRP' will be used herein), goat anti-mouse IgG unconjugated antibody ('abC' will be used herein), and TMB-ELISA substrate with highest sensitivity were purchased from Abcam Inc (Toronto, ON, Canada). NaCl, KCl, Na<sub>2</sub>HPO<sub>4</sub>, KH<sub>2</sub>PO<sub>4</sub>, Tween-20, BSA, 3,3'-diaminobenzidine (DAB), D-(+)-glucose, sucrose, peroxidase from horseradish (HRP), glucose oxidase from aspergillus niger (GOx), deionized water (DI water) and molecular reagent grade pure water were purchased from Sigma-Aldrich (Oakville, ON, Canada). Phosphate buffered saline (PBS) at pH 7.4 was prepared using NaCl, KCl, Na<sub>2</sub>HPO<sub>4</sub>, KH<sub>2</sub>PO<sub>4</sub> and DI water. Complements brand skimmed milk powder was purchased from local store.

## 5.2 Design and fabrication of the LFA-type $\mu$ PAD for counting-based test readout

The design and final fabricated  $\mu$ PAD used in the experiment are shown in the Figure 5.1(a) and (b) respectively. The  $\mu$ PADS were fabricated using a previously reported laser cutting technique [112], where a CO<sub>2</sub> laser beam removes the paper material from foil-backed membranes along the cut line of the design to yield hydrophobic barriers throughout the device. Whatman regenerated cellulose membranes (RC-55) and Amersham Protran 0.45  $\mu$ m nitrocellulose western blotting membranes were used in the fabrication of  $\mu$ PADS for the glucose and human IgE tests respectively. Cellulose paper was used for the glucose test since protein binding was not an issue and it provided faster wicking in comparison to nitrocellulose. The device consists of four zones, which are labelled in Figure 5.1(a) as follows: running liquid zone ‘R’, sample input zone ‘S’, detection zone (containing test dots ‘T1-T3’ and control dot ‘C’), and absorption zone ‘A’. All the zones were patterned on a single sheet of the paper material to eliminate the complexity of merging multiple pads.



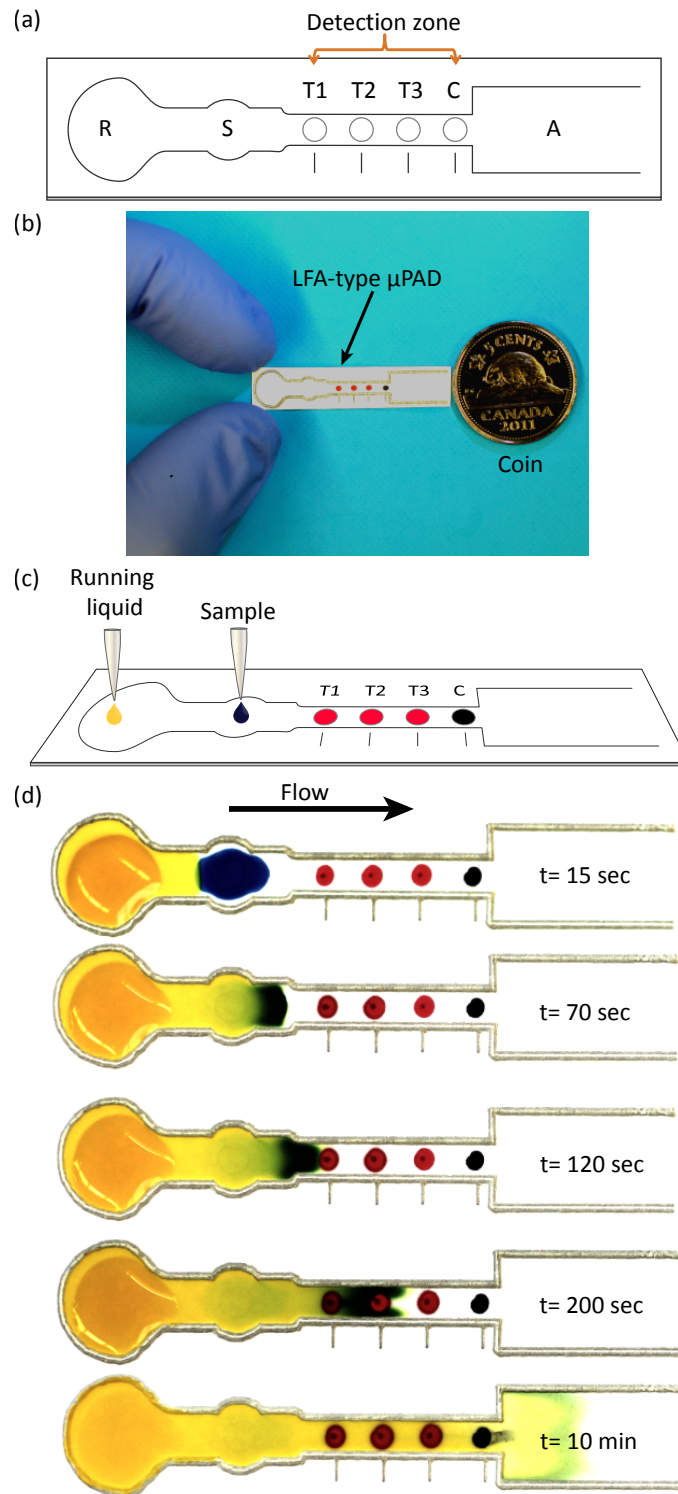


Figure 5.1: (a) Schematic of the LFA-type  $\mu$ PAD designed to analyse small sample volumes. (b) Relative size of the miniaturized  $\mu$ PAD is shown against a Canadian nickel (five cent coin) and finger tips. (c) Schematic of the  $\mu$ PAD showing placement of the simulated sample (blue dye) and simulated running liquid (yellow dye). (d) Photographs of the dye test showing the flow of the simulated sample (blue dye) over time for visual confirmation of successful sample flow across the detection zone, reproduced from Ref. [114].

### 5.3 Operation of the LFA-type $\mu$ PAD

To accommodate the smaller sample volumes, a lateral flow strategy was developed to maximize the amount of analyte that flows over the readout zones and to provide increased consistency, as shown in Figure 5.1. The sample was first pipetted on the ‘S’ zone, then a running liquid was pipetted on the ‘R’ zone, which allowed the sample to flow over the test dots and control dots. The reagent immobilized on the test dots interacted with the analyte present in the sample and provided visual colorimetric signal of analyte detection. The control dot reagent was chosen in such a way so that it can produce colorimetric detection in contact with the sample fluid irrespective of the presence or absence of the analyte.

A preliminary dye test was performed using a  $\mu$ PAD made out of nitrocellulose membrane to visually confirm that the sample flowed over the entire detection zone, as shown in Figure 5.1(c-d). A permanent red ink pen was used to make red circular dots that represent the test dots and a permanent black ink pen was used to make a black dot that represents the control dot. The permanent ink was not washed out by the flowing liquid which is the same behaviour that will be exhibited by the immobilized reagents for the test dots and control dot in analytical devices. A 1  $\mu$ L volume of blue dye was used as the sample and pipetted on the ‘S’ zone, followed by pipetting of 10  $\mu$ L of yellow dye as the running liquid on the ‘R’ zone, as shown in Figure 5.1(c). As the yellow dye was wicked along the device it caused the blue dye to flow over the detection zone, and after 10 minutes all of the blue dye reached the absorption zone ‘A’, which was visually confirmed, as shown in Figure 5.1(d). This

preliminary dye test confirmed that the device design required a running liquid and resulted in the sample fluid flowing over the entire detection zone, which is essential for sufficient analyte-reagent interaction and consistent flow when using small sample volumes.

## 5.4 Spotting reagents

A common approach in barcode-based lateral flow assays is to spot multiple drops of reagent side-by-side and create test lines; however, when a single drop of spotting reagent is placed on a hydrophilic membrane, a circular spot is naturally formed, which is a more simple method to spot the reagents. Therefore to prepare the LFA-type  $\mu$ PADS, a single drop of reagent was spotted on each of the test dots 'T1-T3' and the control dot 'C' where a specific volume of reagent was used to control the size of the dots (0.2  $\mu$ L). The control dot was formed on the membrane by pipetting the reagent as a single drop. The use of a pipette for spotting resulted in some inconsistency in the size of the dots, which is not critical for the control dot but is crucial for the test dots to ensure reproducibility and accuracy of the test result. To overcome the inconsistency associated with pipetting, a syringe pump with micro-bore plastic tubing and an opening fitted with a steel sleeve was used to dispense sub-microlitre reagent volumes and create the test dots, as shown in Figure 5.2. The steel sleeve protected the micro-bore tube from being squeezed by the applied pressure of the finger tips. There are many commercially available drop-wise chemical dispensers which can be used for similar reagent spotting in large scale production of  $\mu$ PADS.

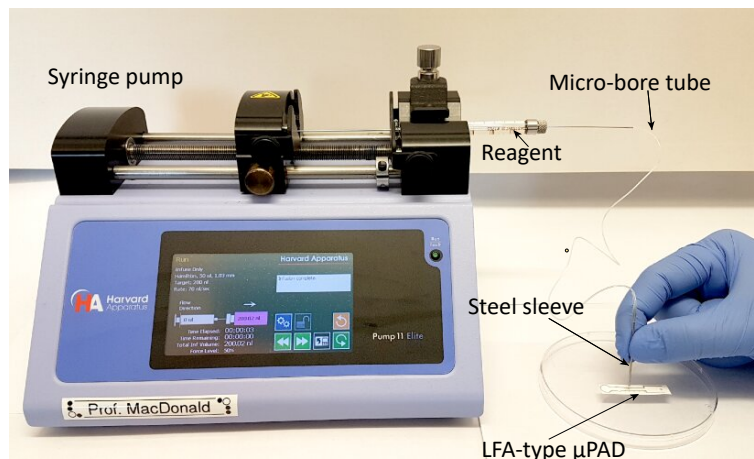


Figure 5.2: Spotting sub-microlitre reagent volumes on the test dots ‘T1-T3’ using a syringe pump, micro-bore tubing, and finger tips, reproduced from Ref. [114].

## 5.5 Device preparation for the glucose test and the test procedure

To demonstrate the efficacy of the miniaturized counting-based  $\mu$ PADs, a glucose test was performed to determine the level of glucose present in simulated blood plasma samples made using five different concentrations of glucose (0, 3, 6, 9 and 12 mmol/L) with BSA (40 mg/mL) in PBS buffer. The glucose levels of 0-12 mmol/L were selected because they represent the range of interest for medical diagnosis [62]. A 0.2  $\mu$ L volume of DAB solution (10 mg/mL in DI water) was spotted on each of the test dots ‘T1-T3’ using the syringe pump, and a 0.2  $\mu$ L volume of DAB-glucose solution (1:1 ratio of 10 mg/mL DAB solution and 20 mg/mL glucose solution made with DI water) was pipetted on the control dot ‘C’. A 0.2  $\mu$ L volume of HRP (800 U/mL in pure water) and 0.2  $\mu$ L volume of GOx (800 U/mL in pure water) were each spotted on the sample input zone ‘S’, as shown in Figure 5.3. The device was allowed to dry

at room temperature for 10 minutes prior to use.

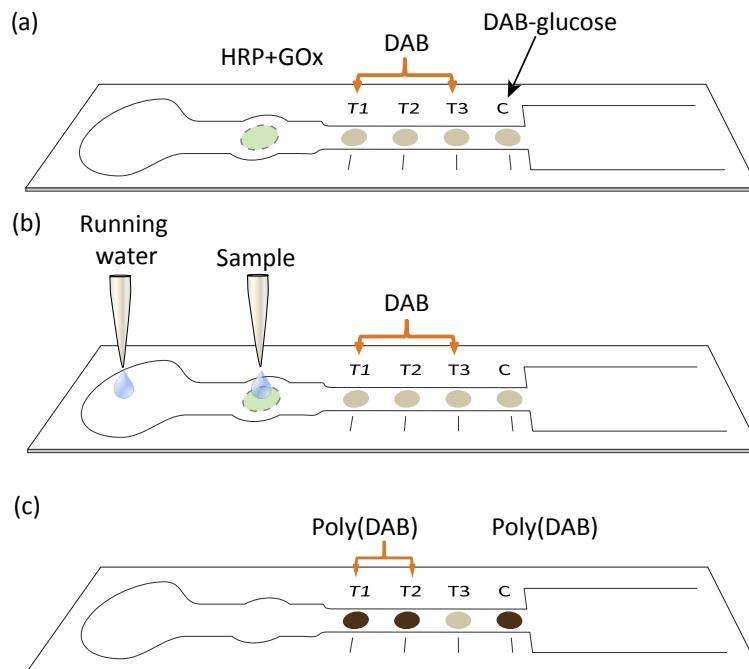


Figure 5.3: Steps for the glucose test: (a) the reagents were spotted on the sample input zone and detection zone of the  $\mu$ PAD, (b) the test was performed by pipetting the simulated blood plasma sample followed by DI water as the running liquid, and (c) colorimetric detection of glucose over the test dots ‘T1-T3’ (with ‘T1’ and ‘T2’ coloured as dark brown as an example of the reaction with glucose), reproduced from Ref. [114].

A 0.5  $\mu$ L sample was dispensed in zone ‘S’ followed by the dispensing of a 10  $\mu$ L volume of DI water in zone ‘R’ which was used as the running liquid for the glucose tests, as shown in Figure 5.3. As the running liquid was wicked along the device it caused the sample to flow over the detection zone. The spotted DAB (test dots) changed from a light brown colour into dark brown poly(DAB) if exposed to HRP, GOx, and glucose, as shown schematically in Figure 5.3(c). At the test dots, glucose is converted to gluconic acid and hydrogen peroxide by glucose oxidase, and subsequently the hydrogen peroxide reacts with DAB in the presence of horseradish

peroxidase and produces dark brown poly(DAB). The glucose is consumed progressively as it flows along the detection zone; therefore higher concentrations of glucose yielded a larger number of dark brown test dots, and the number of dark brown test dots was correlated to the concentration of glucose in the sample. The control dot changed to a dark brown colour regardless of the amount of glucose in the sample, because the control dot was composed of a glucose-DAB mixture, and the HRP and GOx eventually flowed to the control dot, as shown in Figure 5.3. Thus the control dot changing to dark brown provided confirmation that the fluid successfully reached the end of the detection zone and contained enough HRP and GOx for the reactions to occur.

During the test, right after pipetting the sample the LFA-type  $\mu$ PADS were kept inside the petri dish to maintain consistent surrounding for all the test. After the experiment, photographs of the  $\mu$ PADS were captured as test results using a Cannon DSLR camera connected with the computer, as shown in Figure 5.4.

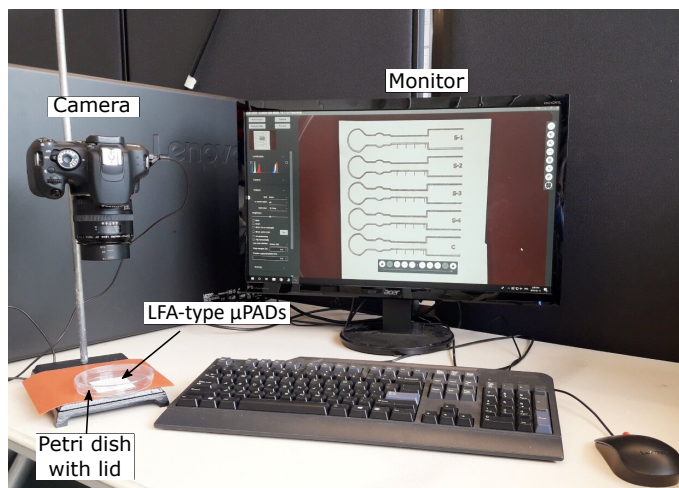


Figure 5.4: The camera set-up to monitor and capture the image of test results obtained from counting-based testing using the LFA-type  $\mu$ PAD

## 5.6 Counting-based results obtained from the glucose test

In order to generate a meaningful semi-quantitative result from a counting-based test, a calibration was required to ensure that the diagnostically important glucose levels had a distinct number of dots that changed colour. This was accomplished by performing several tests while varying the amount of sample volume used. Since the glucose was consumed as the sample flowed over the 3 test dots, using a higher sample volume resulted in more of the dots changing to a dark brown colour. Traditionally, the important diagnostic levels for glucose tests are based on diabetes and hypoglycemia, and glucose concentrations of 0, 3, 6, 9 and 12 mmol/L provide meaningful information about these conditions [62]. A sample volume of 0.5  $\mu$ L was found to generate a distinct number of dots with a dark brown colour change for each of the concentrations; therefore, a 0.5  $\mu$ L sample volume was used in each of the glucose tests reported in this section.

The tests were performed three times (each one is denoted as a set), and for each set five  $\mu$ PADs were fabricated to analyse the five different concentrations of the glucose (0, 3, 6, 9 and 12 mmol/L). Figure 5.5 shows photographs of the detection zone for each  $\mu$ PAD after the glucose tests were completed. A counting of the dark brown dots based on naked eye visualisation of Figure 5.5 reveals that a glucose level of 12 mmol/L corresponded to three dark brown test dots, 9 mmol/L corresponded to two dark brown test dots, 6 mmol/L corresponded to one dark test dot, and 3 mmol/L corresponded to a portion of a test dot with a dark brown colour. The control dot

'C' changed to a dark brown colour in every test, thus confirming that sample flowed to the end of the detection zone.

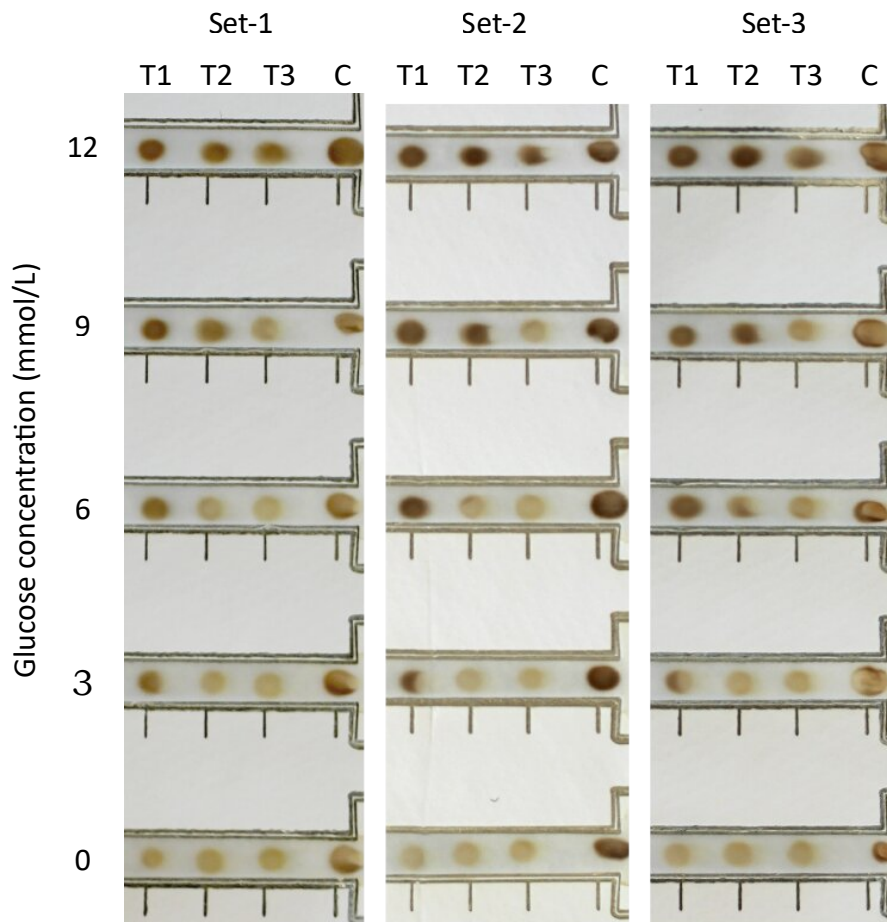


Figure 5.5: Photographs of the detection zones after completion of the glucose tests for three sets of experiments conducted with  $0.5 \mu\text{L}$  of the simulated blood plasma samples containing various concentration of glucose (0-12 mmol/L). The test dots changed to a dark brown colour if they reacted with glucose; therefore the number of dark brown dots in each test corresponds with the level of glucose in the sample, reproduced from Ref. [114].



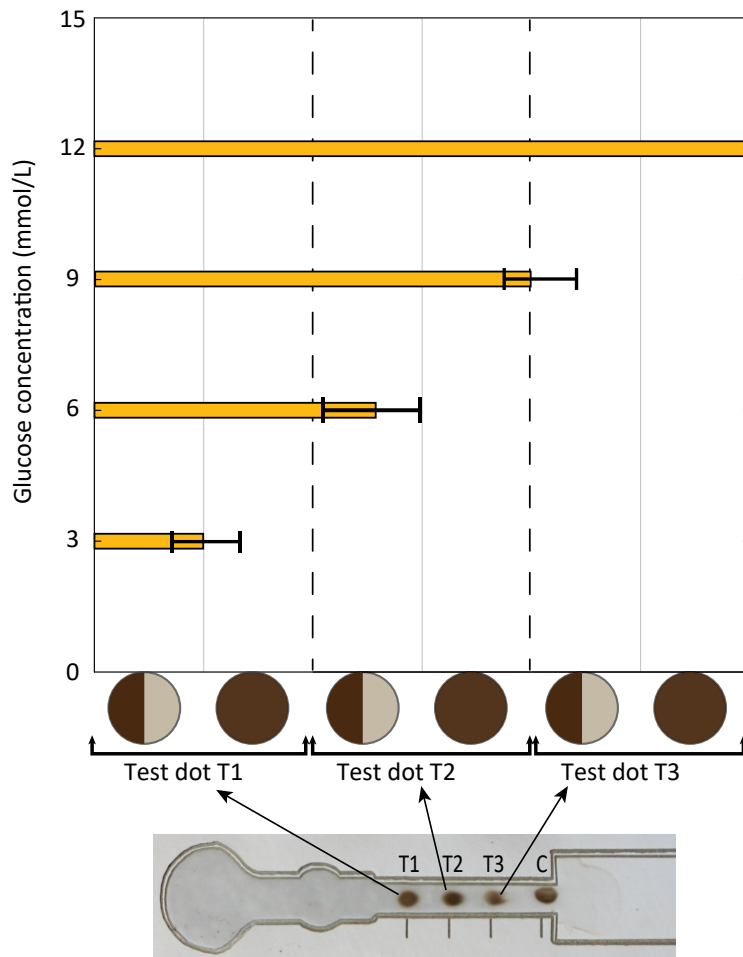


Figure 5.6: The glucose concentrations were plotted against the number of test dots that changed to a dark brown colour. For each test dot, the plot distinguished between the progression of two colorimetric states that were observed: a portion of the test dot changed to a dark brown colour or the entire test dot changed to a dark brown colour, reproduced from Ref. [114].

The results are plotted in Figure 5.6 to provide a graphical interpretation of the findings. Along the bottom of the plot the two colour change types are shown: a portion of the dot changing to dark brown (roughly half), or the entire test dot changing to dark brown. The plot shows that for a glucose level of 12 mmol/L all three test dots ‘T1-T3’ changed to a dark brown colour, for 9 mmol/L, two test dots ‘T1-T2’ changed to a dark brown colour, for 6 mmol/L, one test dot ‘T1’ changed to a dark

brown colour, and for 3 mmol/L only a portion of the first test dot ‘T1’ changed to a dark brown colour. These test results demonstrate that the miniaturized counting-based  $\mu$ PADS can provide a user-friendly semi-quantitative method to monitor the concentration of biomarkers in relation to the important diagnostic ranges associated with different conditions. The small sample volume required will also allow the tests to be integrated with user-friendly sample collection systems such as finger pricking or microneedles.

## 5.7 Device preparation for the IgE test and the test procedure

To demonstrate the efficacy of the miniaturized counting-based  $\mu$ PADS for immunoassays, a human IgE test was performed to determine the total human IgE present in a simulated blood plasma sample prepared in PBS buffer with BSA (40 mg/mL), sucrose (1% w/v), and six different concentrations of IgE (0, 25, 50, 100, 200 and 400 ng/mL). In each  $\mu$ PAD, the test dots ‘T1-T3’ were spotted with 0.2  $\mu$ L of ‘abT’ (1 mg/mL), and the control dot ‘C’ was spotted with 0.2  $\mu$ L of ‘abC’ (1 mg/mL), as shown in Figure 5.7(a). The devices were dried in an incubator after spotting (Heratherm<sup>TM</sup> Compact Microbiological Incubators, Thermo Fisher Scientific, Massachusetts, USA) at 37°C for 30 minutes, as shown in Figure 5.8(a). After drying, the devices were blocked for 15 minutes in a blocking solution made with 5% (w/v) skimmed milk in PBS buffer using a lab rocker platform (Bellco Biotechnology, NJ, USA) at medium speed, as shown in Figure 5.8(b). The blocked devices were washed

for 10 minutes in a washing solution made with 0.05% (v/v) Tween-20 in PBS buffer using the same rocker platform. The washed devices were dried in the incubator at 30°C for 90 minutes and the dried devices were then ready for the IgE testing.

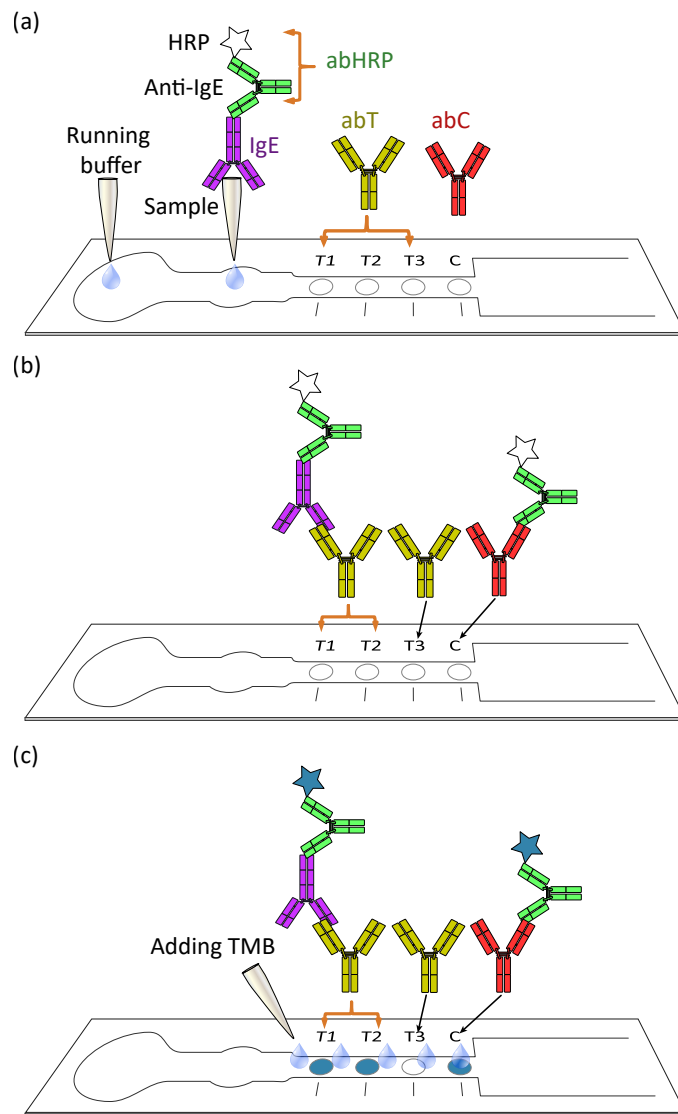


Figure 5.7: Steps for the IgE test: (a) the sample solution (a mixture of the simulated blood plasma (containing IgE) and ‘abHRP’) was placed on the sample input zone followed by the placement of the running buffer in the running liquid input zone, (b) IgE-bound ‘abHRP’ was captured at the test dots, and unbound ‘abHRP’ was captured at the control dot as the sample solution flowed over them, and (c) HRP of the ‘abHRP’ turned blue after adding TMB solution on the detection zone (with ‘T1’ and ‘T2’ shown as blue coloured as an example), reproduced from Ref. [114].

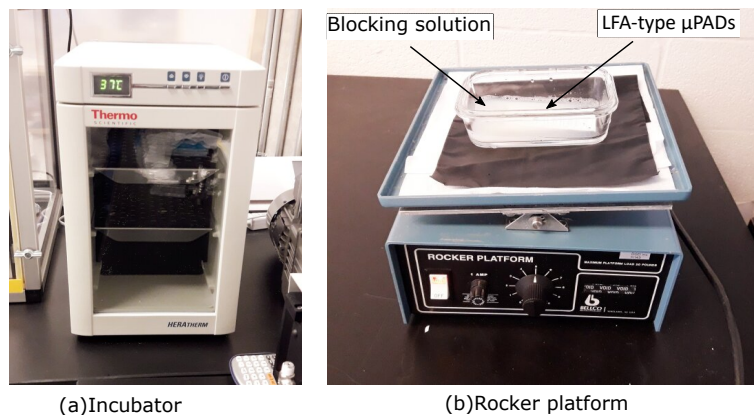


Figure 5.8: The incubator and rocker used in the preparation of the LFA-type  $\mu$ PADS for human IgE test

To perform the IgE test, the simulated blood plasma samples were mixed with ‘abHRP’ ( $1 \mu\text{g}/\text{mL}$ ) to yield a sample solution, which contained IgE bound with the ‘abHRP’ as shown in Figure 5.7(a). A  $1 \mu\text{L}$  sample solution was placed in the sample input zone ‘S’ and immediately after that a  $12 \mu\text{L}$  volume of running buffer (PBS buffer with 2% (v/v) Tween 20) was placed in the running liquid input zone ‘R’, as shown in Figure 5.7(a). As the running liquid was wicked along the device it caused the sample to flow over the detection zone, where the ‘abT’ (test dots) captured IgE bound with ‘abHRP’, and the ‘abC’ (control dot) captured the unbound ‘abHRP’ contained in the sample solution, as shown in Figure 5.7(b). After 10 minutes, the sample reached the absorption zone ‘A’ (after flowing over the test and control dots) and any remaining abHRP that did not bind with a test or control dot was washed away from the detection zone and into the absorption zone. A  $3 \mu\text{L}$  volume of TMB solution was then applied over the detection zone. In the presence of TMB, the IgE bound with ‘abHRP’ at the test dots and the unbound ‘abHRP’ at the control dot changed to a blue colour, as shown in Figure 5.7(c). The horseradish peroxidase

(HRP) reacts with TMB and produces blue coloured TMB-diimine. The test dots only captured IgE bound with ‘abHRP’, therefore the blue colour only appeared in the test dots if human IgE was present in the sample solution as it flowed over each test dot. The IgE was captured progressively as it flowed over each successive test dot; therefore, higher concentrations of IgE yielded a larger number of blue coloured test dots, and the number of blue coloured test dots was correlated to the concentration of IgE in the sample. Unlike the test dots, the control dot captured the unbound ‘abHRP’ in the sample solution regardless of the amount of IgE contained in the sample, and thus a blue coloured control dot provided confirmation that the sample flowed to the end of the detection zone and contained a sufficient amount of ‘abHRP’.

## 5.8 Counting-based test results obtained from the IgE test

Similar to the glucose tests, experiments with different volumes of sample solution were performed, and a sample volume of 1  $\mu$ L was found to be best choice to generate a distinct number of test dots with a colour change corresponding to the critical range of IgE concentrations associated with allergic symptoms [63–65]. The tests were performed three times (each one denoted as a set) and six  $\mu$ PADs were fabricated to analyse each of the six different concentrations of human IgE (0, 25, 50, 100, 200 and 400 ng/mL). Figure 5.9 shows photographs of the detection zone for each  $\mu$ PAD after the IgE tests were completed. A counting of the blue coloured dots based on naked eye visualisation of Figure 5.9 reveals that an IgE concentration of 400 ng/mL

corresponded to three blue coloured test dots, 200 ng/mL corresponded to two and a half test dots, 100 ng/mL corresponded to one and a half test dots, and 50 ng/mL and 25 ng/mL both corresponded to a portion of one test dot changing to a blue colour. The control dot 'C' changed to a blue colour in each test, which confirms that the sample successfully flowed to the end of the detection zone.

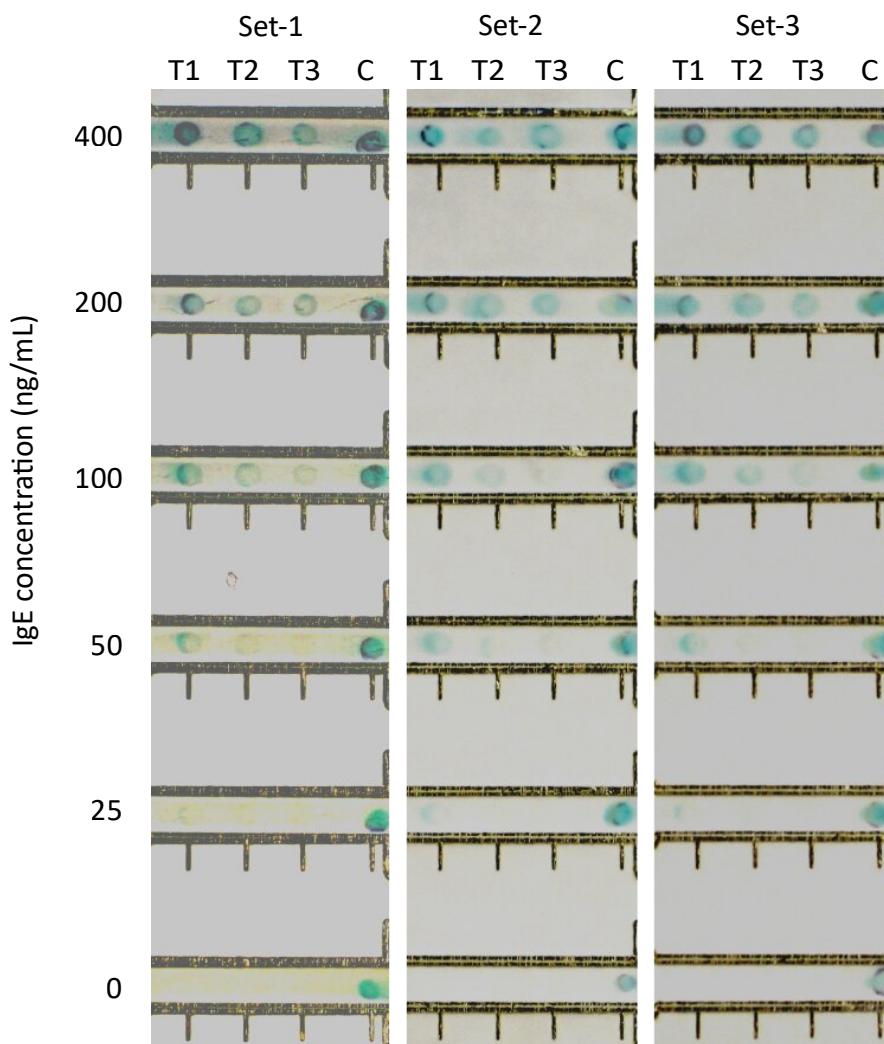


Figure 5.9: Photographs of the detection zones after completion of the IgE tests for three sets of experiments conducted with 1  $\mu$ L of the simulated blood plasma samples containing various concentration of human IgE (0-400 ng/mL). The test dots changed to a blue colour if they bound with IgE; therefore the number of blue dots in each test corresponds with the level of IgE in the sample, reproduced from Ref. [114].

Figure 5.10 provides a graphical interpretation of the findings from the IgE tests. Along the bottom of the plot the two colour change types are shown: a portion of the dot changing to blue (roughly half), or the entire test dot changing to blue. The plot shows that for an IgE concentration of 400 ng/mL corresponded to three blue coloured test dots ‘T1-T3’, 200 ng/mL corresponded to two and a half test dots ‘T1-T3’, 100 ng/mL corresponded to one and a half test dots ‘T1-T2’, and 50 ng/mL and 25 ng/mL both corresponded to a portion of the ‘T1’ test dot changing to a blue colour.

The counting-based approach is valuable for these total IgE tests because a semi-quantitative result provides the important test information in a user-friendly test. According to the literature, in blood plasma three levels of total IgE are commonly considered in medical diagnosis, normal level:  $<48$  ng/mL (20KU/L), moderate level: 48-240 ng/mL (20-100 KU/L), and elevated level:  $>240$  ng/mL (100 KU/L) [63–65]. Each level indicates the probability of allergic symptoms and the probable contribution of allergens in atopic diseases [63]. The concentrations of IgE (0-400 ng/mL) were selected for the miniaturized counting-based  $\mu$ PADs so that the tests can provide a user-friendly approach to predict if the user is within one of the important IgE levels. According to the test results from Figures 5.9 and 5.10, if the blue colour is limited to the first test dot ‘T1’ then it indicates a normal level of total IgE; if the blue colour appears in all three test dots ‘T1-T3’ then it indicates an elevated level of total IgE; and if dots ‘T1-T2’ change to a blue colour this indicates a moderate level of total IgE. This further reinforces the strength of the counting-based approach to provide a semi-quantitative readout that is simple to interpret in comparison with

the interpretation of the intensity of the change in colour.

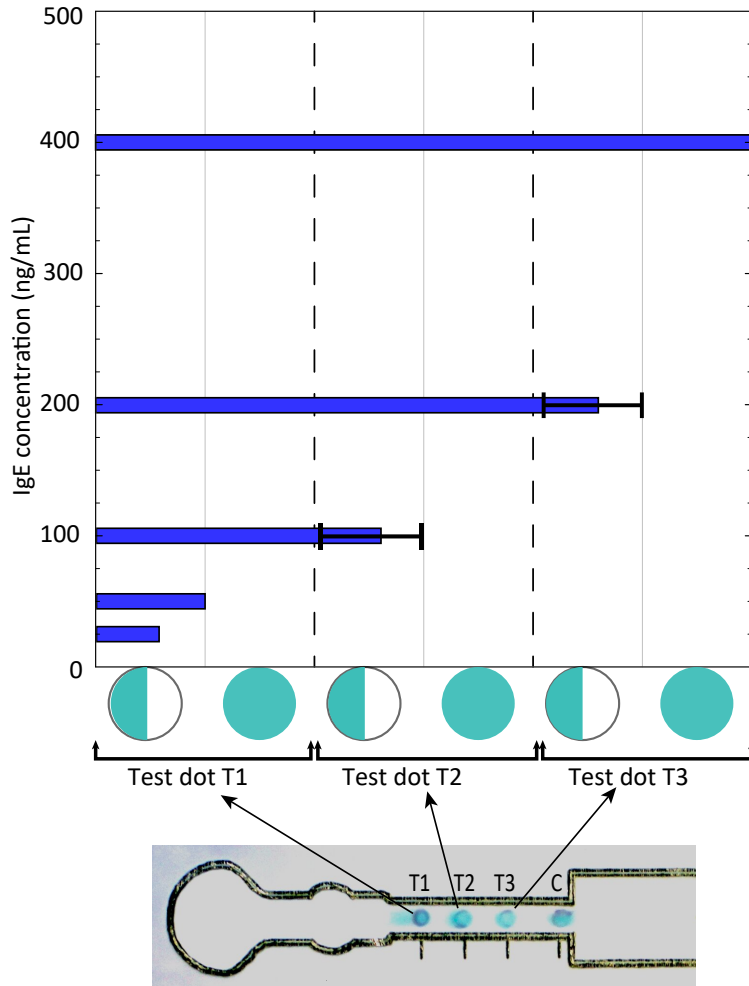


Figure 5.10: The IgE concentrations were plotted against the number of test dots that changed to a blue colour. For each test dot, the plot distinguished between the progression of two colorimetric states that were observed: a portion of the test dot changed to a blue colour or the entire test dot changed to a blue colour, reproduced from Ref. [114].

From the success of the human IgE tests, it can be inferred that similar  $\mu$ PADS made out of nitrocellulose membrane (or any paper material with similar protein binding properties) can be developed for other protein biomarkers present in samples. The use of small sample volumes increases the user-friendly aspect of the tests since simple sample collection methods can be used (such as finger pricking and mi-



croneedles). Distinct colorimetric detection for the target range of an analyte can be achieved by adjusting the sample volume size, test dot size, number of test dots and concentration of immobilized antibody spotted in the test dots. Therefore the miniaturized counting-based  $\mu$ PADS presented here can provide a user-friendly way to provide semi-quantitative information about a wide range of analytes and over a broad range of concentrations.

# Chapter 6

## Conclusion

### 6.1 Fabrication of $\mu$ PADs

#### 6.1.1 Fabrication technique

In the first phase of this study, high-resolution fabrication technique was developed for the fabrication of miniaturized  $\mu$ PADs which provides a number of advantages as compared to the existing fabrication techniques reported in the literature such as simplicity in the fabrication process, rapid, inexpensiveness, one step fabrication and mass production capability. The fabrication technique was based on the material removal process by laser cutting but the foil backing enabled fabrication of miniaturized  $\mu$ PADs with necessary strength required for safe handling. This technique is suitable for adopting in the mass production line which will eventually make the  $\mu$ PADs inexpensive and facilitate the worldwide availability of  $\mu$ PADs for a wide range of diagnostic tests.

### 6.1.2 Fabrication resolution

The high-resolution fabrication technique enabled creating a successful hydrophobic barrier as narrow as  $39 \pm 8 \mu\text{m}$  on the aluminium foil backed 1 Chr chromatography paper which is the narrowest hydrophobic barrier ever reported in the literature. Such precise hydrophobic barrier enabled the development of compact and miniaturized  $\mu\text{PADs}$  where multiple detection zones were placed tightly within a smaller area for multiplexed testing. To determine the physical limit of the miniaturization, the five different types of commercially available paper materials were used to fabricate the smallest features that successfully facilitated capillary flow through the features. The features were fabricated as narrow channels and the widths of the smallest channels fabricated from FP-50, 3MM Chr, 1 Chr, RC-55 and NC were  $139 \pm 8 \mu\text{m}$ ,  $130 \pm 11 \mu\text{m}$ ,  $103 \pm 12 \mu\text{m}$ ,  $45 \pm 6 \mu\text{m}$ , and  $24 \pm 3 \mu\text{m}$  respectively. This part of the study revealed that the paper materials with different physical properties offer a different limit on the miniaturization.

### 6.1.3 Physical properties of paper that limit miniaturization

It was found that the fibre width of a paper material dominates the miniaturization process. A paper material with smaller fibre width allows fabrication of smaller features for the  $\mu\text{PADs}$ . Therefore, to fabricate miniaturized  $\mu\text{PADs}$ , it is better to select paper materials with smaller fibre widths. Another experimental finding is that the narrowest flow path designed in a  $\mu\text{PAD}$  should not be smaller than the thickness of the paper materials because it will cause extreme slow liquid flow unless a device

is designed for such slow flow.

#### **6.1.4 Compact and miniaturized $\mu$ PAD developed for multiplexed testing**

Based on the understanding of hydrophobic barrier and smallest feature size, a compact and miniaturized  $\mu$ PAD was designed and fabricated for multiplexed testing. The device was tested with dyes to check the feasibility of simultaneous testing for eight analytes using a 2  $\mu$ L of sample. The dye test confirmed that the device was suitable for multiplexed testing. To demonstrate the feasibility of the device in medical diagnosis, the glucose test was performed using a 2  $\mu$ L of artificial urine sample and such small volume of sample was enough to provide the colorimetric detection in the eight detection zones spotted with glucose specific reagents. From this success, it can be inferred that these compact and miniaturized  $\mu$ PADs are capable of analysing small sample volume for multiplexed testing.

## **6.2 Flow characterization of small scale channels**

The capillary flow speed through the small-scale channels fabricated from different paper types was measured and analysed. It was found that the flow through the channels follow a similar trend as compared to that of macro-scale channels where wider channels caused quicker flow speeds. However, in the microscale channels, the overall speeds of the capillary flow were significantly slower. The understanding of the flow behaviour through the small scale channels will help in future modelling and

design of user-friendly and miniaturized  $\mu$ PADs with small-scale features.

### **6.3 Diagnostic tests using counting-based miniaturized LFA-type $\mu$ PAD**

A miniaturized LFA-type  $\mu$ PADs was designed and developed with a counting-based colorimetric test readout to analyse small sample volumes (in the sub-microlitre range). The devices were used to provide semi-quantitative information about the concentration of glucose and human IgE present in 0.5 and 1  $\mu$ L of simulated blood plasma samples respectively. The devices successfully provided distinct visual colorimetric detection for varying analyte concentrations where the number of coloured test dots correlated to the analyte concentration. Glucose is a non-protein analyte and IgE is a protein analyte in human blood plasma, therefore it can be inferred that similar devices can be developed to detect other protein and non-protein biomarkers tested in medical diagnosis. The miniaturized counting-based  $\mu$ PADs provide a user-friendly test platform since the counting of coloured dots is more straightforward than interpreting the intensity of a colour change, and the use of small sample volumes will enable the tests to be used with simple sample collection system, such as finger pricking and microneedles.

### **6.4 Inexpensive and user-friendly $\mu$ PADs**

The fabrication technique will enable the fabrication of inexpensive  $\mu$ PADs for a wide range of analytical and diagnostic tests. This method will allow the use of almost

any kind of paper materials in the fabrication, therefore the use of only commercially available paper materials is not a prerequisite. If inexpensive and locally made paper materials are used in the fabrication then overall fabrication cost of the  $\mu$ PADs will eventually become very low. The miniaturization of the  $\mu$ PAD will allow the use of small reagent and sample volume. For blood-based tests, a user-friendly sample collection system (e.g. microneedle) can be integrated with the miniaturized  $\mu$ PAD which will eliminate the user-involvement in sample input and the need for an expert for the venous draw. The inexpensive and user-friendly miniaturized  $\mu$ PADs will be able to provide diagnostic access to the underprivileged people and the people in urgent or emergency medical condition.

## 6.5 Research contributions

This study was undertaken with a broad goal of developing miniaturized  $\mu$ PADs for analytical testing and medical diagnosis. Significant research contributions were made on the way to achieve the goal within the scope of this study. The major contributions of the study are listed below:

1. A new fabrication technique was developed which facilitated the fabrication of inexpensive, compact and miniaturized  $\mu$ PADs. The fabrication technique offered the highest fabrication resolution ever reported in the literature and the technique will enable the fabrication of inexpensive and miniaturized  $\mu$ PADs using a wide range of paper materials.
2. For the first time, it was investigated how the physical properties of the paper

materials limit the miniaturization process. These findings will help in the selection of paper materials based on the dimension of the smallest feature used in the design of the compact and miniaturized  $\mu$ PADs.

3. The miniaturization of  $\mu$ PAD requires the understanding of flow characteristic through small scale features. For the first time, flow through microscale channels were investigated and compared with flow characteristics of larger scale channels.
4. A new design of miniaturized LFA-type  $\mu$ PAD was developed which is suitable for analysing a small sample volume. The devices were fabricated on a single sheet of foil backed paper materials using the newly developed technique which will eliminate the challenges of the miniaturization associated with the conventional fabrication technique used for LFA-type  $\mu$ PAD.
5. A counting-based colorimetric test readout technique was designed and tested with the miniaturized LFA-type  $\mu$ PAD by performing the glucose test and human IgE test. A small volume of simulated blood plasma sample ( $\leq 1 \mu\text{L}$ ) was used in the tests where the conventional LFA-type  $\mu$ PAD required a relatively large volume of sample (25 to 120  $\mu\text{L}$ ) to perform similar counting-based tests.

## 6.6 Recommendation for the future works

The design of compact and miniaturized  $\mu$ PAD reported in chapter 3 and the miniaturized LFA-type  $\mu$ PAD reported in chapter 5 can be used to develop test devices for the wide range of analytical tests including medical diagnosis and environmental monitoring. The chemistry used for a wide range of analytical tests (e.g. blood tests, urine tests, drug tests, poison tests, water quality test etc.) are already established but most of them are designed and calibrated for lab-based tests which require specific lab apparatus and well-trained operators. Therefore, there is a huge opportunity to develop similar miniaturized  $\mu$ PADs reported in this thesis by utilizing the existing chemistry of lab-based tests or by modifying them to make it compatible with the paper materials used in the  $\mu$ PADs.

The miniaturized LFA-type  $\mu$ PAD reported in this thesis can be integrated with a user-friendly sample collection system, such as microneedles. The sample volume should be controlled in the counting-based tests which can be done by incorporating microfluidic valves in the sample collection and input system of the  $\mu$ PAD.



# Bibliography

- [1] A. K. Yetisen, M. S. Akram, and C. R. Lowe. Paper-based microfluidic point-of-care diagnostic devices. *Lab on a Chip*, 13(12):2210–2251, 2013.
- [2] C. Parolo and A. Merkoi. Paper-based nanobiosensors for diagnostics. *Chemical Society Reviews*, 42(2):450–457, 2012.
- [3] E. W. Nery and L. T. Kubota. Sensing approaches on paper-based devices: a review. *Analytical and Bioanalytical Chemistry*, 405:7573+, 2013.
- [4] A. W. Martinez, S. T. Phillips, G. M. Whitesides, and E. Carrilho. Diagnostics for the developing world: microfluidic paper-based analytical devices. *Analytical chemistry*, 82(1):3–10, 2009.
- [5] X. Li and X. Liu. A microfluidic paper-based origami nanobiosensor for label-free, ultrasensitive immunoassays. *Advanced Healthcare Materials*, 5(11):1326–1335, 2016.
- [6] L. Li, X. Huang, W. Liu, and W. Shen. Control performance of paper-based blood analysis devices through paper structure design. *ACS Appl. Mater. Interfaces*, 6(23):21624–21631, 2014.

- [7] J. Hu, S. Wang, L. Wang, F. Li, B. Pingguan-Murphy, T. J. Lu, and F. Xu. Advances in paper-based point-of-care diagnostics. *Biosensors and Bioelectronics*, 54:585–597, 2014.
- [8] F. Figueredo, P. T. Garcia, E. Cortn, and W. K. T. Coltro. Enhanced analytical performance of paper microfluidic devices by using fe<sub>3</sub>o<sub>4</sub> nanoparticles, mwent, and graphene oxide. *ACS Appl. Mater. Interfaces*, 8(1):11–15, 2016.
- [9] N. A. Meredith, C. Quinn, D. M. Cate, T. H. Reilly, J. Volckens, and C. S. Henry. Paper-based analytical devices for environmental analysis. *Analyst*, 141(6):1874–1887, 2016.
- [10] P. Nath, R. K. Arun, and N. Chanda. A paper based microfluidic device for the detection of arsenic using a gold nanosensor. *RSC Advances*, 4(103):59558–59561, 2014.
- [11] S. Z. Hossain, C. Ozimok, C. Sicard, S. D. Aguirre, M. M. Ali, Y. Li, and J. D. Brennan. Multiplexed paper test strip for quantitative bacterial detection. *Anal. Bioanal. Chem.*, 403(6):1567–1576, 2012.
- [12] M. Chowdury, N. Walji, M. A. Mahmud, and B. MacDonald. based microfluidic device with a gold nanosensor to detect arsenic contamination of groundwater in bangladesh. *Micromachines*, 8(3):71, 2017.
- [13] B. M. Jayawardane, W. Wongwilai, K. Grudpan, S. Kolev, M. Heaven, D. Nash, and I. McKelvie. Evaluation and application of a paper-based device for

- the determination of reactive phosphate in soil solution. *J. Environ. Qual.*, 43(3):1081–1085, 2014.
- [14] Y. Kim, G. Jang, and T. S. Lee. New fluorescent metal-ion detection using a paper-based sensor strip containing tethered rhodamine carbon nanodots. *ACS Appl. Mater. Interfaces*, 7(28):15649–15657, 2015. PMID: 26112227.
- [15] S. M. Z. Hossain, R. E. Luckham, M. J. McFadden, and J. D. Brennan. Reagentless bidirectional lateral flow bioactive paper sensors for detection of pesticides in beverage and food samples. *Anal. Chem.*, 81(21):9055–9064, 2009.
- [16] M. Z. Hua, S. Li, S. Wang, and X. Lu. Detecting chemical hazards in foods using microfluidic paper-based analytical devices ( $\mu$ pads): The real-world application. *Micromachines*, 9(1):32, 2018.
- [17] L. S. A. Busa, S. Mohammadi, M. Maeki, A. Ishida, H. Tani, and M. Tokeshi. Advances in microfluidic paper-based analytical devices for food and water analysis. *Micromachines*, 7(5):86, 2016.
- [18] K. L. Peters, I. Corbin, L. M. Kaufman, K. Zreibe, L. Blanes, and B. R. McCord. Simultaneous colorimetric detection of improvised explosive compounds using microfluidic paper-based analytical devices ( $\mu$ pads). *Anal. Methods*, 7(1):63–70, 2015.
- [19] J. Campbell, J. Balhoff, G. Landwehr, S. Rahman, M. Vaithyanathan, and A. Melvin. Microfluidic and paper-based devices for disease detection and diagnostic research. *International journal of molecular sciences*, 19(9):2731, 2018.

- [20] A. W. Martinez, S. T. Phillips, G. M. Whitesides, and E. Carrilho. Diagnostics for the developing world: Microfluidic paper-based analytical devices. *Anal. Chem.*, 82(1):3–10, 2009.
- [21] A. R. Wheeler, W. R. Throdsset, R. J. Whelan, A. M. Leach, R. N. Zare, Y. H. Liao, K. Farrell, I. D. Manger, and A. Daridon. Microfluidic device for single-cell analysis. *Analytical chemistry*, 75(14):3581–3586, 2003.
- [22] I. W. Schie, J. Ruuger, A. S. Mondol, A. Ramoji, U. Neugebauer, C. Krafft, and J. Popp. High-throughput screening raman spectroscopy platform for label-free cellomics. *Analytical chemistry*, 90(3):2023–2030, 2018.
- [23] X. Yu, Y. Xia, Y. Tang, W.-L. Zhang, Y.-T. Yeh, H. Lu, and S.-Y. Zheng. A nanostructured microfluidic immunoassay platform for highly sensitive infectious pathogen detection. *Small*, 13(24):1700425, 2017.
- [24] C. Eid and J. G. Santiago. Assay for listeria monocytogenes cells in whole blood using isotachopheresis and recombinase polymerase amplification. *Analyt.*, 142(1):48–54, 2017.
- [25] Y. Tang, Z. Wang, Z. Li, J. Kim, Y. Deng, Y. Li, J. R. Heath, W. Wei, S. Lu, and Q. Shi. High-throughput screening of rare metabolically active tumor cells in pleural effusion and peripheral blood of lung cancer patients. *Proceedings of the National Academy of Sciences*, 114(10):2544–2549, 2017.

- [26] E. Samiei, M. Tabrizian, and M. Hoorfar. A review of digital microfluidics as portable platforms for lab-on a-chip applications. *Lab on a Chip*, 16(13):2376–2396, 2016.
- [27] K. Yamada, H. Shibata, K. Suzuki, and D. Citterio. Toward practical application of paper-based microfluidics for medical diagnostics: state-of-the-art and challenges. *Lab on a Chip*, 17(7):1206–1249, 2017.
- [28] E. Carrilho, A. W. Martinez, and G. M. Whitesides. Understanding wax printing: A simple micropatterning process for paper-based microfluidics. *Anal. Chem.*, 81(16):7091–7095, 2009.
- [29] M. Jauset-Rubio, M. S. El-Shahawi, A. S. Bashammakh, A. O. Alyoubi, K. Ciara, et al. Advances in aptamers-based lateral flow assays. *TrAC Trends in Analytical Chemistry*, 97:385–398, 2017.
- [30] C. G. Li, H.-A. Joung, H. Noh, M.-B. Song, M.-G. Kim, and H. Jung. One-touch-activated blood multidagnostic system using a minimally invasive hollow microneedle integrated with a paper-based sensor. *Lab on a Chip*, 15(16):3286–3292, 2015.
- [31] S. A. Klasner, A. K. Price, K. W. Hoeman, R. S. Wilson, K. J. Bell, and C. T. Culbertson. Paper based microfluidic devices for analysis of clinically relevant analytes present in urine and saliva. *Analytical and bioanalytical chemistry*, 397(5):1821–1829, 2010.

- [32] S. Corrie, J. Coffey, J. Islam, K. Markey, and M. Kendall. Blood, sweat, and tears: Developing clinically relevant protein biosensors for integrated body fluid analysis. *Analyst*, 140(13):4350–4364, 2015.
- [33] V. Oncescu, D. O’Dell, and D. Erickson. Smartphone based health accessory for colorimetric detection of biomarkers in sweat and saliva. *Lab on a Chip*, 13(16):3232–3238, 2013.
- [34] A. Koh, D. Kang, Y. Xue, S. Lee, R. M. Pielak, J. Kim, T. Hwang, S. Min, A. Banks, P. Bastien, et al. A soft, wearable microfluidic device for the capture, storage, and colorimetric sensing of sweat. *Science translational medicine*, 8(366):366ra165–366ra165, 2016.
- [35] O. Mosley, L. Melling, M. D. Tarn, C. Kemp, M. M. Esfahani, N. Pamme, and K. J. Shaw. Sample introduction interface for on-chip nucleic acid-based analysis of helicobacter pylori from stool samples. *Lab on a Chip*, 16(11):2108–2115, 2016.
- [36] E. Gabriel, P. Garcia, F. Lopes, and W. Coltro. Paper based colorimetric biosensor for tear glucose measurements. *Micromachines*, 8(4):104, 2017.
- [37] J. Li and J. Macdonald. Multiplexed lateral flow biosensors: Technological advances for radically improving point-of-care diagnoses. *Biosensors and Bioelectronics*, 83:177–192, 2016.

- [38] J. C. Jokerst, J. A. Adkins, B. Bisha, M. M. Mentele, L. D. Goodridge, and C. S. Henry. Development of a paper-based analytical device for colorimetric detection of select foodborne pathogens. *Anal. Chem.*, 84(6):2900–2907, 2012.
- [39] A. W. Martinez, S. T. Phillips, M. J. Butte, and G. M. Whitesides. Patterned paper as a platform for inexpensive, low-volume, portable bioassays. *Angewandte Chemie International Edition*, 46(8):1318–1320, 2007.
- [40] C. Zhao and X. Liu. A portable paper-based microfluidic platform for multiplexed electrochemical detection of human immunodeficiency virus and hepatitis c virus antibodies in serum. *Biomicrofluidics*, 10(2):024119, 2016.
- [41] W. Dungchai, O. Chailapakul, and C. S. Henry. Electrochemical detection for paper-based microfluidics. *Analytical chemistry*, 81(14):5821–5826, 2009.
- [42] Z. Nie, C. A. Nijhuis, J. Gong, X. Chen, A. Kumachev, A. W. Martinez, M. Narovlyansky, and G. M. Whitesides. Electrochemical sensing in paper-based microfluidic devices. *Lab on a Chip*, 10(4):477–483, 2010.
- [43] W. Alahmad, K. Uraisin, D. Nacapricha, and T. Kaneta. A miniaturized chemiluminescence detection system for a microfluidic paper-based analytical device and its application to the determination of chromium(iii). *Analytical Methods*, 8(27):5414–5420, 2016.
- [44] L. Ge, S. Wang, X. Song, S. Ge, and J. Yu. 3d origami-based multifunction-integrated immunodevice: low-cost and multiplexed sandwich chemilumines-

- cence immunoassay on microfluidic paper-based analytical device. *Lab on a Chip*, 12(17):3150–3158, 2012.
- [45] J. L. Delaney, C. F. Hogan, J. Tian, and W. Shen. Electrogenated chemiluminescence detection in paper-based microfluidic sensors. *Analytical chemistry*, 83(4):1300–1306, 2011.
- [46] N. K. Thom, G. G. Lewis, K. Yeung, and S. T. Phillips. Quantitative fluorescence assays using a self-powered paper-based microfluidic device and a camera-equipped cellular phone. *RSC Advances*, 4(3):1334–1340, 2014.
- [47] C.-C. Liu, Y.-N. Wang, L.-M. Fu, and Y.-H. Huang. Microfluidic paper-based chip platform for formaldehyde concentration detection. *Chemical Engineering Journal*, 332:695–701, 2018.
- [48] L. Liang, M. Su, L. Li, F. Lan, G. Yang, S. Ge, J. Yu, and X. Song. Aptamer-based fluorescent and visual biosensor for multiplexed monitoring of cancer cells in microfluidic paper-based analytical devices. *Sensors and Actuators B: Chemical*, 229:347–354, 2016.
- [49] S. Chang, J. Seo, S. Hong, D.-G. Lee, and W. Kim. Dynamics of liquid imbibition through paper with intra-fibre pores. *Journal of Fluid Mechanics*, 845:36–50, 2018.
- [50] B. D. MacDonald. Flow of liquids through paper. *Journal of Fluid Mechanics*, 852:1–4, 2018.



- [51] E. Fu, B. Lutz, P. Kauffman, and P. Yager. Controlled reagent transport in disposable 2d paper networks. *Lab Chip*, 10(7):918–920, 2010.
- [52] N. Walji and B. MacDonald. Influence of geometry and surrounding conditions on fluid flow in paper-based devices. *Micromachines*, 7(5):73, 2016.
- [53] C. Castro, C. Rosillo, and H. Tsutsui. Characterizing effects of humidity and channel size on imbibition in paper-based microfluidic channels. *Microfluid. Nanofluid.*, 21(2):21, 2017.
- [54] S. Hong and W. Kim. Dynamics of water imbibition through paper channels with wax boundaries. *Microfluid. Nanofluid.*, 19(4):845–853, 2015.
- [55] A. W. Martinez, S. T. Phillips, G. M. Whitesides, and E. Carrilho. Diagnostics for the developing world: microfluidic paper-based analytical devices, 2009.
- [56] D. M. Cate, S. D. Noblitt, J. Volckens, and C. S. Henry. Multiplexed paper analytical device for quantification of metals using distance-based detection. *Lab on a chip*, 15(13):2808–2818, 2015.
- [57] S. J. Vella, P. Beattie, R. Cademartiri, A. Laromaine, A. W. Martinez, S. T. Phillips, K. A. Mirica, and G. M. Whitesides. Measuring markers of liver function using a micropatterned paper device designed for blood from a fingerstick. *Anal. Chem.*, 84(6):2883–2891, 2012.
- [58] C. G. Li, C. Y. Lee, K. Lee, and H. Jung. An optimized hollow microneedle for minimally invasive blood extraction. *Biomed. Microdevices*, 15(1):17–25, 2013.

- [59] K. Tsuchiya, S. Jinnin, H. Yamamoto, Y. Uetsuji, and E. Nakamachi. Design and development of a biocompatible painless microneedle by the ion sputtering deposition method. *Precision Engineering*, 34(3):461–466, 2010.
- [60] T. Li, A. Barnett, K. L. Rogers, and Y. B. Gianchandani. A blood sampling microsystem for pharmacokinetic applications: Design, fabrication, and initial results. *Lab on a Chip*, 9(24):3495–3503, 2009.
- [61] M. Haq, E. Smith, D. N. John, M. Kalavala, C. Edwards, A. Anstey, A. Morrissey, and J. C. Birchall. Clinical administration of microneedles: skin puncture, pain and sensation. *Biomedical microdevices*, 11(1):35–47, 2009.
- [62] A. D. Association et al. Screening for type 2 diabetes. *Diabetes care*, 27:S11, 2004.
- [63] O. Zetterstöm and S. Johansson. Ige concentrations measured by prist® in serum of healthy adults and in patients with respiratory allergy: a diagnostic approach. *Allergy*, 36(8):537–547, 1981.
- [64] A. Nieters, A. Luczyńska, S. Becker, N. Becker, R. Vermeulen, K. Overvad, K. Aleksandrova, H. Boeing, P. Lagiou, D. Trichopoulos, et al. Prediagnostic immunoglobulin e levels and risk of chronic lymphocytic leukemia, other lymphomas and multiple myeloma-results of the european prospective investigation into cancer and nutrition. *Carcinogenesis*, 35(12):2716–2722, 2014.
- [65] S. H. Olson, M. Hsu, J. L. Wiemels, P. M. Bracci, M. Zhou, J. Patoka, W. R. Reisacher, J. Wang, R. C. Kurtz, D. T. Silverman, et al. Serum immunoglobulin

- e and risk of pancreatic cancer in the prostate, lung, colorectal, and ovarian cancer screening trial. *Cancer Epidemiology and Prevention Biomarkers*, 2014.
- [66] H. Yagoda. Applications of confined spot tests in analytical chemistry: preliminary paper. *Industrial & Engineering Chemistry Analytical Edition*, 9(2):79–82, 1937.
- [67] R. Müller and D. Clegg. Automatic paper chromatography. *Analytical Chemistry*, 21(9):1123–1125, 1949.
- [68] Z. W. Zhong, Z. P. Wang, and G. X. D. Huang. Investigation of wax and paper materials for the fabrication of paper-based microfluidic devices. *Microsyst. Technol.*, 18(5):649–659, 2012.
- [69] Y. Lu, W. Shi, J. Qin, and B. Lin. Fabrication and characterization of paper-based microfluidics prepared in nitrocellulose membrane by wax printing. *Anal. Chem.*, 82(1):329–335, 2010.
- [70] Y. Lu, W. Shi, L. Jiang, J. Qin, and B. Lin. Rapid prototyping of paper-based microfluidics with wax for lowcost, portable bioassay. *Electrophoresis*, 30(9):1497–1500, 2009.
- [71] W. Dungchai, O. Chailapakul, and C. S. Henry. A low-cost, simple, and rapid fabrication method for paper-based microfluidics using wax screen-printing. *Analyst*, 136(1):77–82, 2011.

- [72] Y. Sameenoi, P. N. Nongkai, S. Nouanthavong, C. S. Henry, and D. Nacapricha. One-step polymer screen-printing for microfluidic paper-based analytical device ([small mu ]pad) fabrication. *Analyst*, 139(24):6580–6588, 2014.
- [73] J. Nie, Y. Zhang, L. Lin, C. Zhou, S. Li, L. Zhang, and J. Li. Low-cost fabrication of paper-based microfluidic devices by one-step plotting. *Analytical Chemistry*, 84(15):6331–6335, 2012.
- [74] S. Oyola-Reynoso, A. P. Heim, J. Halbertsma-Black, C. Zhao, I. D. Tevis, S. nar, R. Cademartiri, X. Liu, J.-F. Bloch, and M. M. Thuo. Draw your assay: Fabrication of low-cost paper-based diagnostic and multi-well test zones by drawing on a paper. *Talanta*, 144:289–293, 2015.
- [75] X. Li, J. Tian, T. Nguyen, and W. Shen. Paper-based microfluidic devices by plasma treatment. *Analytical chemistry*, 80(23):9131–9134, 2008.
- [76] V. F. Curto, N. Lopez-Ruiz, L. F. Capitan-Vallvey, A. J. Palma, F. Benito-Lopez, and D. Diamond. Fast prototyping of paper-based microfluidic devices by contact stamping using indelible ink. *RSC Advances*, 3(41):18811–18816, 2013.
- [77] P. de Tarso Garcia, T. M. G. Cardoso, C. D. Garcia, E. Carrilho, and W. K. T. Coltro. A handheld stamping process to fabricate microfluidic paper-based analytical devices with chemically modified surface for clinical assays. *RSC Advances*, 4(71):37637–37644, 2014.

- [78] X. Li, J. Tian, G. Garnier, and W. Shen. Fabrication of paper-based microfluidic sensors by printing. *Colloids and surfaces B: Biointerfaces*, 76(2):564–570, 2010.
- [79] J. Wang, M. R. N. Monton, X. Zhang, C. D. Filipe, R. Pelton, and J. D. Brennan. Hydrophobic solgel channel patterning strategies for paper-based microfluidics. *Lab on a Chip*, 14(4):691–695, 2014.
- [80] K. Abe, K. Suzuki, and D. Citterio. Inkjet-printed microfluidic multianalyte chemical sensing paper. *Analytical Chemistry*, 80(18):6928–6934, 2008.
- [81] J. Olkkonen, K. Lehtinen, and T. Erho. Flexographically printed fluidic structures in paper. *Analytical chemistry*, 82(24):10246–10250, 2010.
- [82] G. Chitnis, Z. Ding, C.-L. Chang, C. A. Savran, and B. Ziaie. Laser-treated hydrophobic paper: an inexpensive microfluidic platform. *Lab on a Chip*, 11(6):1161–1165, 2011.
- [83] C. L. Sones, I. N. Katis, P. J. W. He, B. Mills, M. F. Namiq, P. Shardlow, M. Ibsen, and R. W. Eason. Laser-induced photo-polymerisation for creation of paper-based fluidic devices. *Lab on a Chip*, 14(23):4567–4574, 2014.
- [84] E. M. Fenton, M. R. Mascarenas, G. P. Loopez, and S. S. Sibbett. Multiplex lateral-flow test strips fabricated by two-dimensional shaping. *ACS applied materials & interfaces*, 1(1):124–129, 2008.
- [85] C. Renault, X. Li, S. E. Fosdick, and R. M. Crooks. Hollow-channel paper analytical devices. *Analytical Chemistry*, 85(16):7976–7979, 2013.

- [86] P. Spicar-Mihalic, B. Toley, J. Houghtaling, T. Liang, P. Yager, and E. Fu. Co<sub>2</sub> laser cutting and ablative etching for the fabrication of paper-based devices. *J. Micromech. Microeng.*, 23(6):067003, 2013.
- [87] J. Nie, Y. Liang, Y. Zhang, S. Le, D. Li, and S. Zhang. One-step patterning of hollow microstructures in paper by laser cutting to create microfluidic analytical devices. *The Analyst*, 138(2):671–676, 2013.
- [88] A. W. Martinez, S. T. Phillips, B. J. Wiley, M. Gupta, and G. M. Whitesides. Flash: A rapid method for prototyping paper-based microfluidic devices. *Lab Chip*, 8(12):2146–2150, 2008.
- [89] P. J. He, I. N. Katis, R. W. Eason, and C. L. Sones. Laser-based patterning for fluidic devices in nitrocellulose. *Biomicrofluidics*, 9(2):026503, 2015.
- [90] J. Songok, M. Tuominen, H. Teisala, J. Haapanen, J. Mäkelä, J. Kuusipalo, and M. Toivakka. Paper-based microfluidics: Fabrication technique and dynamics of capillary-driven surface flow. *ACS Appl. Mater. Interfaces*, 6(22):20060–20066, 2014.
- [91] J. Songok and M. Toivakka. Enhancing capillary-driven flow for paper-based microfluidic channels. *ACS Appl. Mater. Interfaces*, 8(44):30523–30530, 2016.
- [92] E. W. Washburn. The dynamics of capillary flow. *The Phys. Rev.*, 17(3):273–283, 1921.

- [93] A. Böhm, F. Carstens, C. Trieb, S. Schabel, and M. Biesalski. Engineering microfluidic papers: Effect of fiber source and paper sheet properties on capillary-driven fluid flow. *Microfluid. Nanofluid.*, 16(5):789–799, 2014.
- [94] E. Elizalde, R. Urteaga, and C. L. A. Berli. Precise capillary flow for paper-based viscometry. *Microfluid. Nanofluid.*, 20(10):135, 2016.
- [95] J. Songok and M. Toivakka. Controlling capillary-driven surface flow on a paper-based microfluidic channel. *Microfluid. Nanofluid.*, 20(4):63, 2016.
- [96] A. W. Martinez, S. T. Phillips, E. Carrilho, S. W. Thomas III, H. Sindi, and G. M. Whitesides. Simple telemedicine for developing regions: camera phones and paper-based microfluidic devices for real-time, off-site diagnosis. *Analytical chemistry*, 80(10):3699–3707, 2008.
- [97] O. Mudanyali, S. Dimitrov, U. Sikora, S. Padmanabhan, I. Navruz, and A. Ozcan. Integrated rapid-diagnostic-test reader platform on a cellphone. *Lab on a Chip*, 12(15):2678–2686, 2012.
- [98] C. T. Gerold, E. Bakker, and C. S. Henry. Selective distance-based k<sup>+</sup> quantification on paper-based microfluidics. *Analytical Chemistry*, 90(7):4894–4900, 2018.
- [99] Y. Chen, W. Chu, W. Liu, and X. Guo. Distance-based carcinoembryonic antigen assay on microfluidic paper immunodevice. *Sensors and Actuators B: Chemical*, 260:452–459, 2018.

- [100] R. Pratiwi, M. P. Nguyen, S. Ibrahim, N. Yoshioka, C. S. Henry, and D. H. Tjahjono. A selective distance-based paper analytical device for copper(ii) determination using a porphyrin derivative. *Talanta*, 174:493–499, 2017.
- [101] X. Wei, T. Tian, S. Jia, Z. Zhu, Y. Ma, J. Sun, Z. Lin, and C. J. Yang. Microfluidic distance readout sweet hydrogel integrated paper-based analytical device ( $\mu$ dish-pad) for visual quantitative point-of-care testing. *Analytical Chemistry*, 88(4):2345–2352, 2016.
- [102] Y.-T. Chen and J.-T. Yang. Detection of an amphiphilic biosample in a paper microchannel based on length. *Biomedical Microdevices*, 17(3):52, 2015.
- [103] K. Yamada, T. G. Henares, K. Suzuki, and D. Citterio. Distance-based tear lactoferrin assay on microfluidic paper device using interfacial interactions on surface-modified cellulose. *ACS Appl. Mater. Interfaces*, 7(44):24864–24875, 2015. PMID: 26488371.
- [104] Y. Sameenoi, P. N. Nongkai, S. Nouanthavong, C. S. Henry, and D. Nacapricha. One-step polymer screen-printing for microfluidic paper-based analytical device ( $\mu$ pad) fabrication. *Analyst*, 139(24):6580–6588, 2014.
- [105] H.-Y. Yin, P.-T. Chu, W.-C. Tsai, and H.-W. Wen. Development of a barcode-style lateral flow immunoassay for the rapid semi-quantification of gliadin in foods. *Food chemistry*, 192:934–942, 2016.



- [106] C. Fang, Z. Chen, L. Li, and J. Xia. Barcode lateral flow immunochromatographic strip for prostate acid phosphatase determination. *Journal of pharmaceutical and biomedical analysis*, 56(5):1035–1040, 2011.
- [107] K.-K. Fung, C. P.-Y. Chan, and R. Renneberg. Development of enzyme-based bar code-style lateral-flow assay for hydrogen peroxide determination. *Analytica chimica acta*, 634(1):89–95, 2009.
- [108] K.-K. Fung, C. P.-Y. Chan, and R. Renneberg. Development of a creatinine enzyme-based bar-code-style lateral-flow assay. *Analytical and bioanalytical chemistry*, 393(4):1281–1287, 2009.
- [109] W. Leung, C. P. Chan, T. H. Rainer, M. Ip, G. W. Cautherley, and R. Renneberg. Infectcheck crp barcode-style lateral flow assay for semi-quantitative detection of c-reactive protein in distinguishing between bacterial and viral infections. *Journal of immunological methods*, 336(1):30–36, 2008.
- [110] J. Cho and S. Paek. Semiquantitative, bar code version of immunochromatographic assay system for human serum albumin as model analyte. *Biotechnology and bioengineering*, 75(6):725–732, 2001.
- [111] S. C. Lou, C. Patel, S. Ching, and J. Gordon. One-step competitive immunochromatographic assay for semiquantitative determination of lipoprotein (a) in plasma. *Clinical chemistry*, 39(4):619–624, 1993.

- [112] M. A. Mahmud, E. J. M. Blondeel, M. Kaddoura, and B. D. MacDonald. Creating compact and microscale features in paper-based devices by laser cutting. *Analyst*, 141(23):6449–6454, 2016.
- [113] M. A. Mahmud, E. J. Blondeel, M. Kaddoura, and B. D. MacDonald. Features in microfluidic paper-based devices made by laser cutting: How small can they be? *Micromachines*, 9(5):220, 2018.
- [114] M. A. Mahmud, E. J. Blondeel, and B. D. MacDonald. Miniaturized counting-based microfluidic paper-based analytical devices for semi-quantitative test readouts. [*Manuscript submitted for publication*].

# Appendices

# Appendix A

## Permissions for reproducing author's own work

Part of Chapter 3 and some portions from other chapters are reproduced from Ref. [112] with permission from the 'Royal Society of Chemistry', according to the publisher an author is allowed to reproduce his published article in the thesis. The copyright policy of the publisher is as follows:

### **Author reusing their own work published by the Royal Society of Chemistry**

You do not need to request permission to reuse your own figures, diagrams, etc, that were originally published in a Royal Society of Chemistry publication. However, permission should be requested for use of the whole article or chapter except if **reusing it in a thesis**. If you are including an article or book chapter published by us in your thesis please ensure that your co-authors are aware of this.

Reuse of material that was published originally by the Royal Society of Chemistry must be accompanied by the appropriate acknowledgement of the publication. The form of the acknowledgement is dependent on the journal in which it was published originally, as detailed in 'Acknowledgements'.

Part of chapter 3, 4 and some portions from other chapters are reproduced from Ref. [113] which is author's own published work. Ref. [113] was published by MDPI where authors retain the copyright and are allowed to reproduce the work in the thesis.



Md Mahmud <md.mahmud@uoit.net>

---

### Use of published work in thesis

---

**support** <support@mdpi.com>  
To: Md Mahmud <md.mahmud@uoit.net>

Thu, Jan 31, 2019 at 11:07 PM

Dear Md. Almostasim,

Thank you for your email. As author of the paper and given that you are the owner of the copyrights, you are entitled to reproduce it in other publications. Please only remember to refer to the work properly. Hope this can help.

Best Regards,

Dimity  
MDPI Support

--

Ms. Dimity Wang  
MDPI Branch Office, Beijing  
Skype: live:8d434a9d1fe4f42f  
E-Mail: [dimity.wang@mdpi.com](mailto:dimity.wang@mdpi.com)

Disclaimer: The information and files contained in this message are confidential and intended solely for the use of the individual or entity to whom they are addressed. If you have received this message in error, please notify me and delete this message from your system. You may not copy this message in its entirety or in part, or disclose its contents to anyone.

[Quoted text hidden]

## Appendix B

### Permission for reproducing figures from literature

## Permission for Figure 1.3

ELSEVIER LICENSE  
TERMS AND CONDITIONS

Apr 23, 2019

This Agreement between Md. A Mahmud ("You") and Elsevier ("Elsevier") consists of your license details and the terms and conditions provided by Elsevier and Copyright Clearance Center.

License Number	4575010803970
License date	Apr 23, 2019
Licensed Content Publisher	Elsevier
Licensed Content Publication	TrAC Trends in Analytical Chemistry
Licensed Content Title	Advances in aptamers-based lateral flow assays
Licensed Content Author	Miriam Jauset-Rubio, Mohammad S. El-Shahawi, Abdulaziz S. Bashammakh, Abdulrahman O. Alyoubi, Ciara K. O'Sullivan
Licensed Content Date	Dec 1, 2017
Licensed Content Volume	97
Licensed Content Issue	n/a
Licensed Content Pages	14
Start Page	385
End Page	398
Type of Use	reuse in a thesis/dissertation
Intended publisher of new work	other
Portion	figures/tables/illustrations
Number of figures/tables/illustrations	1
Format	both print and electronic
Are you the author of this Elsevier article?	No
Will you be translating?	No
Original figure numbers	Fig.1
Title of your thesis/dissertation	Miniaturization of Features in Microfluidic Paper-based Analytical Devices for User-friendly Testing and Diagnosis Using Small Sample Volume
Expected completion date	Apr 2019
Estimated size (number of pages)	115
Requestor Location	Md. A Mahmud 2000 Simcoe St N FEAS, UOIT  Oshawa, ON L1G 0C5 Canada Attn:
Publisher Tax ID	GB 494 6272 12
Total	0.00 USD

## Permission for Figure 1.4

**ELSEVIER LICENSE  
TERMS AND CONDITIONS**

Apr 23, 2019

This Agreement between Md. A Mahmud ("You") and Elsevier ("Elsevier") consists of your license details and the terms and conditions provided by Elsevier and Copyright Clearance Center.

License Number	4574980209914
License date	Apr 23, 2019
Licensed Content Publisher	Elsevier
Licensed Content Publication	Biosensors and Bioelectronics
Licensed Content Title	Multiplexed lateral flow biosensors: Technological advances for radically improving point-of-care diagnoses
Licensed Content Author	Jia Li, Joanne Macdonald
Licensed Content Date	Sep 15, 2016
Licensed Content Volume	83
Licensed Content Issue	n/a
Licensed Content Pages	16
Start Page	177
End Page	192
Type of Use	reuse in a thesis/dissertation
Intended publisher of new work	other
Portion	figures/tables/illustrations
Number of figures/tables/illustrations	1
Format	both print and electronic
Are you the author of this Elsevier article?	No
Will you be translating?	No
Original figure numbers	Fig.1
Title of your thesis/dissertation	Miniaturization of Features in Microfluidic Paper-based Analytical Devices for User-friendly Testing and Diagnosis Using Small Sample Volume
Expected completion date	Apr 2019
Estimated size (number of pages)	115
Requestor Location	Md. A Mahmud 2000 Simcoe St N FEAS, UOIT  Oshawa, ON L1G 0C5 Canada Attn:
Publisher Tax ID	GB 494 6272 12
Total	0.00 USD



## Permission for Figure 1.5(a)

**JOHN WILEY AND SONS LICENSE  
TERMS AND CONDITIONS**



Apr 23, 2019

---

This Agreement between Md. A Mahmud ("You") and John Wiley and Sons ("John Wiley and Sons") consists of your license details and the terms and conditions provided by John Wiley and Sons and Copyright Clearance Center.

License Number	4574981402275
License date	Apr 23, 2019
Licensed Content Publisher	John Wiley and Sons
Licensed Content Publication	Angewandte Chemie International Edition
Licensed Content Title	Patterned Paper as a Platform for Inexpensive, Low-Volume, Portable Bioassays
Licensed Content Author	Andres W. Martinez, Scott T. Phillips, Manish J. Butte, et al
Licensed Content Date	Feb 5, 2007
Licensed Content Volume	46
Licensed Content Issue	8
Licensed Content Pages	3
Type of use	Dissertation/Thesis
Requestor type	University/Academic
Format	Print and electronic
Portion	Figure/table
Number of figures/tables	2
Original Wiley figure/table number(s)	Scheme 1, Figure 1
Will you be translating?	No
Title of your thesis / dissertation	Miniaturization of Features in Microfluidic Paper-based Analytical Devices for User-friendly Testing and Diagnosis Using Small Sample Volume
Expected completion date	Apr 2019
Expected size (number of pages)	115
Requestor Location	Md. A Mahmud 2000 Simcoe St N FEAS, UOIT  Oshawa, ON L1G 0C5 Canada Attn:
Publisher Tax ID	EU826007151
Total	0.00 USD

Permission for Figure 1.5(b)

**Title:** Electrochemical Detection for Paper-Based Microfluidics

**Author:** Wijitar Dungchai, Orawon Chailapakul, Charles S. Henry

**Publication:** Analytical Chemistry

**Publisher:** American Chemical Society

**Date:** Jul 1, 2009

Copyright © 2009, American Chemical Society

Logged in as:  
Md. Mahmud  
Account #:  
3001407692

[LOGOUT](#)

[Home](#) [Account Info](#) [Help](#)

**PERMISSION/LICENSE IS GRANTED FOR YOUR ORDER AT NO CHARGE**

This type of permission/license, instead of the standard Terms & Conditions, is sent to you because no fee is being charged for your order. Please note the following:

- Permission is granted for your request in both print and electronic formats, and translations.
- If figures and/or tables were requested, they may be adapted or used in part.
- Please print this page for your records and send a copy of it to your publisher/graduate school.
- Appropriate credit for the requested material should be given as follows: "Reprinted (adapted) with permission from (COMPLETE REFERENCE CITATION). Copyright (YEAR) American Chemical Society." Insert appropriate information in place of the capitalized words.
- One-time permission is granted only for the use specified in your request. No additional uses are granted (such as derivative works or other editions). For any other uses, please submit a new request.

If credit is given to another source for the material you requested, permission must be obtained from that source.

[BACK](#)

[CLOSE WINDOW](#)

Copyright © 2019 Copyright Clearance Center, Inc. All Rights Reserved. [Privacy statement](#). [Terms and Conditions](#).  
Comments? We would like to hear from you. E-mail us at [customercare@copyright.com](mailto:customercare@copyright.com)

## Permission for Figure 1.5(c)

**ELSEVIER LICENSE  
TERMS AND CONDITIONS**



Apr 23, 2019

---


This Agreement between Md. A Mahmud ("You") and Elsevier ("Elsevier") consists of your license details and the terms and conditions provided by Elsevier and Copyright Clearance Center.

License Number	4574980423057
License date	Apr 23, 2019
Licensed Content Publisher	Elsevier
Licensed Content Publication	Chemical Engineering Journal
Licensed Content Title	Microfluidic paper-based chip platform for formaldehyde concentration detection
Licensed Content Author	Chan-Chiung Liu, Yao-Nan Wang, Lung-Ming Fu, Yu-Han Huang
Licensed Content Date	Jan 15, 2018
Licensed Content Volume	332
Licensed Content Issue	n/a
Licensed Content Pages	7
Start Page	695
End Page	701
Type of Use	reuse in a thesis/dissertation
Intended publisher of new work	other
Portion	figures/tables/illustrations
Number of figures/tables/illustrations	1
Format	both print and electronic
Are you the author of this Elsevier article?	No
Will you be translating?	No
Original figure numbers	Fig. 5
Title of your thesis/dissertation	Miniaturization of Features in Microfluidic Paper-based Analytical Devices for User-friendly Testing and Diagnosis Using Small Sample Volume
Expected completion date	Apr 2019
Estimated size (number of pages)	115
Requestor Location	Md. A Mahmud 2000 Simcoe St N FEAS, UOIT  Oshawa, ON L1G 0C5 Canada Attn:
Publisher Tax ID	GB 494 6272 12
Total	0.00 USD

Permission for Figure 1.5(d)

[Home](#)
[Account Info](#)
[Help](#)

**Title:** Electrogenerated Chemiluminescence Detection in Paper-Based Microfluidic Sensors

**Author:** Jacqui L. Delaney, Conor F. Hogan, Junfei Tian, et al

**Publication:** Analytical Chemistry

**Publisher:** American Chemical Society

**Date:** Feb 1, 2011

Copyright © 2011, American Chemical Society

Logged in as:  
Md. Mahmud  
Account #:  
3001407692

[LOGOUT](#)

**PERMISSION/LICENSE IS GRANTED FOR YOUR ORDER AT NO CHARGE**

This type of permission/license, instead of the standard Terms & Conditions, is sent to you because no fee is being charged for your order. Please note the following:

- Permission is granted for your request in both print and electronic formats, and translations.
- If figures and/or tables were requested, they may be adapted or used in part.
- Please print this page for your records and send a copy of it to your publisher/graduate school.
- Appropriate credit for the requested material should be given as follows: "Reprinted (adapted) with permission from (COMPLETE REFERENCE CITATION). Copyright (YEAR) American Chemical Society." Insert appropriate information in place of the capitalized words.
- One-time permission is granted only for the use specified in your request. No additional uses are granted (such as derivative works or other editions). For any other uses, please submit a new request.

If credit is given to another source for the material you requested, permission must be obtained from that source.

[BACK](#)

[CLOSE WINDOW](#)

## Permission for Figure 1.6(a)

---

**SPRINGER NATURE LICENSE  
TERMS AND CONDITIONS**


---



Apr 23, 2019

---

This Agreement between Md. A Mahmud ("You") and Springer Nature ("Springer Nature") consists of your license details and the terms and conditions provided by Springer Nature and Copyright Clearance Center.

License Number	4574990939618
License date	Apr 23, 2019
Licensed Content Publisher	Springer Nature
Licensed Content Publication	Microfluids and Nanofluids
Licensed Content Title	Dynamics of water imbibition through paper channels with wax boundaries
Licensed Content Author	Seokbin Hong, Wonjung Kim
Licensed Content Date	Jan 1, 2015
Licensed Content Volume	19
Licensed Content Issue	4
Type of Use	Thesis/Dissertation
Requestor type	non-commercial (non-profit)
Format	print and electronic
Portion	figures/tables/illustrations
Number of figures/tables/illustrations	1
Will you be translating?	no
Circulation/distribution	<501
Author of this Springer Nature content	no
Title	Miniaturization of Features in Microfluidic Paper-based Analytical Devices for User-friendly Testing and Diagnosis Using Small Sample Volume
Institution name	n/a
Expected presentation date	Apr 2019
Portions	Fig. 5 (a)
Requestor Location	Md. A Mahmud 2000 Simcoe St N FEAS, UOIT  Oshawa, ON L1G 0C5 Canada Attn:
Total	0.00 USD

Permission for Figure 1.6(b)

**Title:** Diagnostics for the Developing World: Microfluidic Paper-Based Analytical Devices

**Author:** Andres W. Martinez, Scott T. Phillips, George M. Whitesides, et al

**Publication:** Analytical Chemistry

**Publisher:** American Chemical Society

**Date:** Jan 1, 2010

Copyright © 2010, American Chemical Society

Logged in as:  
Md. Mahmud  
Account #:  
3001407692

[LOGOUT](#)

[Home](#) [Account Info](#) [Help](#)

**PERMISSION/LICENSE IS GRANTED FOR YOUR ORDER AT NO CHARGE**

This type of permission/license, instead of the standard Terms & Conditions, is sent to you because no fee is being charged for your order. Please note the following:

- Permission is granted for your request in both print and electronic formats, and translations.
- If figures and/or tables were requested, they may be adapted or used in part.
- Please print this page for your records and send a copy of it to your publisher/graduate school.
- Appropriate credit for the requested material should be given as follows: "Reprinted (adapted) with permission from (COMPLETE REFERENCE CITATION). Copyright (YEAR) American Chemical Society." Insert appropriate information in place of the capitalized words.
- One-time permission is granted only for the use specified in your request. No additional uses are granted (such as derivative works or other editions). For any other uses, please submit a new request.

If credit is given to another source for the material you requested, permission must be obtained from that source.

[BACK](#)

[CLOSE WINDOW](#)

Copyright © 2019 [Copyright Clearance Center, Inc.](#) All Rights Reserved. [Privacy statement](#). [Terms and Conditions](#).  
Comments? We would like to hear from you. E-mail us at [customercare@copyright.com](mailto:customercare@copyright.com)

Permission for Figure 1.7



**Confirmation Number: 11795196**  
**Order Date: 03/01/2019**

---

**Customer Information**

**Customer:** Md, Mahmud  
**Account Number:** 3001407692  
**Organization:** Md, Mahmud  
**Email:** md.mahmud@uoit.net  
**Phone:** +1 (289) 600-6622  
**Payment Method:** Invoice

---

**This is not an invoice**



**Order Details**

[Lab on a chip](#) Billing Status:  
N/A


<p><b>Order detail ID:</b> 71829897  <b>ISSN:</b> 1473-0189  <b>Publication Type:</b> e-Journal  <b>Volume:</b>  <b>Issue:</b>  <b>Start page:</b>  <b>Publisher:</b> ROYAL SOCIETY OF CHEMISTRY  <b>Author/Editor:</b> Royal Society of Chemistry (Great Britain)</p>	<p><b>Permission Status:</b> <span style="color: green;">✔</span> <b>Granted</b>  <b>Permission type:</b> Republish or display content  <b>Type of use:</b> Thesis/Dissertation  <b>Order License Id:</b> 4540500838763</p> <p><b>Requestor type:</b> Academic institution  <b>Format:</b> Print, Electronic  <b>Portion:</b> chart/graph/table/figure  <b>Number of charts/graphs/tables/figures:</b> 1  <b>The requesting person/organization:</b> Md. Almostasim Mahmud  <b>Title or numeric reference of the portion(s):</b> One-touch-activated blood diagnosis, Fig. 1  <b>Title of the article or chapter the portion is from:</b> One-touch-activated blood multidagnostic system using a minimally invasive hollow microneedle integrated with a paper-based sensor.  <b>Editor of portion(s):</b> N/A  <b>Author of portion(s):</b> Cheng Guo Li,<sup>a</sup> Hyou-Arm Joung,<sup>b</sup> Hyungrye Noh,<sup>a</sup> Mun-Bum Song,<sup>c</sup> Min-Gon Kim and Hyungil Jung  <b>Volume of serial or monograph:</b> 15  <b>Issue, if republishing an article from a serial:</b> Issue 16, 2015  <b>Page range of portion:</b> 3286-3292  <b>Publication date of portion:</b> 06 Jul 2015  <b>Rights for:</b> Main product</p>
--	---

**Note:** This item was invoiced separately through our **RightsLink Service**. **Duration of use:** Life of current edition **\$ 0.00**

Permission for Figure 2.1(a-b)

[Home](#)
[Account Info](#)
[Help](#)

**Title:** Understanding Wax Printing: A Simple Micropatterning Process for Paper-Based Microfluidics

**Author:** Emanuel Carrilho, Andres W. Martinez, George M. Whitesides

**Publication:** Analytical Chemistry

**Publisher:** American Chemical Society

**Date:** Aug 1, 2009

Copyright © 2009, American Chemical Society

Logged in as:  
Md. Mahmud  
Account #:  
3001407692

[LOGOUT](#)

**PERMISSION/LICENSE IS GRANTED FOR YOUR ORDER AT NO CHARGE**

This type of permission/license, instead of the standard Terms & Conditions, is sent to you because no fee is being charged for your order. Please note the following:

- Permission is granted for your request in both print and electronic formats, and translations.
- If figures and/or tables were requested, they may be adapted or used in part.
- Please print this page for your records and send a copy of it to your publisher/graduate school.
- Appropriate credit for the requested material should be given as follows: "Reprinted (adapted) with permission from (COMPLETE REFERENCE CITATION). Copyright (YEAR) American Chemical Society." Insert appropriate information in place of the capitalized words.
- One-time permission is granted only for the use specified in your request. No additional uses are granted (such as derivative works or other editions). For any other uses, please submit a new request.

If credit is given to another source for the material you requested, permission must be obtained from that source.

[BACK](#)

[CLOSE WINDOW](#)

Copyright © 2019 [Copyright Clearance Center, Inc.](#) All Rights Reserved. [Privacy statement](#). [Terms and Conditions](#).  
Comments? We would like to hear from you. E-mail us at [customercare@copyright.com](mailto:customercare@copyright.com)



## Permission for Figure 2.1(c)

**JOHN WILEY AND SONS LICENSE  
TERMS AND CONDITIONS**


Apr 23, 2019

---

This Agreement between Md. A Mahmud ("You") and John Wiley and Sons ("John Wiley and Sons") consists of your license details and the terms and conditions provided by John Wiley and Sons and Copyright Clearance Center.

License Number	4574981402275
License date	Apr 23, 2019
Licensed Content Publisher	John Wiley and Sons
Licensed Content Publication	Angewandte Chemie International Edition
Licensed Content Title	Patterned Paper as a Platform for Inexpensive, Low-Volume, Portable Bioassays
Licensed Content Author	Andres W. Martinez, Scott T. Phillips, Manish J. Butte, et al
Licensed Content Date	Feb 5, 2007
Licensed Content Volume	46
Licensed Content Issue	8
Licensed Content Pages	3
Type of use	Dissertation/Thesis
Requestor type	University/Academic
Format	Print and electronic
Portion	Figure/table
Number of figures/tables	2
Original Wiley figure/table number(s)	Scheme 1, Figure 1
Will you be translating?	No
Title of your thesis / dissertation	Miniaturization of Features in Microfluidic Paper-based Analytical Devices for User-friendly Testing and Diagnosis Using Small Sample Volume
Expected completion date	Apr 2019
Expected size (number of pages)	115
Requestor Location	Md. A Mahmud 2000 Simcoe St N FEAS, UOIT  Oshawa, ON L1G 0C5 Canada Attn:
Publisher Tax ID	EU826007151
Total	0.00 USD

Permission for Figure 2.2(a)



**Note:** Copyright.com supplies permissions but not the copyrighted content itself.

1  
PAYMENT
2  
REVIEW
3  
CONFIRMATION

**Step 3: Order Confirmation**

**Thank you for your order!** A confirmation for your order will be sent to your account email address. If you have questions about your order, you can call us 24 hrs/day, M-F at +1.855.239.3415 Toll Free, or write to us at [info@copyright.com](mailto:info@copyright.com). This is not an invoice.

**Confirmation Number: 11795200**  
**Order Date: 03/01/2019**

**Payment Information**

Md. Mahmud  
md.mahmud@uoit.net  
+1 (289) 600-6622  
Payment Method: n/a

If you paid by credit card, your order will be finalized and your card will be charged within 24 hours. If you choose to be invoiced, you can change or cancel your order until the invoice is generated.

---


**Order Details**

**The analyst online**

<p><b>Order detail ID:</b> 71829901  <b>Order License Id:</b> 4540520324580  <b>ISSN:</b> 1364-5528  <b>Publication Type:</b> e-Journal  <b>Volume:</b>  <b>Issue:</b>  <b>Start page:</b>  <b>Publisher:</b> Royal Society of Chemistry  <b>Author/Editor:</b> Society of Public Analysts (Great Britain) ; et al</p>	<p><b>Permission Status:</b> <span style="color: green;">✔</span> <b>Granted</b>  <b>Permission type:</b> Republish or display content  <b>Type of use:</b> Thesis/Dissertation</p> <p><b>Requestor type:</b> Academic institution</p> <p><b>Format:</b> Print, Electronic</p> <p><b>Portion:</b> chart/graph/table/figure</p> <p><b>Number of charts/graphs/tables /figures:</b> 1</p> <p><b>The requesting person/organization:</b> Md. Almostasim Mahmud</p> <p><b>Title or numeric reference of the portion(s):</b> Fig.1</p> <p><b>Title of the article or chapter the portion is from:</b> One-step patterning of hollow microstructures in paper by laser cutting to create microfluidic analytical devices</p>
--	--

**Note:** This item will be invoiced or charged separately through CCC's **RightsLink** service. [More info](#) **\$ 0.00**

Permission for Figure 2.2(b)



**Note:** Copyright.com supplies permissions but not the copyrighted content itself.

1  
PAYMENT

2  
REVIEW

**3  
CONFIRMATION**

**Step 3: Order Confirmation**

**Thank you for your order!** A confirmation for your order will be sent to your account email address. If you have questions about your order, you can call us 24 hrs/day, M-F at +1.855.239.3415 Toll Free, or write to us at [info@copyright.com](mailto:info@copyright.com). This is not an invoice.

**Confirmation Number: 11795198**  
**Order Date: 03/01/2019**

If you paid by credit card, your order will be finalized and your card will be charged within 24 hours. If you choose to be invoiced, you can change or cancel your order until the invoice is generated.

**Payment Information**

Md. Mahmud  
md.mahmud@uoit.net  
+1 (289) 600-6622  
Payment Method: n/a

---

**Order Details**

**Journal of micromechanics and microengineering : structures, devices, and systems**

<p><b>Order detail ID:</b> 71829899  <b>Order License Id:</b> 4540511273554  <b>ISSN:</b> 0960-1317  <b>Publication Type:</b> Journal  <b>Volume:</b>  <b>Issue:</b>  <b>Start page:</b>  <b>Publisher:</b> INSTITUTE OF PHYSICS PUBLISHING  <b>Author/Editor:</b> Institute of Physics (Great Britain) ; American Institute of Physics</p>	<p><b>Permission Status:</b> <span style="color: green;">✔</span> <b>Granted</b>  <b>Permission type:</b> Republish or display content  <b>Type of use:</b> Thesis/Dissertation</p> <p><b>Requestor type:</b> Academic institution</p> <p><b>Format:</b> Print, Electronic</p> <p><b>Portion:</b> chart/graph/table/figure</p> <p><b>Number of charts/graphs/tables /figures:</b> 1</p> <p><b>The requesting person/organization:</b> Md. Almostasim Mahmud</p> <p><b>Title or numeric reference of the portion(s):</b> Figure 2</p> <p><b>Title of the article or chapter the portion is from:</b> CO2 laser cutting and ablative etching for the fabrication of paper-based devices</p>
---	---

**Note:** This item will be invoiced or charged separately through CCC's [RightsLink](#) service. [More info](#) **\$ 0.00**

## Permission for Figure 2.3(a)

**SPRINGER NATURE LICENSE  
TERMS AND CONDITIONS**

Apr 23, 2019

---

This Agreement between Md. A Mahmud ("You") and Springer Nature ("Springer Nature") consists of your license details and the terms and conditions provided by Springer Nature and Copyright Clearance Center.

License Number	4574991154844
License date	Apr 23, 2019
Licensed Content Publisher	Springer Nature
Licensed Content Publication	Microsystem Technologies
Licensed Content Title	Investigation of wax and paper materials for the fabrication of paper-based microfluidic devices
Licensed Content Author	Z. W. Zhong, Z. P. Wang, G. X. D. Huang
Licensed Content Date	Jan 1, 2012
Licensed Content Volume	18
Licensed Content Issue	5
Type of Use	Thesis/Dissertation
Requestor type	non-commercial (non-profit)
Format	print and electronic
Portion	figures/tables/illustrations
Number of figures/tables/illustrations	1
Will you be translating?	no
Circulation/distribution	<501
Author of this Springer Nature content	no
Title	Miniaturization of Features in Micro uidic Paper-based Analytical Devices for User-friendly Testing and Diagnosis Using Small Sample Volume
Institution name	n/a
Expected presentation date	Apr 2019
Portions	Fig. 7
Requestor Location	Md. A Mahmud 2000 Simcoe St N FEAS, UOIT  Oshawa, ON L1G 0C5 Canada Attn:
Total	0.00 USD

## Permission for Figure 2.3(c)

**SPRINGER NATURE LICENSE  
TERMS AND CONDITIONS**



Apr 23, 2019

---

This Agreement between Md. A Mahmud ("You") and Springer Nature ("Springer Nature") consists of your license details and the terms and conditions provided by Springer Nature and Copyright Clearance Center.

License Number	4574991260869
License date	Apr 23, 2019
Licensed Content Publisher	Springer Nature
Licensed Content Publication	Microfluids and Nanofluids
Licensed Content Title	Engineering microfluidic papers: effect of fiber source and paper sheet properties on capillary-driven fluid flow
Licensed Content Author	Alexander Böhm, Franz Carstens, Christian Trieb et al
Licensed Content Date	Jan 1, 2014
Licensed Content Volume	16
Licensed Content Issue	5
Type of Use	Thesis/Dissertation
Requestor type	non-commercial (non-profit)
Format	print and electronic
Portion	figures/tables/illustrations
Number of figures/tables/illustrations	1
Will you be translating?	no
Circulation/distribution	<501
Author of this Springer Nature content	no
Title	Miniaturization of Features in Microfluidic Paper-based Analytical Devices for User-friendly Testing and Diagnosis Using Small Sample Volume
Institution name	n/a
Expected presentation date	Apr 2019
Portions	Fig. 5
Requestor Location	Md. A Mahmud 2000 Simcoe St N FEAS, UOIT  Oshawa, ON L1G 0C5 Canada Attn:
Total	0.00 USD
Terms and Conditions	

Permission for Figure 2.5(a-b)

**Title:** Microfluidic Distance Readout Sweet Hydrogel Integrated Paper-Based Analytical Device ( $\mu$ DiSH-PAD) for Visual Quantitative Point-of-Care Testing

**Author:** Xiaofeng Wei, Tian Tian, Shasha Jia, et al

**Publication:** Analytical Chemistry

**Publisher:** American Chemical Society

**Date:** Feb 1, 2016

Copyright © 2016, American Chemical Society

Logged in as:  
Md. Mahmud  
Account #:  
3001407692

[LOGOUT](#)

[Home](#) [Account Info](#) [Help](#)

**PERMISSION/LICENSE IS GRANTED FOR YOUR ORDER AT NO CHARGE**

This type of permission/license, instead of the standard Terms & Conditions, is sent to you because no fee is being charged for your order. Please note the following:

- Permission is granted for your request in both print and electronic formats, and translations.
- If figures and/or tables were requested, they may be adapted or used in part.
- Please print this page for your records and send a copy of it to your publisher/graduate school.
- Appropriate credit for the requested material should be given as follows: "Reprinted (adapted) with permission from (COMPLETE REFERENCE CITATION). Copyright (YEAR) American Chemical Society." Insert appropriate information in place of the capitalized words.
- One-time permission is granted only for the use specified in your request. No additional uses are granted (such as derivative works or other editions). For any other uses, please submit a new request.



If credit is given to another source for the material you requested, permission must be obtained from that source.

[BACK](#)


[CLOSE WINDOW](#)

Copyright © 2019 Copyright Clearance Center, Inc. All Rights Reserved. [Privacy statement](#). [Terms and Conditions](#).  
Comments? We would like to hear from you. E-mail us at [customercare@copyright.com](mailto:customercare@copyright.com)

Permission for Figure 2.5(c)

[Home](#)
[Account Info](#)
[Help](#)

**ACS Publications**  
Most Trusted. Most Cited. Most Read.

<b>Title:</b>	Distance-Based Tear Lactoferrin Assay on Microfluidic Paper Device Using Interfacial Interactions on Surface-Modified Cellulose	Logged in as: Md. Mahmud Account #: 3001407692
<b>Author:</b>	Kentaro Yamada, Terence G. Henares, Koji Suzuki, et al	<a href="#">LOGOUT</a>
<b>Publication:</b>	Applied Materials	
<b>Publisher:</b>	American Chemical Society	
<b>Date:</b>	Nov 1, 2015	

Copyright © 2015, American Chemical Society

**PERMISSION/LICENSE IS GRANTED FOR YOUR ORDER AT NO CHARGE**

This type of permission/license, instead of the standard Terms & Conditions, is sent to you because no fee is being charged for your order. Please note the following:


- Permission is granted for your request in both print and electronic formats, and translations.
- If figures and/or tables were requested, they may be adapted or used in part.
- Please print this page for your records and send a copy of it to your publisher/graduate school.
- Appropriate credit for the requested material should be given as follows: "Reprinted (adapted) with permission from (COMPLETE REFERENCE CITATION). Copyright (YEAR) American Chemical Society." Insert appropriate information in place of the capitalized words.
- One-time permission is granted only for the use specified in your request. No additional uses are granted (such as derivative works or other editions). For any other uses, please submit a new request.

If credit is given to another source for the material you requested, permission must be obtained from that source.

[BACK](#)

[CLOSE WINDOW](#)

## Permission for Figure 2.5(d)



**Note:** Copyright.com supplies permissions but not the copyrighted content itself.

1  
PAYMENT
2  
REVIEW
3  
CONFIRMATION

**Step 3: Order Confirmation**

**Thank you for your order!** A confirmation for your order will be sent to your account email address. If you have questions about your order, you can call us 24 hrs/day, M-F at +1.855.239.3415 Toll Free, or write to us at [info@copyright.com](mailto:info@copyright.com). This is not an invoice.

**Confirmation Number: 11795201**  
**Order Date: 03/01/2019**

If you paid by credit card, your order will be finalized and your card will be charged within 24 hours. If you choose to be invoiced, you can change or cancel your order until the invoice is generated.

**Payment Information**

Md. Mahmud  
md.mahmud@uoit.net  
+1 (289) 600-6622  
Payment Method: n/a

---

**Order Details**

**The analyst online**

<p><b>Order detail ID:</b> 71829902  <b>Order License Id:</b> 4540530119435  <b>ISSN:</b> 1364-5528  <b>Publication Type:</b> e-Journal  <b>Volume:</b>  <b>Issue:</b>  <b>Start page:</b>  <b>Publisher:</b> Royal Society of Chemistry  <b>Author/Editor:</b> Society of Public Analysts (Great Britain) ; et al</p>	<p><b>Permission Status:</b> <span style="color: green;">✔</span> <b>Granted</b>  <b>Permission type:</b> Republish or display content  <b>Type of use:</b> Thesis/Dissertation  <b>Requestor type:</b> Academic institution  <b>Format:</b> Print, Electronic  <b>Portion:</b> chart/graph/table/figure  <b>Number of charts/graphs/tables/figures:</b> 1  <b>The requesting person/organization:</b> Md. Almostasim Mahmud  <b>Title or numeric reference of the portion(s):</b> Fig.6  <b>Title of the article or chapter the portion is from:</b> One-step polymer screen-printing for microfluidic paper-based analytical device (μPAD) fabrication</p>
--	--

**Note:** This item will be invoiced or charged separately through CCC's **RightsLink** service. [More info](#) **\$ 0.00**



## Permission for Figure 2.6(a-b)

**ELSEVIER LICENSE  
TERMS AND CONDITIONS**

Apr 23, 2019

---

This Agreement between Md. A Mahmud ("You") and Elsevier ("Elsevier") consists of your license details and the terms and conditions provided by Elsevier and Copyright Clearance Center.

License Number	4574980620802
License date	Apr 23, 2019
Licensed Content Publisher	Elsevier
Licensed Content Publication	Food Chemistry
Licensed Content Title	Development of a barcode-style lateral flow immunoassay for the rapid semi-quantification of gliadin in foods
Licensed Content Author	Hsin-Yi Yin, Pei-Tzu Chu, Wen-Che Tsai, Hsiao-Wei Wen
Licensed Content Date	Feb 1, 2016
Licensed Content Volume	192
Licensed Content Issue	n/a
Licensed Content Pages	9
Start Page	934
End Page	942
Type of Use	reuse in a thesis/dissertation
Intended publisher of new work	other
Portion	figures/tables/illustrations
Number of figures/tables/illustrations	2
Format	both print and electronic
Are you the author of this Elsevier article?	No
Will you be translating?	No
Original figure numbers	Scheme1, Fig.2
Title of your thesis/dissertation	Miniaturization of Features in Microfluidic Paper-based Analytical Devices for User-friendly Testing and Diagnosis Using Small Sample Volume
Expected completion date	Apr 2019
Estimated size (number of pages)	115
Requestor Location	Md. A Mahmud 2000 Simcoe St N FEAS, UOIT  Oshawa, ON L1G 0C5 Canada Attn:
Publisher Tax ID	GB 494 6272 12
Total	0.00 USD

## Permission for Figure 2.6(c)

ELSEVIER LICENSE  
TERMS AND CONDITIONS

Apr 23, 2019

---

This Agreement between Md. A Mahmud ("You") and Elsevier ("Elsevier") consists of your license details and the terms and conditions provided by Elsevier and Copyright Clearance Center.

License Number	457498077774
License date	Apr 23, 2019
Licensed Content Publisher	Elsevier
Licensed Content Publication	Analytica Chimica Acta
Licensed Content Title	Development of enzyme-based bar code-style lateral-flow assay for hydrogen peroxide determination
Licensed Content Author	Ka-Kei Fung, Cangel Pui-Yee Chan, Reinhard Renneberg
Licensed Content Date	Feb 16, 2009
Licensed Content Volume	634
Licensed Content Issue	1
Licensed Content Pages	7
Start Page	89
End Page	95
Type of Use	reuse in a thesis/dissertation
Intended publisher of new work	other
Portion	figures/tables/illustrations
Number of figures/tables/illustrations	1
Format	both print and electronic
Are you the author of this Elsevier article?	No
Will you be translating?	No
Original figure numbers	Fig. 7
Title of your thesis/dissertation	Miniaturization of Features in Microfluidic Paper-based Analytical Devices for User-friendly Testing and Diagnosis Using Small Sample Volume
Expected completion date	Apr 2019
Estimated size (number of pages)	115
Requestor Location	Md. A Mahmud 2000 Simcoe St N FEAS, UOIT  Oshawa, ON L1G 0C5 Canada Attn:
Publisher Tax ID	GB 494 6272 12
Total	0.00 USD

Note: Figure 1.1, 2.4 and 2.3(b) are published by MDPI which is an open access journal where reusing a figure with proper reference is allowed.